REPUBLIC OF TÜRKİYE
HARRAN UNIVERSITY
INSTITUTE OF GRADUATE EDUCATION

DOCTORATE THESIS

APPLICATIONS OF ULTRASONICALLY PREPARED COMPOSITE MATERIAL-BASED MODIFIED ELECTRODES IN QUANTITATIVE ANALYSIS

BIKHTIYAR OMAR ABDULLAH ABDULLAH

Thesis Supervisor:
Prof. Dr. MEHMET ASLANOĞLU

Second-supervisor:
Assist. Prof. Dr. Hani K. Ismail ISMAIL

Şanlıurfa
2026

REPUBLIC OF TÜRKİYE
HARRAN UNIVERSITY

DOCTORATE THESIS

APPLICATIONS OF ULTRASONICALLY PREPARED COMPOSITE MATERIAL-BASED MODIFIED ELECTRODES IN QUANTITATIVE ANALYSIS

BIKHTIYAR OMAR ABDULLAH ABDULLAH

Thesis Supervisor:
Prof. Dr. MEHMET ASLANOĞLU

Second-supervisor:
Assist. Prof. Dr. Hani K. Ismail ISMAIL

Şanlıurfa
2026

ACKNOWLEDGEMENT

I would like to express my deepest gratitude to my supervisor **Prof. Dr. Mehmet ASLANOĞLU**, who guided me with their knowledge, experience, and support throughout the development of this thesis, and who made significant contributions to my academic growth. They played a major role in helping me gain a scientific perspective, learn research discipline, and overcome every challenge with a solution-oriented approach.

I would also like to thank my professors and friends in the Department of Chemistry for sharing their knowledge and experience with me throughout my graduate studies and for supporting me in the use of laboratory facilities. I am grateful to my laboratory colleagues **Dr. Tuğçe TEKER, Dr. Şehriban DÜZMEN, and Ebru BEYYAVAŞ**, with whom I had the great pleasure of working during my experimental studies, for their assistance and motivation.

I extend my deepest thanks to my beloved mother (**Nakhshin**) and late father (**Omar**) for their support in completing my doctoral studies, and to my family—(**Ms. Niyan**) and my children—for their patience and endurance., who have never withheld their support and encouragement during this process, and who have always strengthened me with their patience, understanding, and unconditional love. Without their support, the completion of this work would not have been possible.

I would also like to thank my second supervior **Assoc. Prof. Dr. Hani K. Ismail.**

Finally, I would like to thank the Harran University for providing financial support during the execution of this thesis.

This study has been completed with the direct or indirect contributions of many people. I am grateful to each and every one of them.

İÇİNDEKİLER

ABSTRACT

DOCTORATE THESIS

APPLICATIONS OF ULTRASONICALLY PREPARED COMPOSITE MATERIAL-BASED MODIFIED ELECTRODES IN QUANTITATIVE ANALYSIS

BIKHTIYAR OMAR ABDULLAH ABDULLAH

HARRAN UNIVERSITY
INSTITUTE OF GRADUATE EDUCATION

Thesis Supervisor: Prof. Dr. MEHMET ASLANOĞLU
Second-supervisor: Assist. Prof. Dr. Hani K. Ismail ISMAIL
Year:2026, Page : 107

This thesis focuses on the development of advanced voltammetric platforms based on nanostructured electrode modifications for the sensitive, selective, and reliable determination of food additives and bioactive compounds in real samples. Three different electrochemical sensors were fabricated by integrating metal oxide nanoparticles with conductive carbon nanomaterials onto glassy carbon electrodes (GCEs), and their analytical performances were thoroughly evaluated.

In the first study, a voltammetric system was constructed using multi-walled carbon nanotubes (MWCNTs) and aluminum-doped zinc oxide (AZO) nanoparticles to detect sunset yellow, a widely used food dye. Electrochemical impedance spectroscopy (EIS) and cyclic voltammetry (CV) confirmed enhanced charge transfer and a significantly increased electroactive surface area at the MWCNTs/AZO-modified electrode. The sensor demonstrated excellent electrocatalytic activity, achieving a linear range of 4.0×10^{-9}–7.5×10^{-6} M and a detection limit (LOD) of 9.5×10^{-10} M. Successful application to powdered beverages and pharmaceutical syrups validated its accuracy and precision.

The second platform, designed for yohimbine determination in dietary supplements and biological samples, utilized graphene nanoplatelets (GN) and indium tin oxide (ITO) to form a high-performance GCE/GN@ITO electrode. The synergistic combination of GN and ITO resulted in improved electron-transfer kinetics, a wide linear range of 4.0×10^{-9}–2.1×10^{-6} M, and an LOD of 5.0×10^{-10} M, with recovery values close to 100%.

Finally, a GCE modified with a graphene nanoplatelets–antimony tin oxide (ATO-GNP) nanocomposite enabled the selective determination of homovanillic acid (HVA), an important neurological biomarker. The ATO-GNP/GCE platform achieved a linear range of 4.0×10^{-9}–3.5×10^{-6} M and an LOD of 4.5×10^{-10} M, showing strong clinical applicability through accurate measurements in blood and urine samples.

Overall, the developed nanocomposite-based electrochemical sensors offer promising potential for practical applications in food safety control, pharmaceutical analysis, and clinical diagnostics.

KEYWORDS: Graphene, Electroanalysis, Electrochemical sensor, Metallic nanoparticles, Carbon Nanotubes

ABSTRACT

DOKTORA TEZİ

ULTRASONİK YÖNTEMLE HAZIRLANAN KOMPOZİT MALZEME TABANLI MODİFİYE ELEKTROTLARIN KANTİTATİF ANALİZDEKİ UYGULAMALARI

BIKHTIYAR OMAR ABDULLAH ABDULLAH

HARRAN ÜNİVERSİTESİ
LİSANSÜSTÜ EĞİTİM ENSTİTÜSÜ

Tez Danışmanı:Prof. Dr. MEHMET ASLANOĞLU
Yıl:2026, Sayfa : 107

Bu tez çalışması, gerçek örneklerdeki gıda katkı maddeleri ve biyoaktif bileşiklerin hassas, seçici ve güvenilir tayini için nanoyapılı elektrot modifikasyonlarına dayalı gelişmiş voltametrik platformların geliştirilmesine odaklanmaktadır. Bu kapsamda, metal oksit nanoparçacıklarının iletken karbon nanomalzemeleri ile camy karbon elektrot (GCE) yüzeyine entegre edilmesiyle üç farklı elektrokimyasal sensör hazırlanmış ve analitik performansları detaylı olarak değerlendirilmiştir.

İlk çalışmada, yaygın olarak kullanılan bir gıda boyası olan sunset yellow'ın tespiti için çok duvarlı karbon nanotüpler (MWCNTs) ve alüminyum katkılı çinko oksit (AZO) nanoparçacıkları kullanılarak voltametrik bir platform geliştirilmiştir. Elektrokimyasal empedans spektroskopisi (EIS) ve döngüsel voltametri (CV) sonuçları, MWCNTs/AZO ile modifiye edilen elektrotun daha yüksek elektroaktif yüzey alanına ve daha düşük yük transfer direncine sahip olduğunu doğrulamıştır. Sensör, 4.0×10^{-9}–7.5×10^{-6} M lineer çalışma aralığı ve 9.5×10^{-10} M tayin alt sınırı (LOD) ile yüksek elektrokatalitik performans sergilemiştir. Toz içecek ve farmasötik şurup örneklerinde başarıyla uygulanarak yüksek doğruluk ve tekrarlanabilirlik göstermiştir.

İkinci platformda, besin takviyelerinde ve biyolojik örneklerde bulunan yohimbinin seçici tayini için grafen nanoplateletleri (GN) ve indiyum kalay oksit (ITO) kullanılarak GCE/GN@ITO elektrodu geliştirilmiştir. GN ve ITO'nun sinerjik etkisi sayesinde elektron transferi önemli ölçüde iyileşmiş, 4.0×10^{-9}–2.1×10^{-6} M lineer aralık ve 5.0×10^{-10} M LOD değerleri elde edilmiştir. Geri kazanım oranlarının %99.2–100.2 arasında olması yöntemin güvenilirliğini doğrulamıştır.

Son olarak, önemli bir nörolojik biyobelirteç olan homovanilik asidin (HVA) selektif tayini için grafen nanoplatelet–antimon kalay oksit nanokompoziti (ATO-GNP) ile modifiye edilmiş GCE kullanılmıştır. ATO-GNP/GCE platformu, 4.0×10^{-9}–3.5×10^{-6} M lineer aralığı ve 4.5×10^{-10} M LOD değeri ile üstün elektrokatalitik aktivite göstermiş; kan ve idrar örneklerinde yüksek geri kazanım oranları ile klinik uygulama potansiyelini kanıtlamıştır.

Genel olarak, geliştirilen nanokompozit tabanlı elektrokimyasal sensörler; gıda güvenliği, farmasötik analiz ve klinik tanılama alanlarında pratik uygulamalar için son derece umut verici niteliktedir.

ANAHTAR KELİMELER: Grafen, Elektroanaliz, Elektrokimyasal sensör, Metal nanoparçacıklar, Karbon nanotüp

ŞEKİLLER DİZİNİ

ÇİZELGELER DİZİNİ

1. INTRODUCTION

1.1. Food Safety and Synthetic Dyes: Sunset Yellow as a Case Study

Ensuring food safety is a fundamental public health priority, as consumers expect the foods they eat to be both visually appealing and harmless to human health (Fan et al., 2024). Over the past several decades, the food industry has increasingly used additives to improve the sensory, nutritional, and storage properties of food products. Among these additives, synthetic dyes hold a crucial place due to their ability to enhance the appearance, attractiveness, and marketability of foods. Color plays a major psychological role in consumers' purchasing decisions; a vividly colored product is often perceived as fresher, tastier, or of higher quality. However, the widespread use of artificial food dyes has raised important concerns about their potential health effects. One of the most extensively used synthetic colorants is an azo dye known as sunset yellow (E110), which provides a bright orange-yellow shade to many commercially processed foods and beverages. The increasing focus on food safety has driven continuous scientific evaluation of this dye, its benefits, and its potential risks (Fan et al., 2024).

Sunset yellow, belongs to the azo dye family. These dyes contain an –N=N– azo linkage that connects aromatic structures, contributing to their vivid coloration and stability. Sunset Yellow is derived from petroleum-based raw materials and is known for its high solubility in water, heat resistance, and strong color retention during processing and storage. Due to these advantages, it has been approved as a permitted food colorant in many regions including the European Union, where it is labeled as E110, and in the United States under the designation FD&C Yellow No. 6. Despite its global acceptance, some countries maintain stricter regulations or have banned its use based on toxicological concerns (Garkani Nejad et al., 2022a).

The food industry uses sunset yellow to achieve or restore an appealing color in products that may lose their natural appearance during processing. It is commonly incorporated into flavored soft drinks, powdered drink mixes, confectionery, ice cream, bakery items, chips, sauces, snack foods, breakfast cereals, and even pharmaceuticals such as syrups and tablets. Natural colorants such as carotenoids, turmeric, or annatto may serve similar purposes, but they often suffer from limitations including instability to light and heat, variability in shade, and high cost. In contrast, Sunset Yellow offers consistency and affordability, making it especially attractive for mass-produced foods (Fan et al., 2024, Garkani Nejad et al., 2022a, Shume et al., 2023).

While its technological advantages are clear, health-related concerns have led scientists and regulators to scrutinize Sunset Yellow carefully. One of the primary issues is its potential to cause allergic and intolerance reactions in susceptible individuals. People who are asthmatic or sensitive to aspirin may exhibit symptoms like hives, rashes, or respiratory difficulties after consuming Sunset Yellow-containing foods. Another major topic of concern involves behavioral effects in children. Research, including widely referenced studies from the United Kingdom, has suggested that certain synthetic dyes—among them sunset yellow—when consumed in mixtures with preservatives such as sodium benzoate, may contribute to increased hyperactivity and attention-related disorders in children. Although the findings are not universally conclusive, they were influential enough that the European Union mandated warning labels on products containing specific dyes, stating that they "may have an adverse effect on activity and attention in children." This regulatory step highlights the importance of exercising caution even when scientific outcomes remain under discussion (Fan et al., 2024, Garkani Nejad et al., 2022a, Shume et al., 2023).

Beyond behavioral concerns, Sunset Yellow has also been examined for its possible toxicological effects at the cellular and organ level. After ingestion, it is partially broken down by intestinal bacteria, forming aromatic amines. Some amines are considered potentially harmful due to their mutagenic or carcinogenic characteristics. Studies in animal models have reported oxidative stress, DNA damage, and changes in liver and kidney tissue after high or prolonged exposure. However, regulatory authorities maintain that these effects generally occur at doses much higher than those permitted in foods. To ensure consumer safety, authoritative organizations such as the Joint FAO/WHO Expert Committee on Food Additives (JECFA), the U.S. Food and Drug Administration (FDA), and the European Food Safety Authority (EFSA) have established acceptable daily intake (ADI) values, typically ranging from 1–4 mg per kg of body weight. As long as consumption remains within these guideline limits, the dye is considered safe for the general population (Fan et al., 2024, Garkani Nejad et al., 2022a, Shume et al., 2023).

Another dimension of the safety evaluation concerns the metabolic and microbiological implications of synthetic dye consumption. Early findings suggest that azo dyes may disrupt the balance of the gut microbiota, which plays a key role in digestion, immunity, and mental health. Although studies in this field are still emerging, the possibility of long-term effects on the gastrointestinal system

reinforces the importance of continuous research. Children are particularly vulnerable, not only because of their lower body weight but also because they tend to consume a higher proportion of dyed foods such as soft drinks, candies, and snacks. Therefore, monitoring food consumption patterns is essential to prevent excessive exposure.

In response to public concern and evolving scientific evidence, many manufacturers have begun replacing Sunset Yellow with natural alternatives wherever feasible. This transition is supported by consumer preferences shifting toward "clean-label" products that avoid synthetic chemicals. However, the replacement is not always straightforward. Natural pigments often face technological hurdles, such as instability under acidic or high-temperature conditions, which can shorten product shelf life or alter flavor. As a result, synthetic dyes like Sunset Yellow continue to play a role in the food industry, and their use must be balanced with rigorous safety evaluation and transparent labelling (Li et al., 2025a, Fan et al., 2024).

Advanced analytical technologies facilitate the monitoring of Sunset Yellow in food products to ensure that regulatory limits are not exceeded. Techniques such as high-performance liquid chromatography (HPLC), spectrophotometry, mass spectrometry, and emerging electrochemical sensing methods enable rapid and sensitive detection, improving quality control in manufacturing and regulatory laboratories. The development of these methods also contributes to food fraud prevention, as the intentional overuse of low-cost dyes poses risks in unregulated markets (Fan et al., 2024).

In conclusion, sunset yellow remains an important synthetic colorant widely used in the global food industry due to its appealing color, stability, and low cost. Nevertheless, ongoing research on its potential health impacts has led to stricter regulations, improved labeling policies, and a growing shift toward natural color alternatives. Ensuring food safety requires a careful balance between technological efficiency and public health protection. As scientific understanding advances, regulatory frameworks must continue to evolve, encouraging responsible use and supporting consumer education. Ultimately, the safety of food dyes like Sunset Yellow will rely on continuous monitoring, adherence to established intake limits, and broader industry efforts to innovate safer and more sustainable coloring solutions.

1.2. Drugs in Food Supplements: Yohimbine

Food supplements have become a major segment of the global health and nutrition market, often positioned as natural, safe products designed to enhance performance, endurance, weight loss, or overall well-being (Fu et al., 2022, Hodapp et al., 2022). However, increasing evidence indicates that some supplements contain pharmacologically active substances, either unintentionally due to contamination or deliberately added to increase product effectiveness (Fu et al., 2022, Hodapp et al., 2022). One such compound that has raised significant scientific and regulatory concern is yohimbine, an alkaloid derived from Pausinystalia yohimbe, a plant native to Central Africa. While yohimbine has long been used in traditional medicine and approved in certain countries as a pharmaceutical agent, its widespread inclusion in dietary supplements—especially those marketed for sexual enhancement and fat loss—creates serious food safety issues (Fu et al., 2022, Hodapp et al., 2022). Assessing the pharmacological function, possible toxicity, and regulatory challenges surrounding yohimbine is therefore essential in the context of safeguarding public health.

Yohimbine is an indole alkaloid primarily extracted from the bark of the yohimbe tree and synthetically available as yohimbine hydrochloride. Scientifically, it functions as an α2-adrenergic receptor antagonist, meaning it blocks receptors that normally inhibit noradrenaline release. This action leads to increased sympathetic nervous system activity, elevated heart rate, and enhanced circulation. Historically, yohimbine was used to treat sexual dysfunction, particularly erectile difficulties in men, due to its ability to stimulate blood flow to the pelvic region. It has also been explored for potential therapeutic use in depression, low libido, and certain autonomic nervous system disorders (Hodapp et al., 2022, Zhu et al., 2021, Zhao et al., 2021).

In recent years, yohimbine has gained enormous popularity in the global dietary supplement market. Products containing yohimbine are commonly promoted for weight loss and enhanced fat metabolism, increased energy and athletic performance, sexual enhancement in both men and women, appetite suppression and bodybuilding and fitness improvements (Hodapp et al., 2022, Zhu et al., 2021, Zhao et al., 2021)..

The pharmacological mechanism that contributes to weight loss benefits involves increased lipolysis. By blocking α2-receptors in adipose tissue, yohimbine

promotes the release of stored fat, especially under conditions of low insulin such as fasting. This has made yohimbine a frequent ingredient in bodybuilding supplements aimed at reducing body fat percentage while preserving muscle mass. In the sexual enhancement market, yohimbine is marketed as a natural viagra, although the compound is anything but mild or risk-free (Hodapp et al., 2022).

The major concern related to yohimbine in food supplements lies in the variability of its concentration and the absence of strict regulatory control. Unlike pharmaceutical products, supplements are often sold without standardized dosing or medical supervision. Analytical studies investigating commercial supplements have revealed substantial inconsistencies between labeled and actual yohimbine content, with some products containing significantly higher concentrations than declared. This poses a serious risk to consumers, especially because yohimbine has a narrow therapeutic window, and its side effects increase rapidly with dose (Hodapp et al., 2022, Zhu et al., 2021, Zhao et al., 2021).

Yohimbine is known to produce a wide range of adverse effects, particularly affecting the cardiovascular and central nervous systems. Commonly reported side effects include elevated heart rate, high blood pressure, anxiety, jitteriness, headaches, nausea, and sweating. At higher doses, yohimbine may trigger panic attacks, heart palpitations, arrhythmias, or dangerous hypertensive episodes. Individuals with underlying medical conditions—such as cardiovascular disease, psychological disorders, or kidney problems—are especially vulnerable. Cases of hospitalization and even fatalities have been linked to excessive yohimbine consumption in supplements (Hodapp et al., 2022, Zhu et al., 2021, Zhao et al., 2021).

Beyond direct toxicity, interactions with other drugs pose additional hazards. Because yohimbine influences neurotransmitter levels and blood pressure regulation, it may interact unpredictably with antidepressants, antihypertensive drugs, stimulants, or recreational substances. Such interactions further complicate its uncontrolled use in the general population. The presence of yohimbine in multi- ingredient supplements may amplify stimulant effects when combined with caffeine or other thermogenic agents, raising the risk of severe cardiovascular outcomes (Zhu et al., 2021).

Psychological effects also demand attention. Yohimbine has been shown to increase anxiety by intensifying activity in the central noradrenergic pathways. For

individuals predisposed to mental health issues, even small doses may trigger agitation, insomnia, or panic symptoms. As supplements are frequently marketed as stress relievers or performance enhancers, consumers may remain unaware that the product contains a substance capable of worsening psychological conditions (Zhu et al., 2021).

Regulatory perspectives on yohimbine vary widely around the world. In the United States, yohimbine is classified as a prescription drug when marketed for therapeutic purposes but is allowed as a dietary supplement ingredient if extracted from yohimbe bark. This regulatory ambiguity has enabled the supplement industry to use yohimbine widely without pharmaceutical-grade controls. In contrast, several European countries have stricter regulations or bans due to safety concerns, and products containing yohimbine may be treated as medicines rather than foods. Regulatory agencies emphasize that supplements should not contain undeclared or unapproved pharmacologically active substances, yet enforcement remains challenging given the vast and rapidly expanding market (Hodapp et al., 2022, Zhu et al., 2021, Zhao et al., 2021).

Another factor complicating risk assessment is the uncertain composition of plant-derived extracts. Yohimbe bark contains multiple alkaloids in addition to yohimbine, some of which may contribute to toxicity but remain uncharacterized. Extract quality depends on plant source, extraction method, purity levels, and intentional or accidental adulteration. Consequently, supplements labeled as containing “yohimbe extract” may exhibit unpredictable potency and pharmacological effects, creating additional uncertainty for consumers and regulators (Hodapp et al., 2022, Zhu et al., 2021, Zhao et al., 2021).

Public health concerns regarding yohimbine have led researchers to develop advanced analytical methods for detecting and quantifying the compound in supplements. Techniques like high-performance liquid chromatography (HPLC), mass spectrometry, and electrochemical sensing provide precise measurements to monitor compliance and identify mislabeled products. Such tools are essential in combating food fraud, supporting risk assessment, and informing regulatory action (Hodapp et al., 2022, Zhu et al., 2021, Zhao et al., 2021).

Consumer education is also an important part of managing safety. Many individuals mistakenly assume that any ingredient of plant origin is inherently safe, which is not the case with yohimbine. Awareness campaigns emphasizing the need

for professional consultation before using supplements containing stimulant or drug-like compounds could help reduce health risks. Healthcare professionals, including nutritionists and pharmacists, should be equipped with current information on yohimbine toxicity as supplement use continues to grow (Hodapp et al., 2022, Zhu et al., 2021, Zhao et al., 2021).

Looking forward, the challenge lies not only in regulating specific substances like yohimbine but also in addressing the broader issue of pharmaceuticals entering the supplement marketplace. Robust oversight, standardized labeling, and strict enforcement against adulteration are crucial to prevent the misuse of compounds with pharmacological potency. At the same time, further research on dose-dependent toxicity, long-term exposure, and vulnerable populations is needed to strengthen scientific evidence that supports regulatory decisions (Hodapp et al., 2022, Zhu et al., 2021, Zhao et al., 2021).

In conclusion, yohimbine represents a clear example of how pharmacologically active agents can infiltrate the food supplement market under the guise of being natural enhancers. While it can produce desired effects such as increased fat metabolism and improved sexual function, its narrow safety margin and potential for serious cardiovascular, neurological, and psychological side effects make its uncontrolled use a major food safety concern. The lack of standardization, variable content in supplements, and insufficient consumer awareness amplify the risks associated with its use. Protecting public health requires comprehensive regulatory action, accurate product testing, transparent labeling, and ongoing scientific evaluation. As the popularity of dietary supplements continues to rise, ensuring that they are both effective and safe remains an essential responsibility for health authorities and the scientific community (Hodapp et al., 2022, Zhu et al., 2021, Zhao et al., 2021).

1.3. Detection of Pharmaceutical and Biomarker Compounds in Biological Fluids

Biological fluids such as blood, urine, and cerebrospinal fluid (CSF) contain a wide range of endogenous and exogenous chemical compounds that can serve as diagnostic indicators of disease or provide evidence of drug metabolism. Detecting these compounds with high sensitivity and selectivity is essential in clinical diagnostics, pharmacokinetics, forensic toxicology, and neuroscience research. Among these biomolecules, homovanillic acid (HVA) holds particular importance

due to its close connection with dopamine metabolism. As dopamine plays vital roles in cognition, motor control, reward mechanisms, and neuroendocrine regulation, disturbances in its biochemical pathways can signal the presence of severe neurological and psychiatric disorders. Therefore, the sensitive analysis of HVA in biological fluids has become a valuable approach for understanding and monitoring dopaminergic function, guiding diagnosis, and assessing therapeutic outcomes (Hrdlicka et al., 2021, Soliman et al., 2025).

Homovanillic acid (4-hydroxy-3-methoxyphenylacetic acid) is the major metabolite formed through the enzymatic degradation of dopamine. In the central nervous system, dopamine undergoes oxidative deamination by monoamine oxidase (MAO), followed by conversion by catechol-O-methyltransferase (COMT), ultimately producing HVA, which is then transported into the bloodstream and excreted in urine. Because dopamine itself is highly unstable, rapidly metabolized, and present at extremely low concentrations in peripheral fluids, HVA serves as a more accessible and reliable indirect biomarker of dopaminergic activity. Under physiological conditions, HVA levels reflect the rate of dopamine turnover, making its measurement clinically meaningful for monitoring neural function (Hrdlicka et al., 2021, Soliman et al., 2025).

The determination of HVA is especially relevant in neurological disease diagnosis. Abnormal levels are associated with a variety of disorders. Reduced HVA concentrations in CSF are commonly observed in Parkinson's disease, where the progressive loss of dopaminergic neurons leads to insufficient dopamine production. Conversely, elevated HVA levels may indicate excessive dopaminergic activity, as seen in conditions such as schizophrenia or neuroblastoma, a pediatric cancer originating from neural crest cells. In fact, urinary HVA quantification is an established screening and diagnostic tool for neuroblastoma, often used alongside vanillylmandelic acid (VMA). Monitoring HVA levels during treatment provides insights into therapeutic efficacy and potential recurrence. The compound has also been studied for its involvement in attention-deficit hyperactivity disorder (ADHD), autism spectrum disorders, and drug addiction, further expanding its clinical importance (Hrdlicka et al., 2021, Soliman et al., 2025).

The accurate detection of HVA in biological fluids requires analytical methods that combine high sensitivity, stability, and selectivity (He et al., 2022, Ning et al., 2014, Tian et al., 2025). Traditional laboratory techniques include chromatographic methods. Chromatography has long been favored due to the

electroactive nature of HVA and the high detection sensitivity it allows. The electrochemical response arises from the oxidation of HVA's phenolic functional group, enabling quantification at nanomolar levels. Mass spectrometry offers additional advantages through structural identification and improved specificity, essential when assessing samples with complex biological matrices (Hrdlicka et al., 2021).

Sample preparation is a crucial step in the detection process because biological fluids contain proteins, salts, and a multitude of interfering molecules that may hinder accurate quantification. Techniques such as solid-phase extraction (SPE) are widely used to isolate HVA from urine or CSF, concentrating and purifying the analyte before chromatographic analysis. Advances in microextraction techniques aim to reduce solvent use and processing time while maintaining high extraction efficiency. These improvements support the development of rapid diagnostic platforms suitable for clinical practice (He et al., 2022, Ning et al., 2014, Tian et al., 2025).

Despite its strengths, chromatography remains costly, time-consuming, and limited to well-equipped laboratories. In recent years, electrochemical sensing platforms have emerged as a promising alternative for real-time, low-cost, and portable HVA monitoring. The electrochemical detection of HVA has benefited significantly from the advent of nanomaterial-based electrode modifiers, which enhance electron transfer and increase electroactive surface area. Modified glassy carbon electrodes (GCEs) incorporating materials such as carbon nanotubes, graphene derivatives, metal oxides, or conductive polymers have demonstrated remarkable advances in sensitivity and selectivity. These improvements are particularly important for detection in complex matrices, where interfering species such as ascorbic acid and uric acid coexist and exhibit overlapping oxidation potentials (Zhu et al., 2018, Khamlichi et al., 2017, Rene Pfeifera et al., (2019 , T. Selvaraju and Ramaraj, 2007, Mulla et al., 2009, Buleandra et al., 2025, Dejmkova et al., 2017, Goyal et al., 2024, Wang et al., 2025, Wu et al., 2025, Jin et al., 2025, Qi et al., 2025, Liu et al., 2025a).

Several voltammetric strategies for the detection of HVA have been reported using various electrode materials and surface modifications (Blanco-López et al., 2007, Hatefi-Mehrjardi et al., 2014, Shishkanova et al., 2018, Yolanda Dineiro et al., 2005, Shishkanova et al., 2023, O'Neill, 2005). For instance, a poly(aminosalicylic acid)-modified pencil graphite electrode was applied for the recovery of HVA in

urine samples and achieved a sensitivity of 0.03462 μA/μM and an LOD of 1.82×10-6 M within the range of 3.0×10-6–6.14×10-5 M (Santhy Antherjanam et al., 2023). Carbon nanotube-based electrodes functionalized with zinc ferrite oxide (ZFO) nanoparticles exhibited enhanced electrocatalytic activity and adsorption efficiency, providing a sensitivity of 6.679 μA/μM and an LOD of 1.4×10-7 M (Khulood Abu Al-Ola et al., 2021). GCE modified by polymers, such as poly(neutral red) and nafion yielded LODs of 8.0×10-7 M and 1.2×10-6 M, respectively (Simona Baluchováa et al., 2018), A carbon electrode modified with leucine enabled an LOD of 1.0×10-7 M and a linear range of 4.0×10-7–1.0×10-4 M, demonstrating high selectivity in urine samples (Khamlichi et al., 2017). Likewise, a screen-printed electrode modified with a coumarin derivative of Troger's base (CTB) and graphite
(G) achieved an LOD of 2.2×10-6 M and a sensitivity of 1.7105 μA/μM in blood samples (Shishkanova et al., 2018). Moreover, a voltammetric sensor based on a molecularly imprinted polymer (MIP) presented a linear response for 5×10-8–1×10-5 M HVA concentrations with an LOD of 7×10-9 M (Diñeiro et al., 2005).

Despite these promising advances, many reported HVA sensors still suffer from limitations such as relatively high detection limits, narrow linear ranges, and limited stability or reproducibility under complex biological conditions. Therefore, the design of new hybrid electrode materials that can provide enhanced electrochemical response and reliable performance for HVA determination remains of high interest.

In conclusion, homovanillic acid is a critical biochemical marker that provides valuable information on dopamine metabolism and neurological health. Its detection in biological fluids supports the diagnosis and monitoring of disorders like Parkinson's disease, schizophrenia, and neuroblastoma, while contributing to pharmacological research and forensic assessments. Ongoing advancements in electrochemical and chromatographic methods are bringing enhanced sensitivity, rapid processing, and point-of-care diagnostic capabilities closer to clinical implementation. As understanding of dopaminergic function deepens, the precise and reliable quantification of HVA will remain an essential component of biomedical analysis aimed at improving patient care and advancing neuroscientific knowledge.

1.4. Advantages of Electrochemical Sensors as Electrocatalysts in Sensing Applications

Electrochemical sensors stand at the forefront of modern analytical science

owing to their exceptional sensitivity, rapid response, low operational cost, and adaptability to a wide range of applications, including environmental monitoring, pharmaceutical analysis, biomedical diagnostics, and food safety. Their ability to convert chemical information directly into an electrical signal enables real-time, on-site detection, which is increasingly critical in today's complex supply chains and healthcare environments (Sun et al., 2025, Shan et al., 2025, Patil et al., 2025).

The effectiveness of electrochemical sensors is deeply linked to the electrocatalytic properties of the electrode materials. Bare electrodes such as glassy carbon, gold, or platinum often demonstrate limited sensitivity for many analytes due to slow electron transfer kinetics and insufficient surface area. To overcome these limitations, researchers have increasingly incorporated nanostructured electrocatalysts—metal nanoparticles, metal oxides, carbon-based nanomaterials, and hybrid composites—onto electrode surfaces. These materials provide a dramatically higher density of active sites, enhanced conductivity, and superior catalytic activity, enabling more efficient oxidation or reduction of target analytes (Sun et al., 2025, Shan et al., 2025, Patil et al., 2025).

One of the primary advantages of electrochemical sensors is their compatibility with nanostructured catalytic materials, which can be tailored to match the redox characteristics of specific analytes. Nanomaterials exhibit unique physicochemical properties such as quantum confinement, high surface-to-volume ratio, and tunable electronic structure, all contributing to improved catalytic performance (Sun et al., 2025, Shan et al., 2025, Patil et al., 2025).

Electrochemical sensing platforms also benefit from their versatility in employing various voltammetric and amperometric techniques, such as cyclic voltammetry (CV), square-wave voltammetry (SWV), and electrochemical impedance spectroscopy (EIS). These methods enable the quantitative evaluation of analytes with high precision and low detection limits. When combined with nanomaterial-based electrocatalysts, these techniques can achieve limits of detection in the nanomolar or even picomolar range (Sun et al., 2025, Shan et al., 2025, Patil et al., 2025).

From an electrocatalytic perspective, the incorporation of advanced materials significantly reduces the overpotential required for analyte oxidation or reduction. Lower overpotentials translate into sharper peak shapes, better signal-to-noise ratios, and increased selectivity, particularly for analytes prone to interference from

structurally similar compounds. Moreover, electrocatalytic surfaces can facilitate preferential adsorption on surfaces via hydrogen bonding, π–π interactions, or electrostatic attraction, enhancing analytical sensitivity (Sun et al., 2025, Shan et al., 2025, Patil et al., 2025).

Hybrid nanomaterials—such as metal oxide–carbon nanotube composites, graphene–metal nanoparticle hybrids, or polymer-coated metal oxides—combine multiple functionalities, yielding synergistic effects. Such materials enhance both electron transfer and mass transport, enabling electrodes to operate efficiently in complex matrices such as biological fluids or food extracts. For example, carbon-based materials act as conductive scaffolds, while metal nanoparticles offer catalytic centers, producing powerful sensing interfaces (Sun et al., 2025, Shan et al., 2025, Patil et al., 2025).

The cost-effectiveness of electrochemical sensors also makes them appealing for widespread use. Unlike chromatography-based techniques, electrochemical sensors do not require expensive consumables, high-pressure pumps, or large volumes of organic solvents. The fabrication process for modified electrodes—using drop-casting, electrodeposition, or simple mixing—remains inexpensive and scalable, facilitating mass production for industrial and regulatory laboratories (Sun et al., 2025, Shan et al., 2025, Patil et al., 2025).

Moreover, electrochemical sensors demonstrate excellent selectivity when properly engineered. Selective recognition can be achieved through molecular imprinting, surface functionalization, nanostructuring, or the use of biomimetic interfaces. In the context of electrocatalysis, surface chemistry can be tuned to enhance interactions with target molecules while suppressing interference from undesired species. For example, functional groups on carbon nanomaterials can be oxidized to promote hydrogen bonding, while metal oxides can provide Lewis acidic sites that interact strongly with analytes containing amine or hydroxyl groups (Sun et al., 2025, Shan et al., 2025, Patil et al., 2025).

Electrochemical sensors also excel in real-time monitoring. Unlike chromatographic methods that require batch processing, electrochemical devices provide instantaneous signals proportional to analyte concentration, allowing continuous monitoring in dynamic systems. This feature is particularly useful in biomedical diagnostics, environmental monitoring, and food safety inspection, where time-sensitive decisions are required (Sun et al., 2025, Shan et al., 2025, Patil et al.,

2025).

In conclusion, electrochemical sensing technologies offer a powerful combination of sensitivity, specificity, portability, affordability, and adaptability. These advantages stem largely from the integration of electrocatalytic nanomaterials that dramatically enhance electron transfer and surface reactivity. As research in nanotechnology continues to progress, the performance of electrochemical sensors is expected to improve further, making them indispensable tools across multiple scientific and industrial sectors.

1.5. Sensitivity-Enhancing Role of Graphene Nanoplatelets as Electrocatalysts

Graphene nanoplatelets (GNPs) are among the most prominent advanced carbon-based nanomaterials used to enhance electrocatalytic performance in electrochemical sensors. GNPs are small, flat fragments with a multilayer graphene structure and high surface area, which significantly improve the electronic properties of electrodes. It is known that GNPs accelerate the electron-transfer kinetics involved in oxidation and reduction reactions of target analytes. In this respect, GNPs serve as critical electrocatalysts in enhancing the sensitivity of electrochemical sensors (Jiménez-Suárez and Prolongo, 2020, Liu et al., 2023, Lu et al., 2024).

One of the most important advantages of GNPs is their exceptionally high electrical conductivity. The π–π conjugation system formed by sp^2-hybridized carbon atoms within the honeycomb lattice provides rapid electron-transport capability. This high conductivity allows electrochemical reactions occurring on the electrode surface to take place at lower overpotentials, increasing the signal strength while reducing energy consumption. Therefore, GNP-modified electrodes enable the detection of target analytes with sharper and more pronounced peaks (Jiménez-Suárez and Prolongo, 2020, Liu et al., 2023, Lu et al., 2024).

Additionally, the high specific surface area of GNPs increases the number of active sites available for the interaction of analyte molecules with the electrode surface. This expanded active surface facilitates the adsorption of analytes—especially those present at low concentrations—thus improving the signal- to-noise ratio. Therefore, GNP-based electrodes provide an ideal platform for trace- level detection. The literature reports that electrodes modified with GNPs achieve ultra-low detection limits for many biomolecules, toxic chemicals, and pharmaceutical compounds (Rodsud and Limbut, 2019, Jiménez-Suárez and

Prolongo, 2020, Deng et al., 2017, Zhou et al., 2016).

Another key feature of GNPs is their structural stability and chemical durability. Graphene-based materials are highly resistant to oxidation, acid-base conditions, and physical deformation. This increases the long-term stability of GNP-modified electrodes. High repeatability and reproducibility are critical, especially in sensitive measurements such as food safety and clinical analyses. The robust structure of GNPs offers an important advantage in ensuring such reliability (Rodsud and Limbut, 2019, Jiménez-Suárez and Prolongo, 2020, Deng et al., 2017, Zhou et al., 2016).

Furthermore, the suitability of GNPs for surface functionalization makes them highly versatile electrocatalysts. GNPs can contain oxygen-functional groups or be readily modified, enabling their easy integration with metal nanoparticles, polymers, biomolecules, and other nanomaterials. These hybrid structures exhibit enhanced electrochemical performance due to synergistic electrocatalytic interactions. For example, when combined with metal nanoparticles, GNPs can increase both the electron-transfer rate and the number of active sites, resulting in much more powerful sensing platforms (Rodsud and Limbut, 2019, Jiménez-Suárez and Prolongo, 2020, Deng et al., 2017, Zhou et al., 2016).

The ease of mass production and cost-effectiveness of GNPs further broadens their application areas. Large quantities of GNPs can be obtained through graphene oxide reduction processes, mechanical exfoliation, or chemical synthesis techniques. Thus, the scalability of GNP-based electrodes is high, making them suitable for industrial applications. GNPs are widely used in diverse fields, including food safety analysis, environmental pollutant monitoring, biosensing, and pharmaceutical detection (Rodsud and Limbut, 2019, Jiménez-Suárez and Prolongo, 2020, Deng et al., 2017, Zhou et al., 2016).

In conclusion, graphene nanoplatelets are ideal electrocatalysts and surface-modification materials for voltammetry sensors due to their superior electrical conductivity, large surface area, chemical stability, low cost, ease of functionalization, and strong electrocatalytic synergism. GNP-based composite materials provide a remarkable advantage over conventional electrodes, particularly in the sensitive quantification of pharmaceutical agents. The literature strongly indicates that GNPs will play an increasingly central role in the design of future electrochemical sensors.

1.6. Carbon Nanotubes as Electrocatalysts

Carbon nanotubes (CNTs) are among the most influential nanomaterials developed in the last three decades and have revolutionized the field of voltammetric sensing. Structurally, CNTs consist of rolled graphene sheets organized into seamless cylindrical tubes, classified based on the number of layers as single-walled CNTs or multi-walled CNTs. Their extraordinary electrical, mechanical, and surface properties enable remarkable improvements in electron transfer and catalytic activity at electrode surfaces, making them exceptional electrocatalysts for the development of high-performance voltammetry sensors. Due to these advantages, CNT-modified electrodes have been used extensively to detect environmental contaminants, pharmaceuticals, neurotransmitters, and biomarkers at trace levels (Hidalgo et al., 2025).

One of the primary advantages of CNTs is their exceptionally high electrical conductivity. The π-conjugated sp^2 carbon lattice of CNTs supports ballistic electron transport along their tubular axis, enabling extremely fast charge transfer between the electrode surface and target analytes. This property is particularly valuable in the oxidation and reduction of molecules with slow electron-transfer kinetics on bare electrodes. CNT modification reduces overpotential, increases peak current, and enhances signal definition. Studies have demonstrated that CNT-based electrodes exhibit far superior sensitivity and lower detection limits compared to traditional materials. Thus, CNTs serve as efficient electrocatalysts, facilitating rapid redox reactions and boosting analytical response (Hidalgo et al., 2025).

Another major feature of CNTs is their large electroactive surface area. Their high aspect ratio and mesoporous structure result in increased adsorption sites where analyte molecules can interact with the electrode surface. This enhances pre-concentration effects, improves mass transport during electrochemical processes, and significantly boosts responsiveness toward low-concentration analytes. As a consequence, CNT-modified electrodes frequently exhibit broad linear dynamic ranges and excellent sensitivity — essential characteristics for practical sensing applications in fields such as clinical diagnostics or food safety. The ability to work efficiently in trace analyte detection has driven widespread adoption of CNTs in sensor fabrication (Hidalgo et al., 2025).

Beyond conductivity and surface area, CNTs are recognized for their robust

chemical and mechanical stability. Highly graphitic CNTs resist oxidation, corrosion, and structural degradation even in harsh chemical environments, making them suitable for repeated measurements and long-term sensor operation. This is crucial for real-world deployment in challenging sample matrices such as biological fluids, food extracts, and industrial wastewaters. Additionally, CNT-based electrodes typically provide excellent repeatability and reproducibility. Since sensor lifetime and operational consistency are important criteria for commercialization, CNTs play a central role in bridging laboratory research and industrial sensing technologies (Hidalgo et al., 2025).

A noteworthy advantage of CNTs is their ability to be readily functionalized. Pristine CNTs exhibit hydrophobic surfaces and a tendency to bundle due to van der Waals interactions, which can limit their dispersion and accessibility of active sites. To overcome this, surface modification through chemical oxidation, polymer coating, or nanoparticle attachment is frequently applied. Functionalized CNTs with oxygen-containing groups (e.g., –COOH, –OH) show improved dispersion in aqueous suspensions, better interfacial bonding with electrode binders, and enhanced electrocatalytic activity (Hidalgo et al., 2025, Ghasemi et al., 2024).

CNTs are also exceptional platform materials for hybrid nanocomposites. The combination of CNTs with metal nanoparticles and metal oxides frequently generates synergistic interactions. Metal nanoparticles contribute catalytic active sites, while CNTs provide conductive pathways to rapidly transfer electrons generated during redox reactions. These hybrid nanocomposites often exhibit dramatically enhanced electrocatalytic performance compared to their individual components alone. For example, CNT-metal oxide nanocomposite electrodes have shown exceptional capability for detecting pharmaceuticals with extremely low detection limits in real samples (Hidalgo et al., 2025, Ghasemi et al., 2024).

In conclusion, carbon nanotubes serve as highly effective electrocatalysts that substantially enhance the analytical performance of electrochemical sensors. Their exceptional conductivity, high electroactive surface area, strong structural durability, and customizable surface chemistry allow for superior electron transfer, increased sensitivity, wide linear working ranges, and remarkably low detection limits. Their ability to form multifunctional nanocomposites enables synergistic electrocatalytic behavior, paving the way for new-generation sensing technologies. As research into safer, more sustainable fabrication and functionalization strategies advances, CNT-based electrodes will continue to play a dominant role in both commercial and

emerging electroanalysis applications. The remarkable versatility of CNTs ensures their ongoing importance in exploring innovative solutions for pharmaceutical detection, biochemical monitoring, and environmental protection.

1.7. Metal Oxide Nanoparticles as Electrocatalysts in Sensing Applications

Metal oxide nanoparticles have emerged as highly effective electrocatalysts in electrochemical sensing due to their outstanding catalytic activity, tunable physicochemical properties, high surface-to-volume ratio, and ability to facilitate rapid electron transfer. Various metal oxides were widely integrated into electrode surfaces for enhancing sensitivity and overall analytical performance in detecting chemical and biological analytes. The nanoscale dimensions of metal oxide particles result in an exceptionally large density of active sites where redox reactions can occur. This high surface area lowers the overpotential, increases current response, and accelerates electron transfer kinetics. Additionally, many metal oxides possess intrinsic semiconducting properties, allowing them to act as both electron mediators and catalytic centers in electrochemical reactions. Their surfaces often contain oxygen vacancies or defect sites, which enhance adsorption and electron transfer interactions with analyte molecules (Teker and Aslanoglu, 2021, Subramanian et al., 2024, Rafiq et al., 2024, Teker and Aslanoglu, 2024).

Metal oxide nanoparticles are particularly effective in promoting redox reactions for a wide range of chemicals, like pharmaceuticals, neurotransmitting drugs, amino acids, and environmentally important toxic pollutants. The catalytic efficiency of metal oxide nanoparticles can be further enhanced by controlling particle size, shape, and crystallinity, which influences surface energy, active site density, and electron mobility. Transition metal oxides often exhibit multiple oxidation states, enabling reversible redox cycling that amplifies electrochemical signals in voltammetric sensing applications. A key advantage of metal oxide nanoparticles is their ability to form hybrid nanocomposites with carbon-based nanomaterials such as graphene nanoplatelets, carbon nanotubes, and carbon nanofibers, as well as with conductive polymers. In these composites, the carbonaceous scaffold provides excellent conductivity and mechanical stability, while the metal oxide nanoparticles supply active catalytic sites. This synergistic combination improves electron transfer efficiency, expands electroactive surface area, and allows ultra-sensitive detection, often achieving nanomolar or even picomolar detection limits (Teker and Aslanoglu, 2021, Subramanian et al., 2024, Rafiq et al., 2024, Teker and Aslanoglu, 2024).

Overall, metal oxide nanoparticles have established themselves as cornerstone materials in modern electrochemical sensing. Their high catalytic activity, tunable surface chemistry, and synergistic interactions with carbon-based or polymeric nanomaterials enable sensitive, selective, and reproducible detection of a wide variety of analytes. By reducing overpotentials, amplifying signals, and expanding electroactive surfaces, MONPs continue to play a pivotal role in the development of high-performance voltammetric sensors and next-generation electroanalytical devices.

1.8. Advantages of Nanostructured Composite Materials in Electroanalysis

Electrodes modified with nanostructured composite materials exhibit significantly superior performance in electroanalytical applications compared to conventional electrodes. The large active surface area, high electrocatalytic activity, rapid charge transfer, and strong adsorptive properties provided by nanocomposites enable these electrodes to produce sensitive, reliable, and highly reproducible analytical results. These features offer a critical advantage particularly in applications such as enrionmental monitoring, quality control of pharmaceutical formulations and food analysis where analytes must be detected at very low concentrations (Rodsud and Limbut, 2019, Beyyavaş and Aslanoglu, 2024, Düzmen et al., 2024).

One of the most important advantages of nanocomposite-based electrodes is their ability to significantly expand the linear working range. In conventional electrodes with flat surfaces, such as bare glassy carbon electrodes (GCE), surface saturation may occur at high analyte concentrations due to limited available active sites, which results in a loss of linearity. In contrast, the hierarchical surface morphology of nanostructured composites allows analyte molecules to interact more effectively with the surface and provides more sites for electron transfer. Therefore, a wide linear range can be achieved, covering extremely low to high concentration levels. This property is particularly valuable in screening studies of complex matrices and routine analyses requiring a broad concentration range (Rodsud and Limbut, 2019, Beyyavaş and Aslanoglu, 2024, Düzmen et al., 2024).

Another important advantage is the substantially reduced limit of detection (LOD). Nanocomposites enhance the interaction between the analyte and the electrode surface, thereby increasing the electron-transfer rate. Additionally, the high surface-to-volume ratio of nanomaterials improves the signal-to-noise ratio, allowing

the detection of even very small changes in current. As a result, nanocomposite-modified electrodes can be effectively used for the determination of toxic substances, drug residues, and biomarkers at ultra-low levels. The ability to achieve lower LOD values has made these electrodes indispensable tools in modern electroanalytical chemistry (Rodsud and Limbut, 2019, Beyyavaş and Aslanoglu, 2024, Düzmen et al., 2024).

The sensitivity of nanocomposite electrodes is also significantly improved. Such enhancement is mainly attributed to the catalytic acceleration of electrochemical reactions by nanostructures and their ability to lower the energy barrier for oxidation or reduction of the analyte. Furthermore, the high electrical conductivity of nanomaterials reduces the surface resistance, allowing the electrode to respond more rapidly and generate stronger current signals. Increased sensitivity ensures that even trace amounts of analytes within a sample can be reliably distinguished and quantified, providing a major advantage in applications requiring high accuracy (Rodsud and Limbut, 2019, Beyyavaş and Aslanoglu, 2024, Düzmen et al., 2024).

2. PREVIOUS STUDIES

2.1. Determination of Dyes in Food Samples

Sunset yellow, a widely used colorant, is used for improving the taste, appearance and texture of food products (Yang et al., 2022). In the last few decades, sunset yellow is also being used in food industry due to providing stability in food products (Li et al., 2022). Sunset yellow is commonly used in beverages such as juices and drink mixes to enhance their visual appeal, consistency, and overall color (Garkani Nejad et al., 2022). However, synthetic food dyes are hazardous, toxic and harmful to human organism (Ji et al., 2016, Sahraei et al., 2013). High levels of sunset yellow consumption have been linked to various harmful effects, including damage to DNA (Qin et al., 2019). For this reason, the concentration of sunset yellow in food items should be carefully regulated. The acceptable daily intake should remain below 2.5 µg per gram of body weight (Wang et al., 2013). However, some countries tolerate amounts of sunset yellow in beverages up to 100.0 µg/mL (Gómez et al., 2012). Developing a sensitive analysis method for such a dye compound is important for food safety and human health.

Chromatography (Qin et al., 2019), spectrophotometry (Ai et al., 2018) and capillary electrophoresis (Yi et al., 2018) were performed for the determination of dye compounds. Nevertheless, the primary drawback of the techniques mentioned above is that they involve lengthy and time-intensive procedures when applied to food analysis.

Voltammetry, as a flexible analytical method, offers high sensitivity along with strong accuracy and reliable precision in sample analysis (Sakthivel et al., 2018, de Lima et al., 2020, El-Gendy et al., 2023, Khazaee Nejad et al., 2024, Mohammed et al., 2016, Asran et al., 2023, Mohamed et al., 2021).

Researchers have described multiple voltammetric approaches employing different electrode materials to detect and quantify colorants in food samples.(Ji et al., 2022, Sun et al., 2023, Figueira Alves et al., 2022, Tajik and Beitollahi, 2022, Balram et al., 2022). Carbon electrodes can provide a wide potential window, lower background current response, and chemical inertness for electroanalysis (Kolozof et al., 2020, Tahtaisleyen et al., 2020, Tran et al., 2019). Electrochemistry of different colorants have been studied on GCE (Sierra-Rosales et al., 2018). In addition, nanostructured modified electrodes have large surface area, allowing rapid electron transfer (Marquez-Mariño et al., 2018, He et al., 2018). Gomez and co-workers

proposed a sensitive voltammetric method for the detection of a food coloring dye (Gómez et al., 2012). The authors also reported that high sensitivity and good selectivity can be achieved in the analysis of food products by voltammetric methods (Wu et al., 2021, Penagos-Llanos et al., 2020, Darabi and Shabani-Nooshabadi, 2021, Kaya et al., 2021). For example, voltammetry at electrodes modified with graphene transducers and carbon nanotubes (Li et al., 2022), chitosan (Peña- Gonzalez, 2018), Fe-BTC framework (Ji et al., 2022), graphene/graphene-metallic oxide nanoparticles (Li et al., 2019a, Pogacean et al., 2019, Ding et al., 2019, Li et al., 2019b), molecularly imprinted polyprrole (Xu et al., 2012), polymers (Koyun, 2018, Rozi et al., 2018), lanthanide metal-organic framework (Cai et al., 2019), FeNi3 nanoalloy (Hajmalek et al., 2021), Eu3+/Cu2O nanostructures (Foroughi et al., 2021b), silver-poly(cysteine) (Tang et al., 2016), Fe3O4-SiO2 and MWCNTs (Arvand et al., 2015), nanocomposite of zeolitic imidazolate-cobalt-tannic acid (Setoudeh et al., 2020), ZnO/Fe3O4/carbon composite (Foroughi et al., 2021a), CuS crystals (Li et al., 2019a), and composite of indium-NiO nanoparticles (Moarefdoust et al., 2021) showed increased sensitivity and good selectivity. However, MWCNTs have excellent chemical and physical properties and can be used in materials, electrocatalysis and environmental sciences. Hybrid nanomaterials with MWCNTs were utilized in electroanalysis due to highly enhanced responses. Moreover, the composite of metals and MWCNTs enabled sensitive measurements and provided low detection limits. Zinc oxide (ZnO) has high popularity owing to its attractive properties such as low cost, non-toxicity, resource abundance, superior thermal and chemical stability (Regmi et al., 2023). ZnO possesses has high electron density and n-type conductivity owing to intrinsic defects such as Zn interstitials and O vacancies (Regmi et al., 2023). Additionally, doping ZnO with aluminum has proven to be effective in creating high-quality transparent electrodes (Regmi et al., 2023, García-Salinas et al., 2023). AZO, an aluminum- doped ZnO film, has high optical and electrical properties and is successfully utilized in display and photovoltaic materials (Regmi et al., 2023, García-Salinas et al., 2023, Singh and Scotognella, 2023). AZO films are used in flexible solar cells owing to their desirable mechanical properties, high optical transparency and high electrical conductivity (Regmi et al., 2023, García-Salinas et al., 2023, Alkahlout et al., 2014, Singh and Scotognella, 2023). Additionally, AZO films are known to provide enhanced flexibility and durability of materials, maintaining their optical and electrical properties even under stretching and bending conditions (Regmi et al., 2023, García-Salinas et al., 2023, Alkahlout et al., 2014).

In study, we present a sensitive voltammetric platform constructed on a GCE

with MWCNTs and nanoparticles of aluminium doped zinc oxide (AZO) by means of ultrasonication. The proposed platform (GCE/MWCNTs/AZO) exhibited great improvement in voltammetric behavior of sunset yellow. The GCE/MWCNTs/AZO system enabled good accuracy and high precision for the determination of sunset yellow in beverages and pharmaceuticals. The novelty of the proposed modified electrode relates to the ability to detect sunset yellow in beverages and pharmaceuticals containing interfering species, proving its practical applicability with good accuracy and high sensitivity. Moreover, due to its high electrochemically active surface area, good electrical conductivity, strong adsorption capacity and the presence of surface oxygen vacancies of AZO, it showed a high improvement in the voltammetric behavior of sunset yellow, providing a low detection limit and a wide linear working range.

2.2. Determination of Drugs in Food Supplements

Yohimbine is a stimulant and is used for its ability to improve body composition as well as symptoms of erectile dysfunction (Fu et al., 2022, Hodapp et al., 2022). Yohimbine supplements can be used for weight loss since its ability to increase lipolysis (Hodapp et al., 2022). However, yohimbine causes abdominal pain, dizziness, anxiety, nervousness and nausea (Hodapp et al., 2022, Zhu et al., 2021). Moreover, toxic effect yohimbine in herbal products has been reported (Hodapp et al., 2022). Case reports with yohimbine use also indicated high blood pressure, cardiac arrhythmias, anxiety and agitation (Hodapp et al., 2022, Zhu et al., 2021, Zhao et al., 2021). Dietary yohimbine supplements have been mislabelled in the US and the content found in the products raises warnings of potential harm (Hodapp et al., 2022). Zhu and co-workers also reported severe acute intoxication and poisoning cases (Zhu et al., 2021). Therefore, a reliable method for quantifying yohimbine is required for clinical and health issues. Determination of yohimbine was conducted using chromatography (Mittal et al., 2000), spectroscopy (Farouk et al., 2011), and flow amperometry (Švorc and Kalcher, 2014). Current analytical methods for yohimbine detection, such as chromatography, are often time-consuming, expensive, and require specialized equipment, limiting their application in routine quality control. However, voltammetric detection provides good reproducibility, high selectivity and excellent sensitivity in electroanalysis (Azab, 2019, Chandana et al., 2024, Jeevitha et al., 2024, M.B. Shivaswamy et al., 2024, Gowda et al., 2025). Additionally, voltammetric sensors enable rapid, cost-effective, and precise analysis, making them particularly suitable for monitoring the quality of yohimbine-containing products (Rodsud and Limbut, 2019, Beyyavaş and Aslanoglu, 2024, Düzmen et al.,

2024). Authors also prepared a procedure for determining yohimbine in supplements by boron-doped diamond electrodes (Švorc et al., 2014). In contrast, electrodes made from carbon exhibit minimal background current, are chemically stable, and allow for a broader potential range during measurements (David et al., 2015, Fernandez et al., 2018, Karabiberoğlu et al., 2013, Ghorbani-Bidkorbeh et al., 2010). Electrodes enhanced with nanostructured materials demonstrate strong electrocatalytic performance, offer an expanded surface area, and facilitate rapid electron transfer (Manikandan et al., 2018, Trani et al., 2017, Ghorbani-Bidkorbeh et al., 2010, Xu et al., 2013, Karapınar et al., 2024). Moreover, graphene nanopowders possess exceptional physical characteristics and display outstanding electrical conductivity when applied as electrocatalytic materials (Jiménez-Suárez and Prolongo, 2020, Pereira et al., 2020). Voltammetric procedures by coating GCEs with graphene, graphene-dysprosium oxide and carbon nanofibers-erbium oxide were used to quantify yohimbine (Rodsud and Limbut, 2019, Beyyavaş and Aslanoglu, 2024, Düzmen et al., 2024). Additionally, nano-materials with metallic nanoparticles based materials also showed high reproducibility, and enabled lower LOD in electroanalysis (Düzmen and Aslanoglu, 2023). Rare earth metals demonstrate outstanding performance when employed in electrocatalytic sensing applications and in supercapacitor technologies.(Carcione et al., 2023, Wang et al., 2024). Furthermore, ITO shows high conductivity in various applications as energy convertor (Li et al., 2022). Authors also reported that ITO has prominent characteristics such as stable chemical and physical behavior (Ottoni et al., 2016). This study focuses on the development of a voltammetric sensor for the reliable determination of yohimbine in dietary supplements, addressing the need for more accessible and efficient analytical tools to ensure product safety and prevent health risks. By modifying GCEs with GN and ITO, GCE/GN@ITO shows good electrochemical performance, offering a large surface area, reduced Rct, and remarkable catalytic activity. This innovative platform was applied to detect yohimbine in supplements, providing a reliable and sensitive tool for accurate analysis. The synergy between GN's high conductivity and ITO's electrocatalytic properties, enhanced by oxygen vacancies, significantly improves the electron transfer and interaction with the analyte. The proposed electrochemical sensor exhibited improved peak definition, higher current response, and lower oxidation potential for yohimbine compared to both bare and singly modified electrodes. These characteristics make the GCE/GN@ITO sensor an ideal candidate for sensitive electrochemical detection. Additionally, the platform outperforms existing detection methods by offering superior sensitivity, a key feature for precise and reliable analysis in various applications. This advancement establishes a new benchmark in

analytical accuracy and precision, particularly for the detection of bioactive compounds like yohimbine. Overall, the integration of ITO and GN into a single electrode material represents a significant step forward in the development of high-performance sensors, with broad implications for electrochemical sensing in various applications.

2.3. Determination of Drugs in Biological Samples

Homovanillic acid (HVA) is a major end-product of dopamine metabolism and serves as an important biomarker for assessing dopaminergic activity in the human nervous system (Hrdlicka et al., 2021). Abnormal levels of HVA in biological fluids such as blood and urine have been linked to various neurological disorders, including Parkinson's disease, schizophrenia, and neuroblastoma (Hrdlicka et al., 2021). Monitoring HVA concentrations in complex media is therefore crucial for early diagnosis, therapeutic monitoring, and clinical research on neurodegenerative and psychiatric diseases (Hrdlicka et al., 2021).

To date, various methods were developed for quantifying HVA, including high-performance liquid chromatography-tandem mass spectrometry (HPLC-MS) (Romero-Alfano et al., 2025), liquid chromatography–tandem mass spectrometry (Iwasaki et al., 2022), high-precision liquid chromatography with electrochemical detection (Borchers and Pieler, 2010), and spectroscopy (Devika Sudha Ravindran et al., 2021). Although these methods provide high accuracy and selectivity, they typically require complex and time-consuming sample pretreatment, expensive instrumentation, and skilled operators. In contrast, electrochemical techniques have attracted considerable attention because of their simplicity, rapid response, and suitability for point-of-care diagnostics (Zhu et al., 2018, Khamlichi et al., 2017, Rene Pfeifera et al., (2019 , T. Selvaraju and Ramaraj, 2007, Mulla et al., 2009, Buleandra et al., 2025, Dejmkova et al., 2017, Goyal et al., 2024).

Several voltammetric strategies for the detection of HVA have been reported using various electrode materials and surface modifications (Blanco-López et al., 2007, Hatefi-Mehrjardi et al., 2014, Shishkanova et al., 2018, Yolanda Dineiro et al., 2005, Shishkanova et al., 2023, O'Neill, 2005). For instance, MWCNT/zinc ferrite nanostructure coated carbon paste electrode enabled a working range of 4.1×10-7 to 3.2×10-6 M with an LOD of 1.4×10-7 M (Khulood Abu Al-Ola et al., 2021), glassy carbon electrodes modified GCE modified by polymers, such as poly(neutral red) and nafion with detection limits of 8.0×10-7 M and 1.2×10-6 M,

respectively (Simona Baluchováa et al., 2018), and electropolymerization of 4-aminosalicylic acid modified pencil graphite electrode yielded a working range of 3.0×10-6 to 6.1×10-5 M with an LOD of 1.8×10-6 M (Santhy Antherjanam et al., 2023) have been employed to enhance the sensitivity of HVA detection. However, many of these sensors still suffer from limitations such as relatively high LODs and narrow linear ranges for reliable applications. Therefore, developingf novel materials that can further improve the electrochemical response towards HVA remains highly desirable.

Metal oxide nanoparticles were shown as good candidates for modification due to providng high surface area, good conductivity, chemical stability, and catalytic properties (Hassan A.M. Hendawy and Khaled, 2025, Abbas et al., 2021). Among these, antimony tin oxide (ATO) is a highly conductive n-type semiconductor material that has attracted growing interest for electrochemical sensing applications because of its excellent electrical conductivity, chemical inertness, and strong catalytic activity (Li et al., 2015, Ren et al., 2020, Baytak et al., 2016, Amutha et al., 2022). ATO nanoparticles can effectively promote electron transfer processes, reduce overpotentials, and enhance oxidation kinetics for target analytes (Baytak et al., 2016).

GNPs, composed of stacked graphene layers, offer outstanding features like a large surface area, good conductivity, robust strength, and abundant edge-plane sites that enhance electron transfer (Jiménez-Suárez and Prolongo, 2020). GNPs have been widely incorporated into voltammetry sensors for the detection of small molecules, drugs, antioxidants, and environmental pollutants (Rodsud and Limbut, 2019, Jiménez-Suárez and Prolongo, 2020, Deng et al., 2017, Zhou et al., 2016).

Combining ATO nanoparticles with GNPs in a hybrid nanocomposite creates a synergistic sensing interface that integrates the large surface area and high conductivity of GNPs and the catalytic functionality of ATO. This strategy is expected to significantly enhance the analytical performance of voltammetric sensors for the trace-level determination of HVA in complex biological matrices.

In this thesis, we aimed to develop a sensitive voltammetric sensor with a GNP/ATO nanocomposite on GCE for the determination of HVA. The electrochemical behavior of the voltammetry sensor was characterized using cyclic voltammetry and electrochemical impedance spectroscopy, and its detection performance was systematically optimized. The developed platform exhibited

excellent analytical features, including high sensitivity, stability, good reproducibility, low detection limit and a wide linear working range. The platform was successfully applied for detecting HVA in urine and blood, demonstrating its promising potential for clinical diagnostics and neurological disease monitoring.

3. MATERIALS AND METHODS

3.1. Materials

Sunset yellow (dye content 95%), yohimbine and homovanillic acid (HVA, ≥99% purity)and tartrazine (dye content 97%) were purchased from Sigma-Aldrich (USA). Multi-walled carbon nanotubes (MWCNTs, >95%, OD: 20–30 nm), graphene nanoplatelets (GNP, thickness <2–8 nm, lateral size 4–12 μm), aluminium- doped zinc oxide nanopowder (AZO, 15 nm, 99.99+%), antimony tin oxide nanopowder (ATO, 30 nm), and indium tin oxide nanopowder (ITO) were obtained from US-Nano Chemical Company (USA) and used as received. Graphene nanoplatelets (GN) were similarly purchased from US-Nano, USA.

All other chemicals and solvents were reagent grade and purchased from Merck or Sigma-Aldrich. Stock solutions of analytes were freshly prepared in PBS, which served as the supporting electrolyte in all voltammetric analyses. Before each experiment, the electrochemical cell was deaerated by bubbling high-purity nitrogen gas through the solution for several minutes to remove dissolved oxygen.

Yohimbine containing tablets were sourced from Trendyol, an e-commerce platform based in Turkey. All reagents were used without further purification unless otherwise stated.

3.2. Instrumentation

Voltammetric measurements were carried out using a PGSTAT-12 model Autolab potentiostat along with a GCE, Ag/AgCl in 3.0 M KCl and Pt rod as working, reference and counter electrodes, respectively. GCEs were obtained from BASi while reference and counter electrodes were purchased from Metrohm. A pH meter purchased from Metrohm was used for adjusting pH values. SEM-mapping images, EDX spectrum and XRD pattern were all recorded on a Zeiss Evo50 model of electron microscope and Ultima III model of X-ray diffractometer, respectively.

3.3. Preparation of Electrochemical Platforms

3.3.1. Preparation of GCE/MWCNTs/AZO

GCEs were polished with 0.05 μm alumina slurry on a polishing pad before use. Then, GCEs were placed in acetone and sonicated for 10 min. Afterwards, GCEs were electrochemically activated in 0.1 M PBS (pH7) by scanning from -0.4 V to 1.2

V at a scan rate of 100 mV/s by cyclic voltammetry. Then, 5.0 mg MWCNTs and 2.5 mg AZO were dispersed in chloroform. The mixture was sonicated for 60 min prior to modify the surface of GCE. 3.0 µL suspension was pipetted and dropped on GCE and then left to dry in air. Modified electrode was rinsed with distilled water. The electrode was also electrochemically activated prior to use in electro-analysis. For this purpose, cyclic voltammetry was performed for recording multiple scans with the proposed electrode in 0.1 M PBS at pH 7 in a potential window from -0.4 V to 1.2 V. The electro-activation of the proposed electrode was completed once a stable background voltammogram was obtained. A schematic presentation of developing GCE/MWCNTs/AZO and its application is presented in Figure 3.1.

Figure 3.1. Preparation and use of GCE/MWCNTs/AZO

3.3.2. Prepatation of Voltammetric Sensor of GCE/GN@ITO

GC electrodes were polished with 0.3 and 1.0 µm alumina to obtain a mirror-like finish. GCE was rinsed with distilled water. Then, the electrode were activated by cyclic voltammetry (CV) to obtain stable background voltammograms. Afterwards, 5 mg of GN and 1 mg ITO were dispersed in 25 ml chloroform. The suspension was then sonicated for 60 minutes. Then, GC electrodes were coated with 5 µL GN-ITO. GC electrodes modified with GN@ITO were activated in a potential window of -1.0~1.0 V by CV. A simple illustration of the preparation of the platform and its voltametric usage is presented in Figure 3.2.

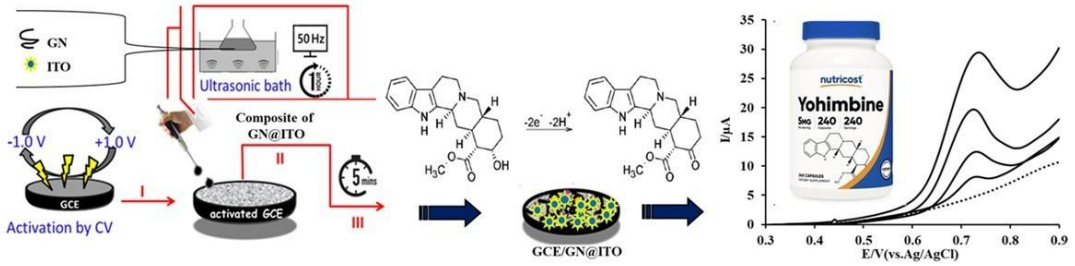

Figure 3.2. Preparation of and use of GCE/GN@ITO

3.3.3. Preparation of the electrohcemical sensor of ATO–GNP/GCE

Prior to the electrode modification, GC electrode was mechanically polished to a mirror-like finish using a 0.3 μm alumina slurry, thoroughly rinsed with deionized water, and sonicated in acetone for 5 min. Electrochemical pretreatment was then performed by cyclic voltammetry (CV) between –0.6 V and +1.0 V in 0.1 M PB (pH 7.0) to stabilize the baseline and ensure a clean, active surface.

For the preparation of the material of the ATO–GNP suspension, 5 mg of GNPs and 1 mg of ATO nanoparticles were dispersed in chloroform and sonicated for 1 hour to obtain a uniform and stable dispersion. 5 μL aliquot of the resulting suspension was carefully drop-cast on GCE and left to dry under ambient conditions. The ATO–GNP/GCE platform was then electrochemically activated in 0.1 M PB by CV prior to its use for the determination of HVA. A schematic representation of process is shown in Figure 3.3. The solid and dotted CVs correspond to the voltammograms of the first and second scans, respectively.

Figure 3.3. Schematic illustration and use of the proposed sensor

3.4. Preparation of samples and analysis

3.4.1. Preparation of samples for the quantification of dye content

2.0 g powder was weighed and dissolved in 0.1 M PBS. Then, dilutions were carried out by PBS. The sample was ultra-sonicated for 10 min. The sample was then pipetted and transferred to a 50 mL beaker to immerse the proposed platform for 210 sec. The platform was then rinsed with distilled water and transferred to an electrochemical cell for the electroanalysis of sample.

5.0 ml pediatric syrup was accurately transferred to a flask and then diluted with 0.1 M PBS at pH 7. The pediatric syrup sample was also ultrasonicated for 10 min. Then, a supernatant was then transferred to a 50 mL beaker to immerse the proposed platform for 210 sec. The GCE/MWCNTs/AZO system was rinsed with distilled water and transferred to a cell for analysis.

3.4.2. Preparation of samples for the determination of yohimbine

The contents of three capsules were accurately weighed, and the average mass of a single capsule was dispersed in 10 mL of methanol. The solution was diluted to 25 mL using PBS and subjected to sonication for 10 minutes to ensure homogeneity. A known volume of the prepared solution was then taken to the electrochemical cell for analysis.

3.4.3. Prepration of samples for the determination of homovanillic acid

To assess the applicability of the electrochemical platform, artificial blood and artificial urine were used to study.

Prior to analysis, the artificial blood sample was first filtered using Whatman No. 1 filter paper to remove any particulates, then diluted by mixing 1 mL of blood with 0.1 M PB (pH 7.0). Artificial urine sample was prepared in a similar manner by diluting urine with PB. All prepared samples were gently vortexed to ensure homogeneity before analysis.

These mild pretreatment steps were deliberately chosen to avoid the use of organic solvents or deproteinization agents that could adsorb or degrade HVA. The satisfactory recovery values confirmed that no measurable analyte loss occurred during filtration or dilution.

For quantitative evaluation, the standard addition method was employed. Known concentrations of HVA standard solution were spiked into the filtered artificial blood and urine samples, and SWV measurements were recorded after each addition under optimized conditions. Calibration plots of anodic peak current versus HVA were constructed, and HVA contents were calculated from the extrapolated intercepts. The recovery values were calculated as (found concentration/added concentration)×100% to assess accuracy and matrix effects.

4. FINDINGS

4.1. The Application of GCE/MWCNTs/AZO to Quantify Sunset Yellow in Drinks

4.1.1. Characterization of the proposed sensor

The material of AZO was characterized by means of SEM, EDX and XRD techniques. SEM images (Figure 4.1) and mapping images (Figure 4.2) show AZO on MWCNTs. The EDX spectrum also exhibited that the material is composed of C, O, Al and Zn (Figure 4.3). However, Au is observed owing to the coating procedure before SEM measurements. The XRD pattern also confirmed the presence of MWCNT and AZO. The response of MWCNTs was observed at 26°. However, peaks observed at 2θ = 32°, 34°, 36° 47.5°, 57°, and 63° are assigned to AZO (Figure 4.4).

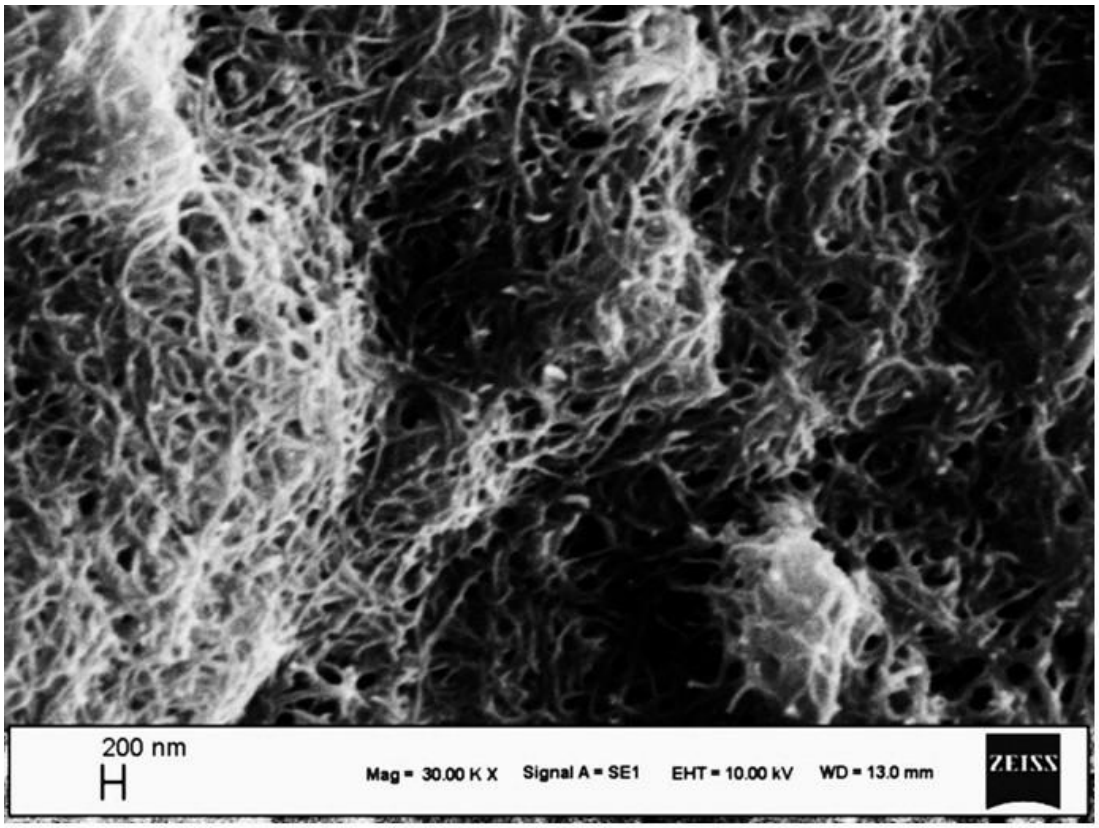

Figure 4.1. A SEM image of MWCNTs-AZO

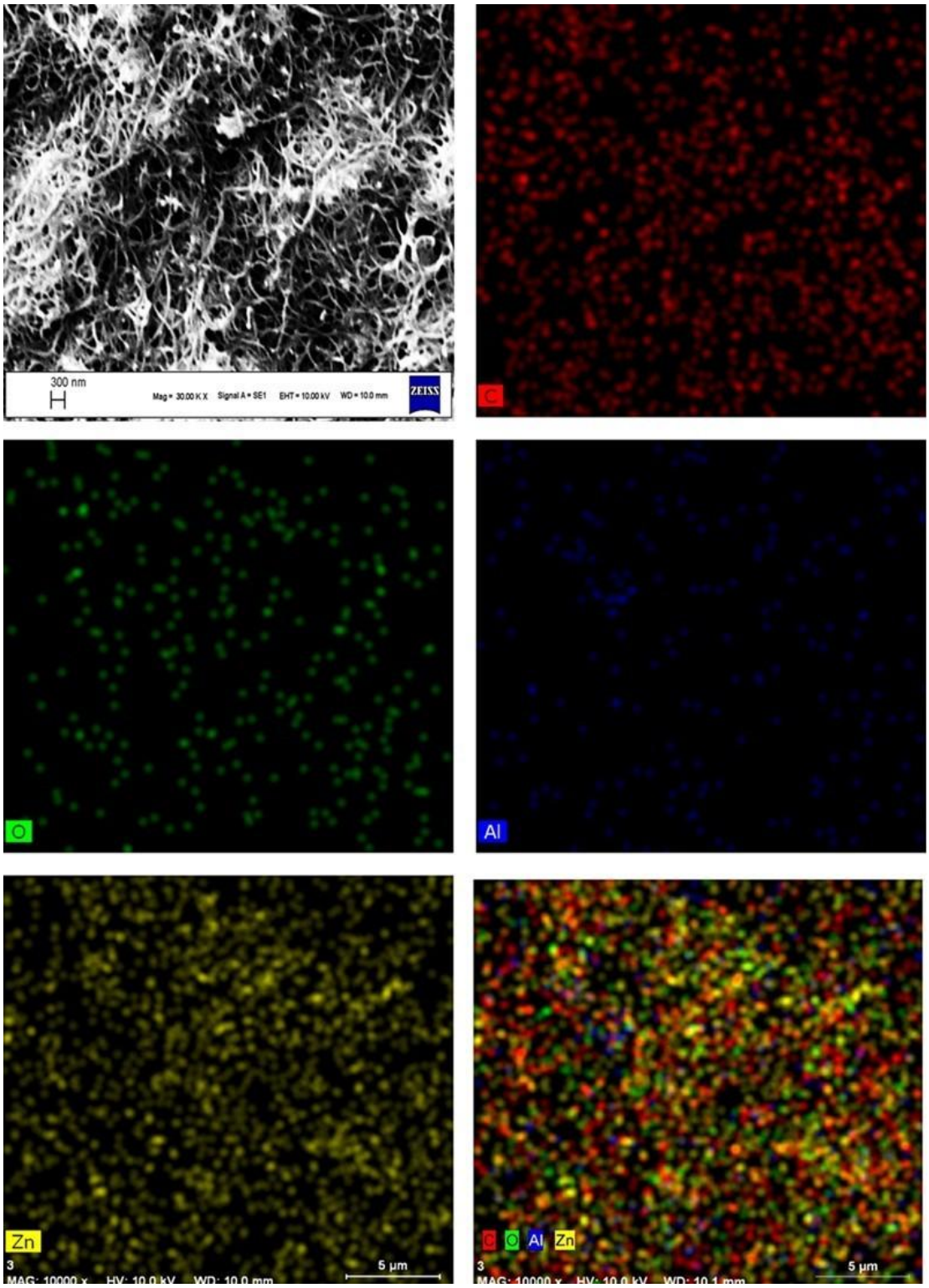

Figure 4.2. Mapping images of the proposed material

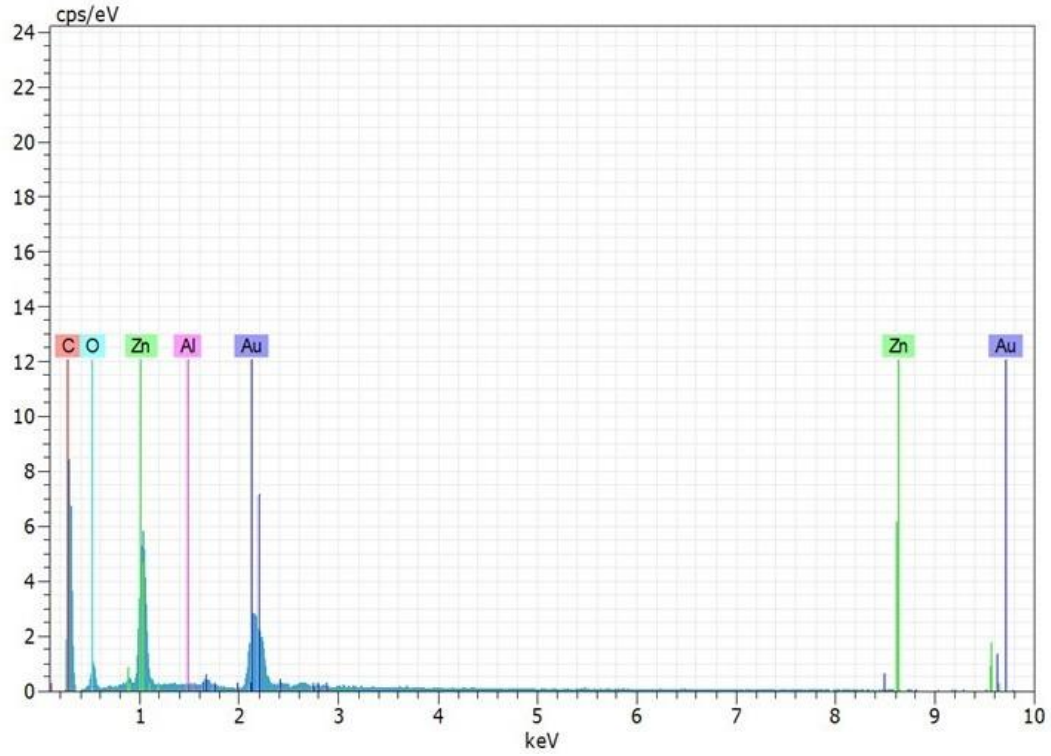

Figure 4.3. EDX spectrum of the proposed material

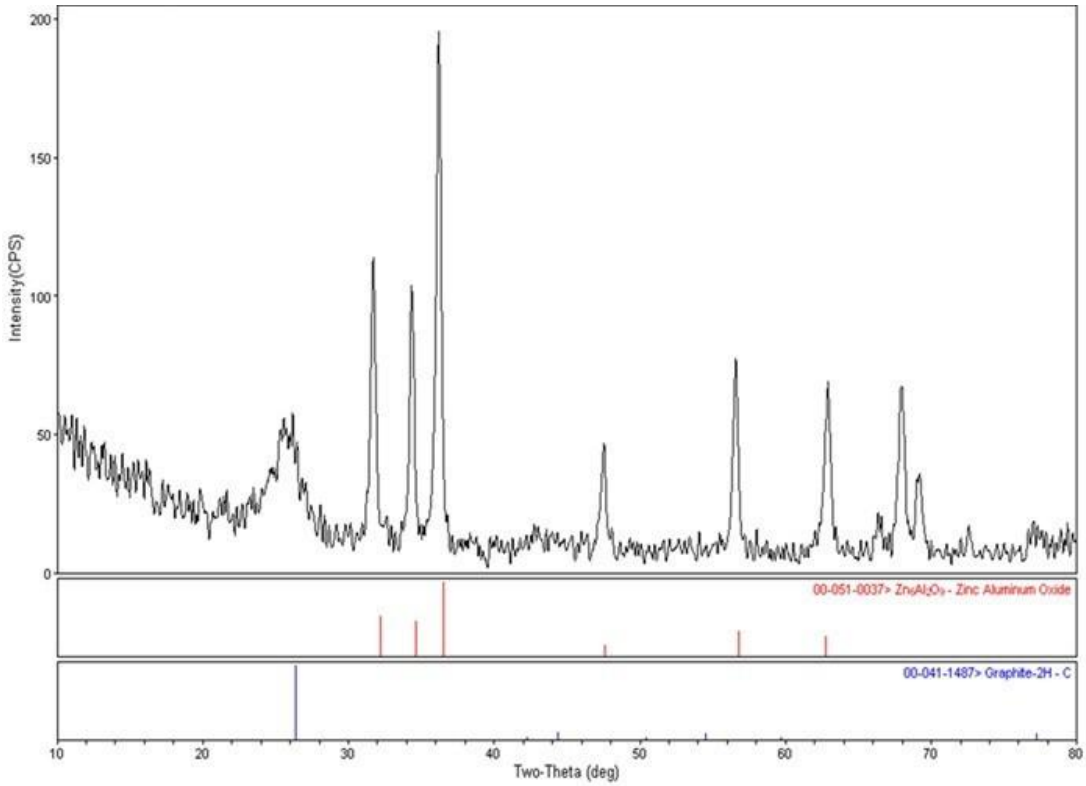

Figure 4.4. XRD spectrum of the proposed material

4.1.2. Optimization of the proposed electrochemical sensor

The GCE/MWCNTs/AZO system was kept in dye solution for various time

periods, rinsed with distilled water and then transferred to the voltammetric cell to record voltammograms using 3.0 µL of black suspension. Voltammetric measurements showed that a period of 210 s was appropriate to achieve the maximum current response (Figure 4.5A). The amount of suspension of the modifying material was also examined. Figure 4.5B showed that the no remarkable increase in peak response was observed for values higher than 3.0 µL of black suspension at an accumulation time of 210 s. The dependence of pH value of voltammetry of sunset yellow showed that the highest response was obtained at pH

7. The optimized parameters for square wave voltammetry (SWV) were determined as step potential of 5 mV, amplitude of 20 mV and frequency of 20 Hz.

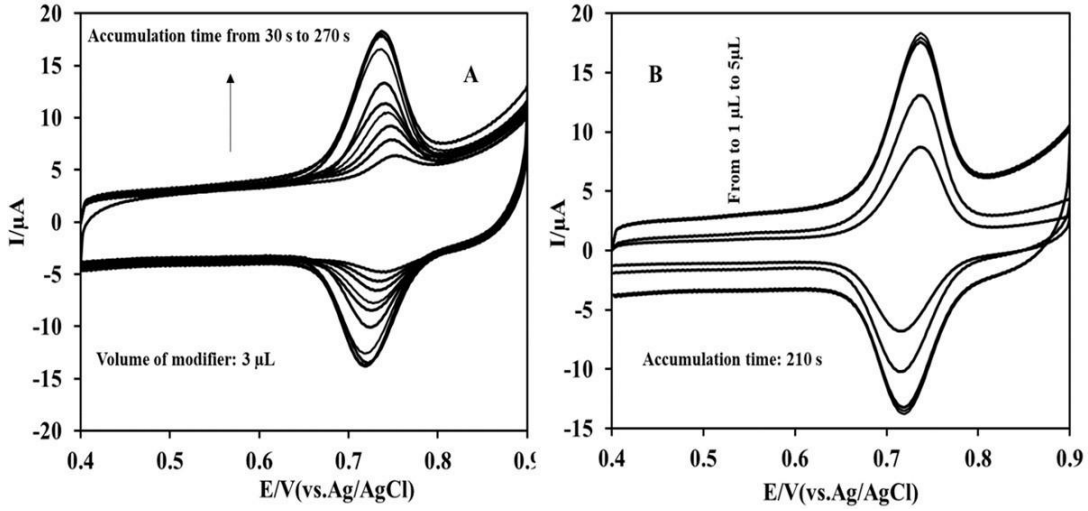

Figure 4.5. (A) CVs of dye for various period of time. (B) CVs of sunset yellow at different volumes.

4.1.3. Electrochemical impedance measurement

The study of charge transfer resistance (Rct) were carried out using EIS spectroscopy at a frequency range of 0.01 Hz – 1 MHz for an amplitude of 25 mV. The Rct values were determined by semicircle plots of Nyquist diagrams (Figure 6). EIS study yielded Rct values of 595 Ω, 398 Ω, 270 Ω and 79 Ω for GCE (a), GCE/MWCNTs (b), CGE/AZO (c) and GCE/MWCNTs/AZO (d, respectively. The reduced value of Rct obtained at the proposed platform indicated that GCE/MWCNTs/AZO activated an excellent electron pathway for sensing applications.

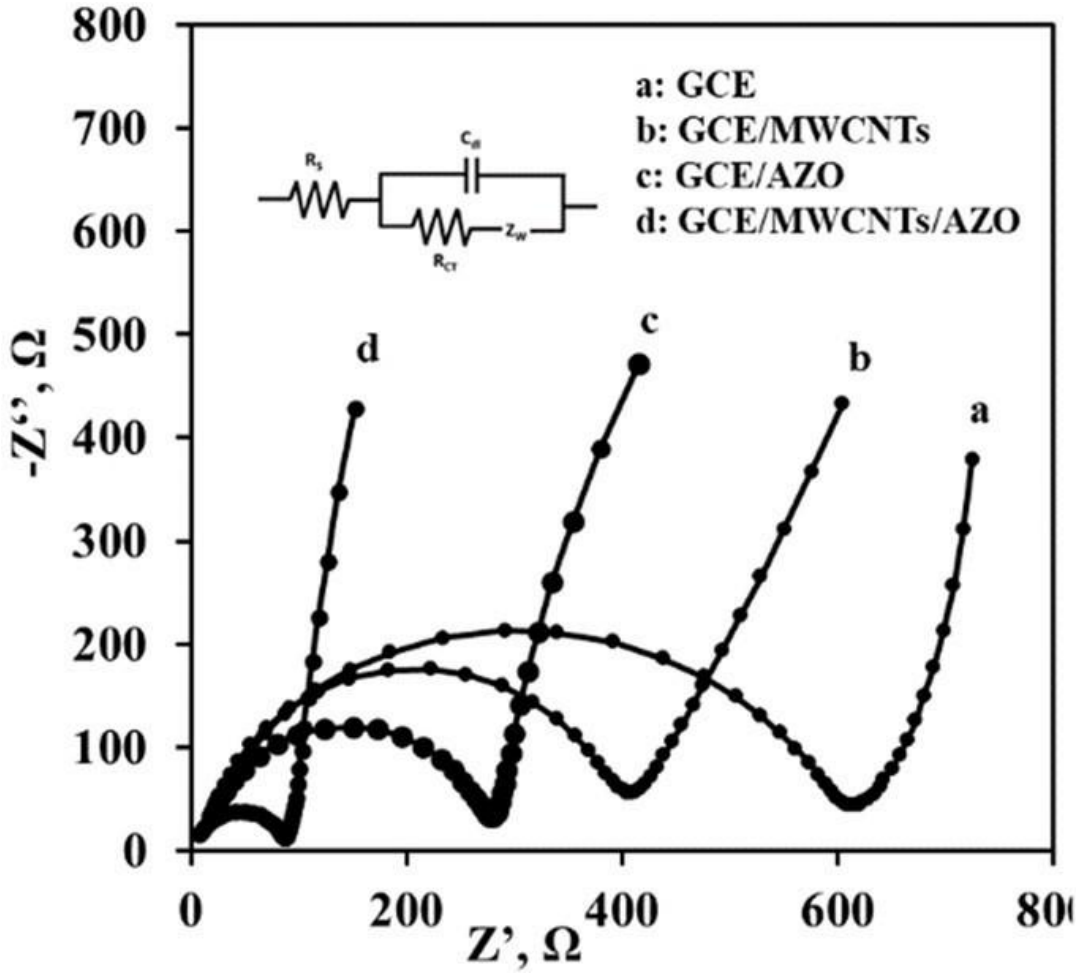

Figure 4.6. Curves recorded by EIS at various electrodes

4.1.4. Determination of electroactive area

Determination of active surface area was accomplished by recording cyclic scans of 1 mM potassium ferriccyanide in 0.1 M KCl by utilizing Randles–Sevcik equation. Voltammograms of electrodes are compared at 50 mV/s as given in Figure 4.7. The electrochemically active surface area was calculated by means of the plots of Ip versus v1/2. Electrochemically active surface area of 0.066, 0.26, 0.36 and 0.49 cm2 were calculated for GCE, GCE/MWCNTs, and GCE/MWCNTs/AZO. Voltammetric study showed that AZO and MWCNTs modified electrode possessed the highest value of surface area.

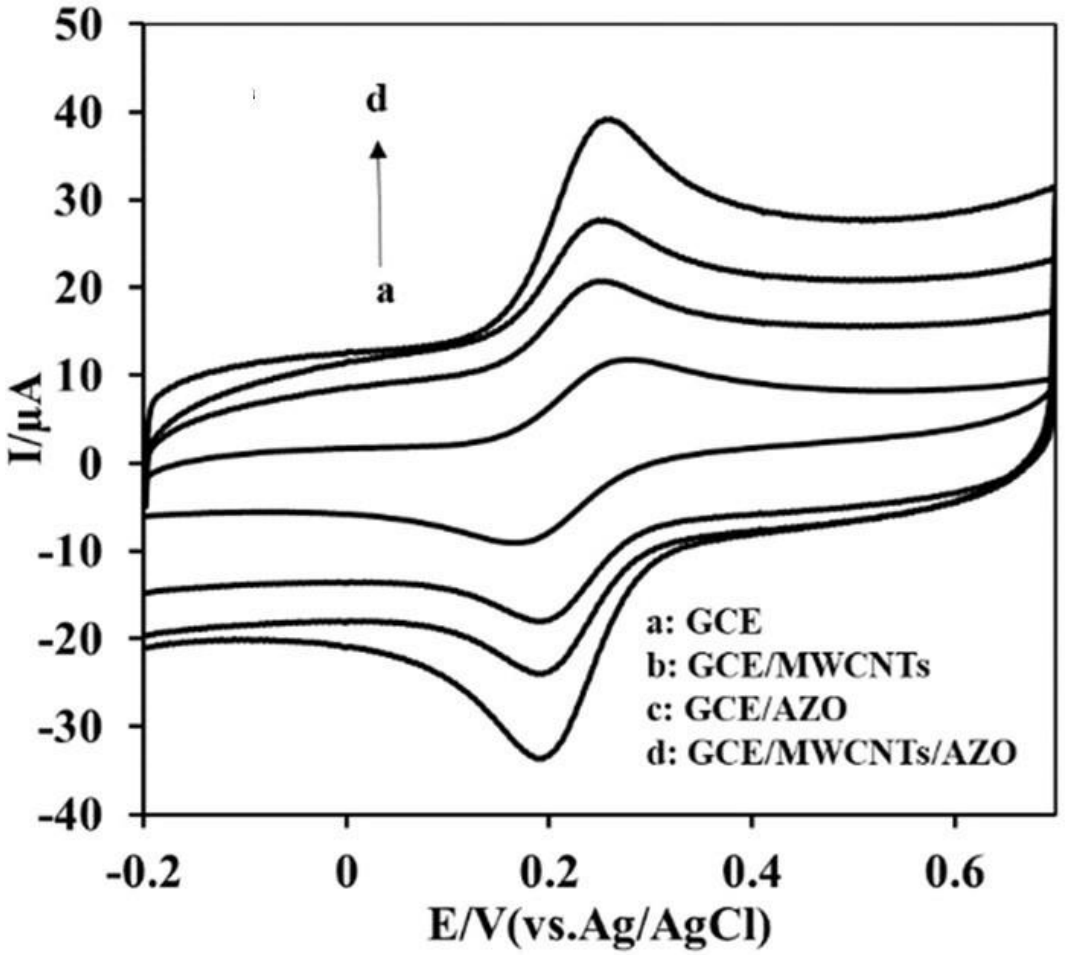

Figure 4.7. CVs for 1 mM K3[Fe(CN)6] for various electrodes.

4.1.5. Voltammetric behavior of sunset yellow

Cyclic voltammograms of 10 μM dye compound recorded for an accumulation time of 210 s at various electrodes are presented in Figure 4.8. GCE showed broad anodic peak for the dye at 0.766 V. No cathodic peaks were observed in the reverse scan. However, an improved oxidation peak at Epa of 0.756 V and a cathodic peak at Epc of 0.717 V for sunset yellow were observed at GCE/MWCNTs. The peak potential separation (ΔEp) between anodic and cathodic peaks were 39 mV. Moreover, a GCE modified with MWCNTs-AZO (GCE/MWCNTs/AZO) highly improved redox couple for sunset yellow and exhibited a sharp oxidation peak was observed at 0.737 V, while a reduction peak was observed at 0.719 V a with an ΔEp of 18 V. Obviously, the value of Epa was shifted lower potential values in the order from GCE to GCE/MWCNTs, and GCE/MWCNTs/AZO, indicating higher electrocatalytic activity of GCE/MWCNTs/AZO when compared to unmodified GCE and GCE/MWCNTs. The increase of the electroactive surface area led to a high improvement in the voltammetric behavior of sunset yellow including lower ΔEp,

high peak response and the lower charge transfer resistance value due to the strong synergistic effect between AZO and MWCNTs.

An expected characteristic of electroactive adsorbates is that the potential difference between the peak potentials of the waves can be less than 29 mV for a two electron process (Margonis et al., 2021). The lower value of ΔEp indicates faster electrode reaction (Yang et al., 2017).

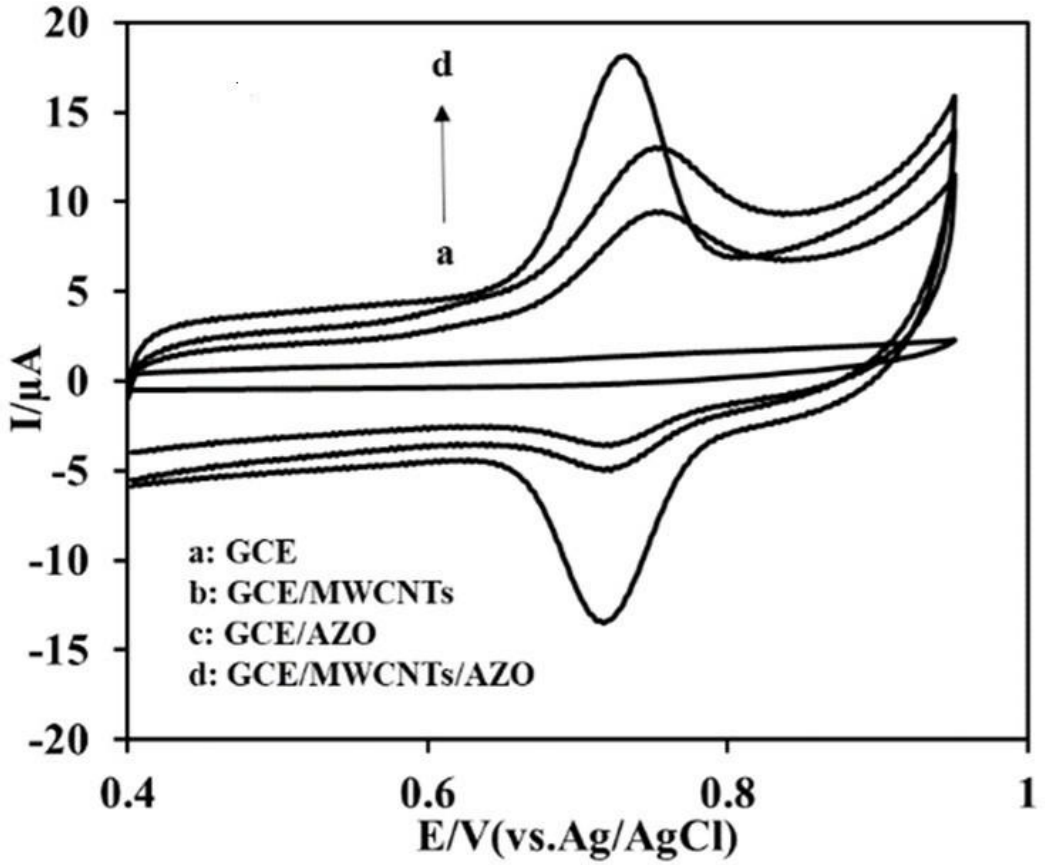

Figure 4.8. CVs of sunset yellow at various electrodes.

The composite of MWCNTs-AZO nanoparticles can promote an increase in surface area, leading to an increase in mass transfer and decreased overpotential. The mechanism for the determination of sunset yellow can be attributed to the surface oxygens on AZO nanoparticles (Zhang et al., 2021, Nimbalkar et al., 2019). Oxygen atoms can interact with sunset yellow, i.e., -OH, -N=N, and enable the oxidation of sunset yellow (Nimbalkar et al., 2019, Zhang et al., 2021).

The effect of scan rate on voltammetry of dye compound was studied at scan rates between 50 mV/s and 300 mV/s in order to obtain the electrode reaction

mechanism. CVs of 10 µM sunset yellow are presented in Figure 4.9A. A graph of Ip -v showing a linear plot, was presented in Figure 4.9B. Furthermore, the slope of logI-logv was close to 1, suggesting an adsorptive process for the dye compound on GCE/MWCNTs/AZO (Figure 4.9C).The influence of scan rate on peak potentials used to estimate the number of electrons in dye process on GCE/MWCNTs/AZO by utilizing the Laviron model (Laviron, 1974) is presented in Figure 4.9D.

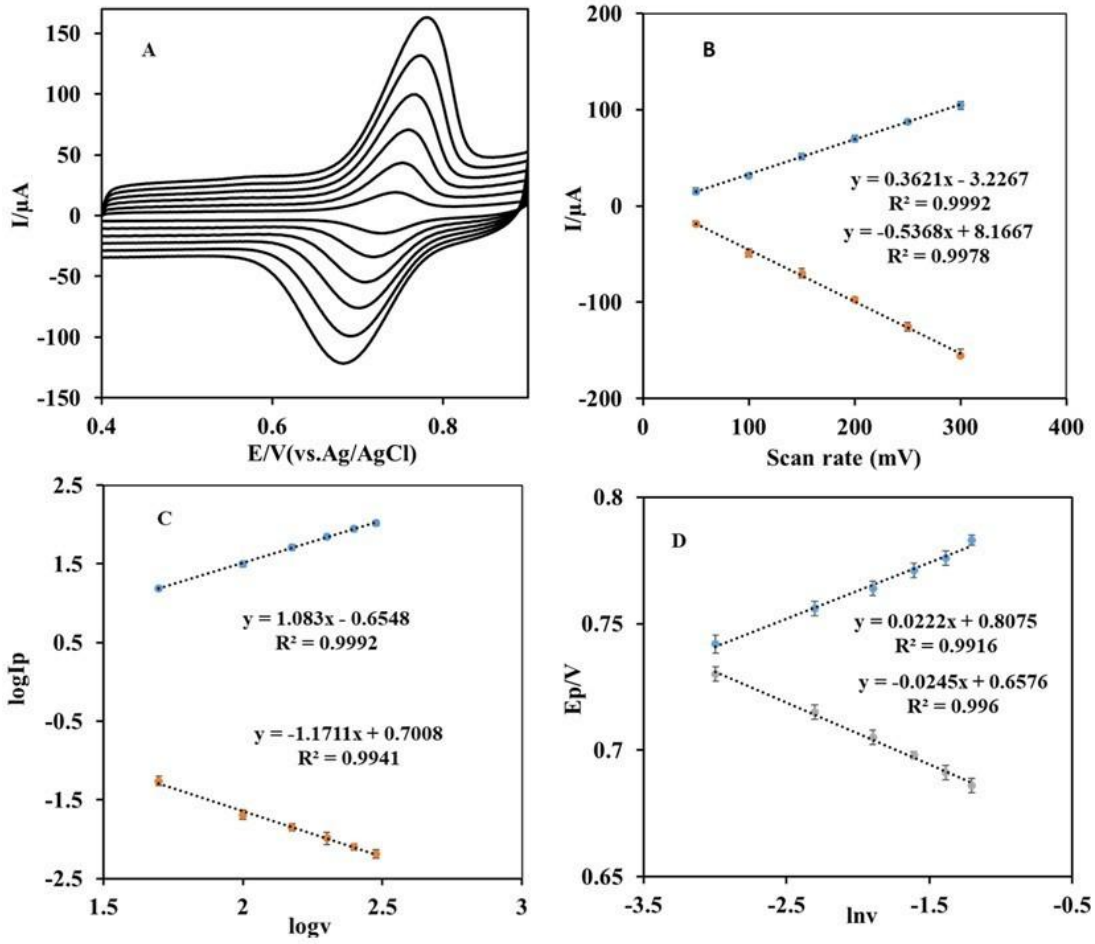

Figure 4.9. . (A) CVs of sunset yellow for various scan rates. (B) A graph of Ip vs. sweep rates. (C) Graph of logI vs. logv. (D) Graph of Epa vs. lnv.

Both Epa and Epc were determined to be linear according to the Napierian logarithm of sweep rate (lnv). The equations are given below: Epa (V) = 0.0222lnv (V/s) + 0.8075 (R^2 = 0.9916) and Epc (V) = -0.0245lnv (V/s) + 0.6576 (R^2 = 0.9960). Based on the these equations, the slopes of Epa-lnv and Epc-lnv are equal to RT/(1–α)nF and RT/αnF, respectively (Ding et al., 2019). The value of αn was 1.15. The value of electron-transfer coefficient (α) was estimated to be 0.52 and the value of n was found to be 2.2 for for the dye compound. These results suggest that that the process proceeds by a two-electron oxidation on GCE/MWCNTs/AZO (Ebube

Uwaya and Bisetty, 2023, Chebotarev et al., 2019).

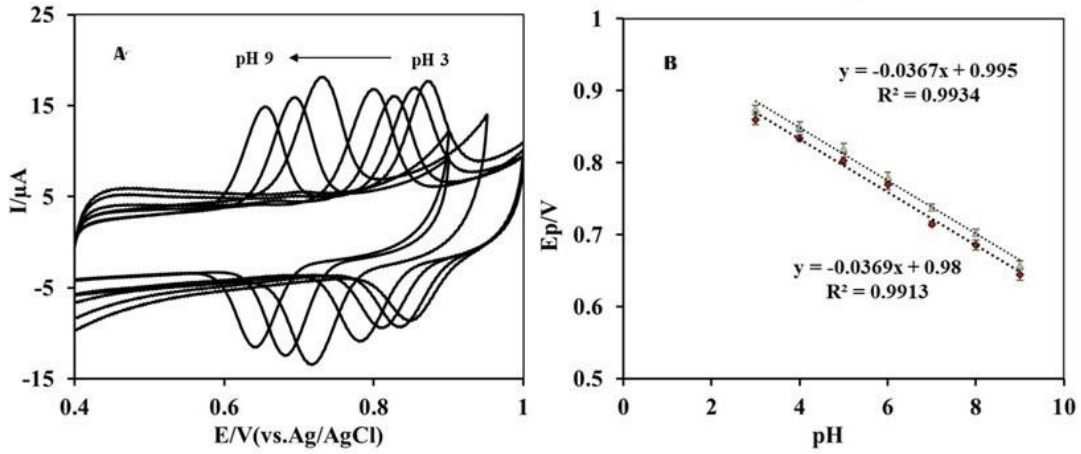

Figure 4.10. (A) CVs of sunset yellow for pH values. (B) A plot of Epa versus pH.

GCE/MWCNTs/AZO was also used for the determination of the number of protons for the electrode reaction of sunset yellow. For this purpose, voltammograms of sunset yellow were recorded at various pH values and these are presented in Figure 4E. Based on the following equation, the slope of Figure 4F was found to be -0.036 V/pH. This shows one-proton and two-electron transfer in the process of dye compound, which is also in agreement with previous studies (Chebotarev et al., 2019, Ebube Uwaya and Bisetty, 2023).

The optimum value of solution pH for the determination of dye was found to be 7 since the sharpest peak was seen in pH 7. Based on the number of electrons and proton calculated at GCE/MWCNTs/AZO, the possible electrode reaction of sunset yellow is presented in Scheme 2 (Ebube Uwaya and Bisetty, 2023).

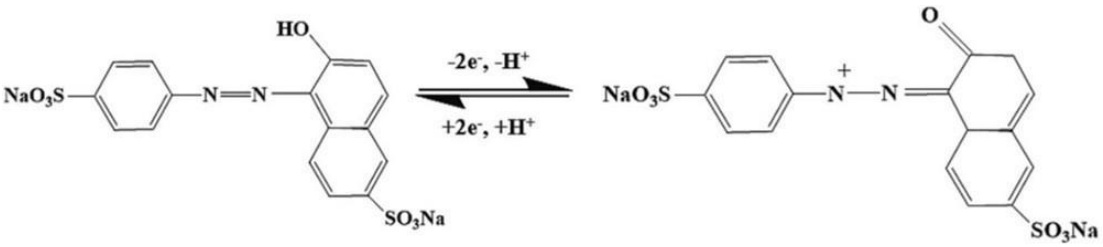

Figure 4.11. The electrode reaction of dye compound on GCE/MWCNTs/AZO

4.1.6. Calibration at GCE/MWCNTs/AZO

Square wave voltammetry (SWV) was used to determine the linear working range and detection limit (LOD) for sunset yellow at GCE/MWCNTs/AZO. Voltammograms for various dye concentrations are given in Figure 4.12A.

Graph of current against concentrations yielded a dynamic linear working range (Figure 4.12B). The linear working ranges are 4.0×10-9–4.0×10-7 M and 4.0×10-7–7.5×10-6 M, respectively.

The calibration study showed regression equations such as Ip(μA)=44.3C(μM)+2.45 (R2=0.9900) and Ip(μA) = 7.5C(μM)+33.76 (R2=0.9990). The value of LOD obtained at GCE/MWCNTs/AZO was 9.5×10-10 M.

The results observed on GCE/MWCNTs/AZO can be compared with previous values (Table 4.1). Data indicate that GCE/MWCNTs/AZO provide lower detection limit and a large working range for the dye compound in comparison with previous studies (Penagos-Llanos et al., 2019, Chebotarev et al., 2019, Dorraji and Jalali, 2017, Qiu et al., 2016, Tang et al., 2016, Li et al., 2019a, Gan et al., 2013, Deng et al., 2016).

This can be attributed not only to the synergistic effect between MWCNTs-AZO surface area and the ability of the nanostructured composite to efficiently promote electron exchange between the electrode surface and sunset yellow, but also to the presence of surface oxygen vacancies of AZO nanoparticles and its excellent conductivity (Ebube Uwaya and Bisetty, 2023, Borchers and Pieler, 2010).

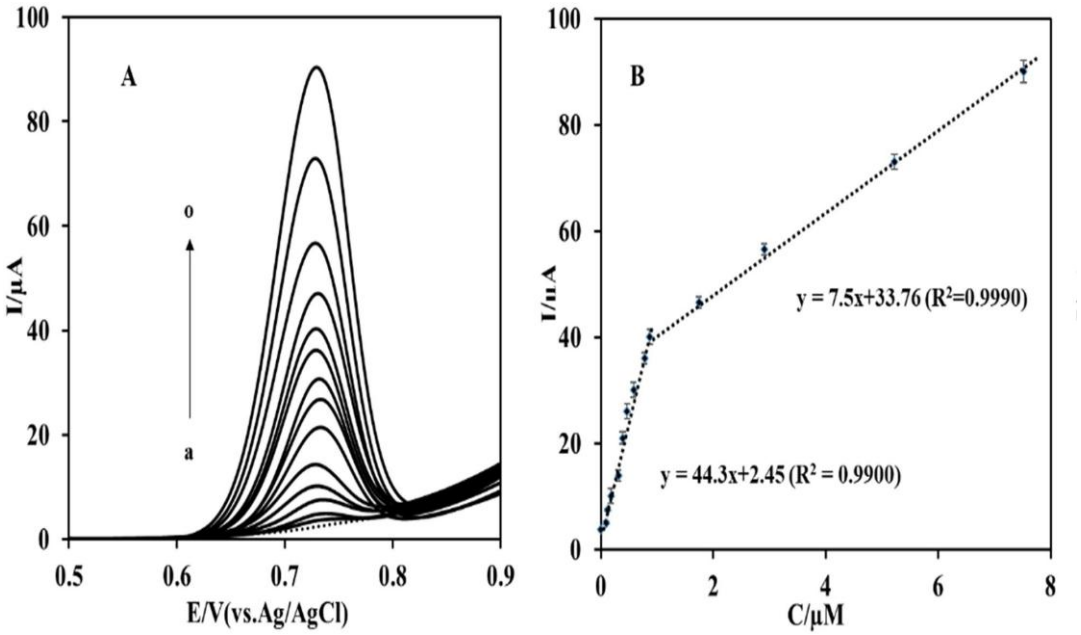

Figure 4.12. (A) SWVs for increasing concentrations of dye compound. (B) Plot of current vs. concentration.

Table 4.1. A comparison table of analytical parameters of various electrodes

Electrode material	Sunset yellow		Reference
	LOD (M)	Linear range (M)	
Cobalt complex	3.0×10^{-7}	1.2×10^{-7}–3.0×10^{-6}	(Penagos-Llanos et al., 2019)
Graphene oxide-MWCNTs	2.5×10^{-8}	9.0×10^{-8}–8.0×10^{-6}	(Qiu et al., 2016)
ZnO-cysteic acid	3.0×10^{-8}	1.0×10^{-7}–3.0×10^{-6}	(Dorraji and Jalali, 2017)
Ag-L-csyteine	7.5×10^{-8}	5.0×10^{-7}–3.0×10^{-4}	(Tang et al., 2016)
CuS	6.0×10^{-9}	1.0×10^{-7}–3.0×10^{-4}	(Li et al., 2019a)
Silica-cetylpyridinium chloride	5.0×10^{-9}	2.0×10^{-8}–2.0×10^{-6}	(Chebotarev et al., 2019)
Au-graphene oxide	2.4×10^{-9}	1.0×10^{-8}–3.0×10^{-6}	(Deng et al., 2016)
Ni-Graphene	2.2×10^{-9}	7.4×10^{-9}–4.4×10^{-7}	(Gan et al., 2013)
GCE/MWCNTs/AZO	9.5×10^{-10}	4.0×10^{-9}–7.5×10^{-6}	This study

4.1.7. Reproducibility, stability and selectivity

The repeatability, reproducibility, stability as well as selectivity are important analytical parameters for any method. Repeatability of GCE/MWCNTs/AZO was studied by recording voltamograms sunset yellow. The RSD% value of 10 repetitive scans of 10 µM sunset yellow was 2.2 %.

Additionally, the mean RSD% value of three electrodes was calculated to be 2.3%. These results indicated excellent repeatability and reproducibility of GCE/MWCNTs/AZO.

The stability of the proposed electrode was also good enough since the reduction in response of 10 µM dye compound was less than 6% in 10 days.

The selectivity of GCE/MWCNTs/AZO towards dye compound in a solution with tartrazine was also investigated. CVs of various concentrations of of dye compound were recorded in a solution of 20 µM tartrazine (Figure 4.13A). SWVs of various dye concentrations in a solution with 20 µM tartrazine at GCE/MWCNTs/AZO in 0.1 M PBS at pH 7.0 are also presented in Figure 4.13B. The response of increasing concentrations of dye was not affected by the presence of tartrazine. Additionally, ascorbic acid, glucose, sodium, potassium, nitrate and chloride have no remarkable influence on the response of sunset yellow (Figure 4.14). These indicated good selectivity of GCE/MWCNTs/AZO.

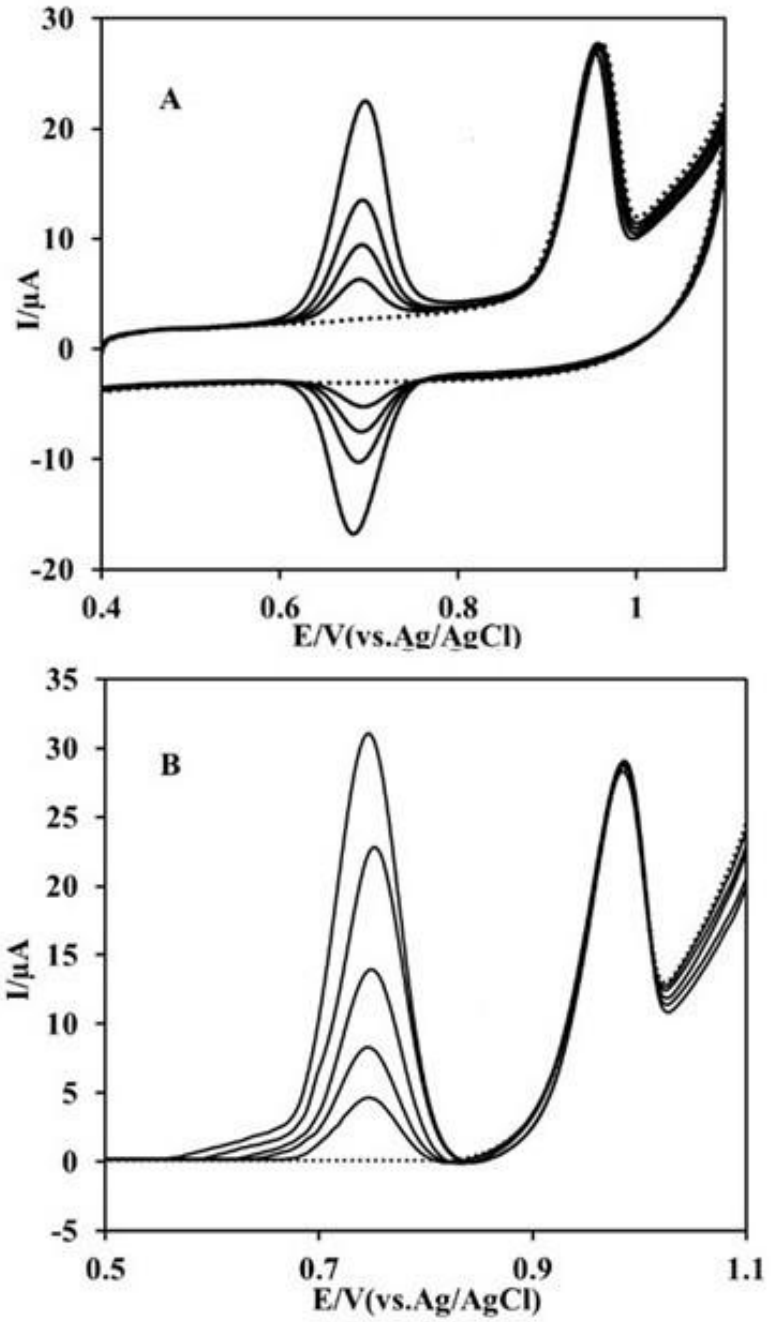

Figure 4.13. (A) CVs of different dye concentrations with tartrazine. (B) SWVs of different dye concentrations with tartrazine.

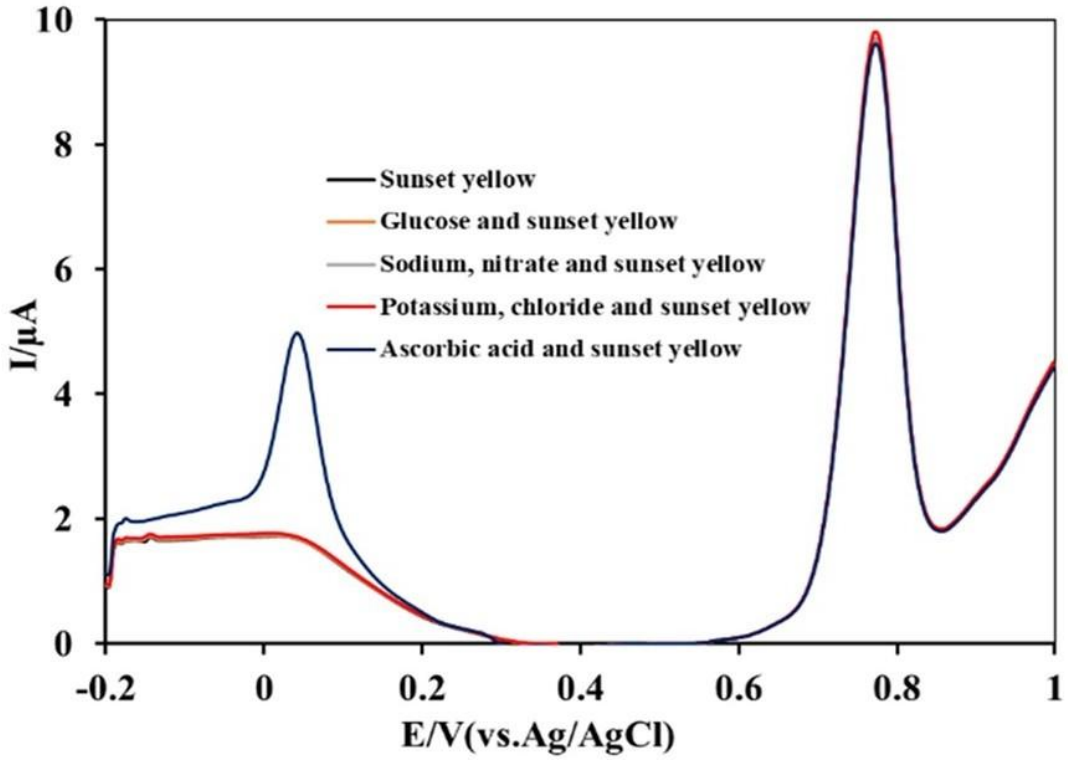

Figure 4.14. SWVs of sunset yellow with various species.

4.1.8. Analysis of samples

The developed method with GCE/MWCNTs/AZO was used for the analysis of a nation-wide consumed powder drink for the determination of dye compound. The results are presented in Table 4.2.

Voltammograms of the powder beverage and various additions of sunset yellow are given in Figure 4.15A. A graph of peak response versus concentration appears in Figure 4.15B. The dye content was calculated as 96.50±1.35 mg/kg. Also, recovery values of 99.0%-100.8% with RSD% values of 1.4%-2.1% obtained by GCE/MWCNTs/AZO were acceptable and reasonable.

For a comparison, the powder drink sample was also analysed by UV-vis spectroscopic method. Figure 4.15C presents the spectra of the powder drink in the absence and presence of sunset yellow. Figure 4.15D presents the plot of absorbance against concentration. Data can be found in Table 4.2. The dye content obtained by UV-vis was 95.5±2.1 mg/kg. The spectroscopic method yielded recoveries between 98.0% and 101.1%.

Statistical analysis of beverage with GCE/MWCNTs/AZO and UV was carried out by t-test. A t-value of 0.69 was found at a confidence level of 95. These

revealed negligible differences between the two methods with a confidence level of 95% (<2.77).

Additionally, the GCE/MWCNTs/AZO system was also applied to determine the sunset yellow content of pediatric syrup. Figure 4.15E presents the voltammograms of dye compound in pediatric syrup. Figure 4.15F shows a plot of current against concentration.

Dye content of the pharmaceutical preparation was 22.54±0.31 µM. As given in Table 4.3, good recoveries obtained by the GCE/MWCNTs/AZO system indicated that the platform can be applied for dye content in complex matrices..

Consequently, the results of the analysis of powder drink indicated that GCE/MWCNTs/AZO can provide excellent results of dye content.

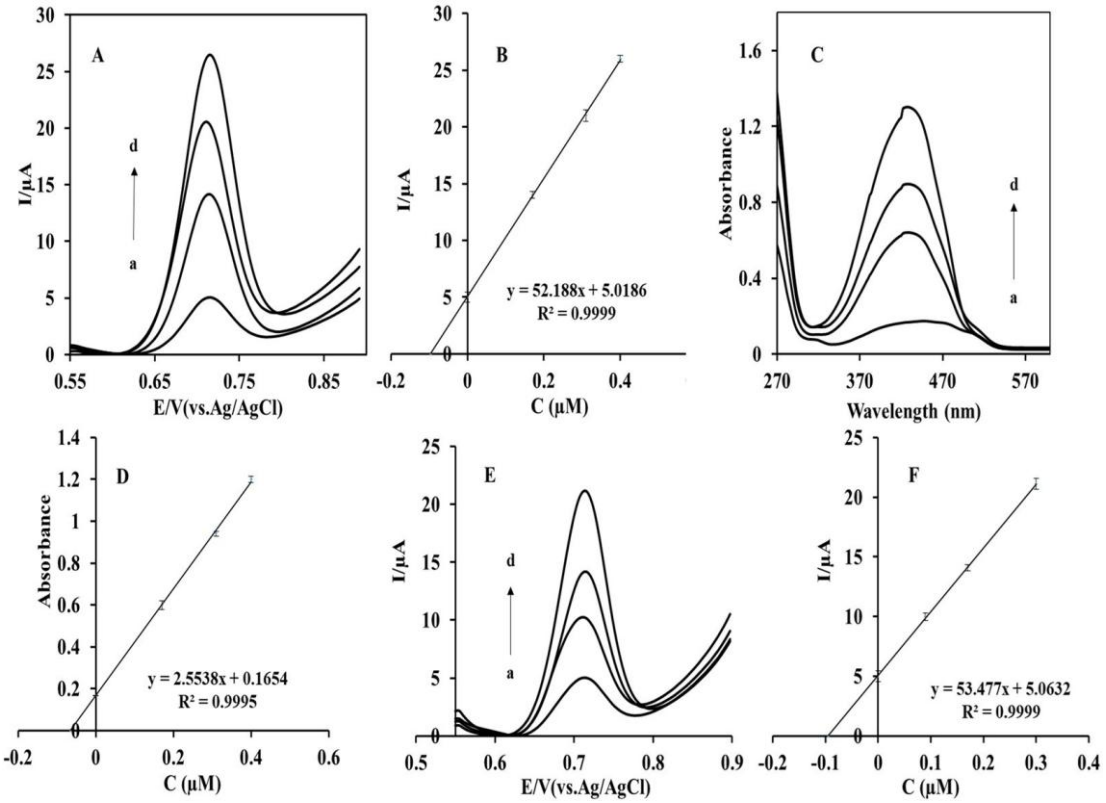

Figure 4.15. Figure 6. (A) SWVs of the analysis of beverage sample and standard additions of dye. (B) Linear graph for the response of currents againts concentrations. C) Spectra of dye sample (and stardard additions. (D) A linear graph of the response vs. dye concentrations. E) SWVs of pediatric syrup and standard additions of sunset yellow. (F) A linear graph of response against dye concentrations obtained from SWV srudy

Table 4.2. Analysis of a nation-wide consumed powder drink

Method	Sunset yellow (mg/kg)	Added (nM)	Expected (nM)	Found (nM)	Recovery	RSD
Square Wave Voltammetry	96.50±1.35	-	-	96.0±1.3	-	1.4
		170.0	266.0	268.0±5.0	100.8	1.9
		310.0	406.0	402.0±8.0	99.0	2.0
		400.0	496.0	500.0±7.0	100.8	1.4
UV-vis Spectroscopy	95.50±2.10	-	-	64.0±1.4	-	2.2
		170.0	234.0	234.9±6.8	100.4	2.9
		310.0	374.0	368.0±9.2	98.4	2.5
		400.0	464.0	469.8±9.8	101.3	2.1

Table 4.3. Electroanalysis of pharmaceutical preparation

Method	Sunset yellow (µM)	Added (nM)	Expected (nM)	Found (nM)	Recovery	RSD
Pediatric syrup	22.54±0.31	-	-	95.0±1.3	-	1.4
		90.0	185.0	187.0±2.0	101.1	1.1
		170.0	265.0	263.0±5.0	99.2	1.9
		300.0	395.0	394.0±8.0	99.8	2.0

4.2. The application of GCE/GN@ITO: Sensitive Determination of Yohimbine in Food Supplements

4.2.1. Characterization of surface material

The surface morphology and composition of the electrode materials were investigated using SEM, EDX, and XRD.

SEM images of GCE modified with GN and the GN@ITO composite are shown in Figure 4.16. The micrograph of GN@ITO reveals a uniform distribution of ITO nanoparticles across the graphene surface, suggesting successful integration of the two components.

Elemental mapping images (Figure 4.17) further confirm the even dispersion of ITO particles on the GN. The corresponding EDX spectrum (Figure 4.18) displays peaks for tin (Sn), indium (In), oxygen (O), carbon (C), and gold (Au). The presence of gold is attributed to the standard gold-coating process used during SEM sample preparation.

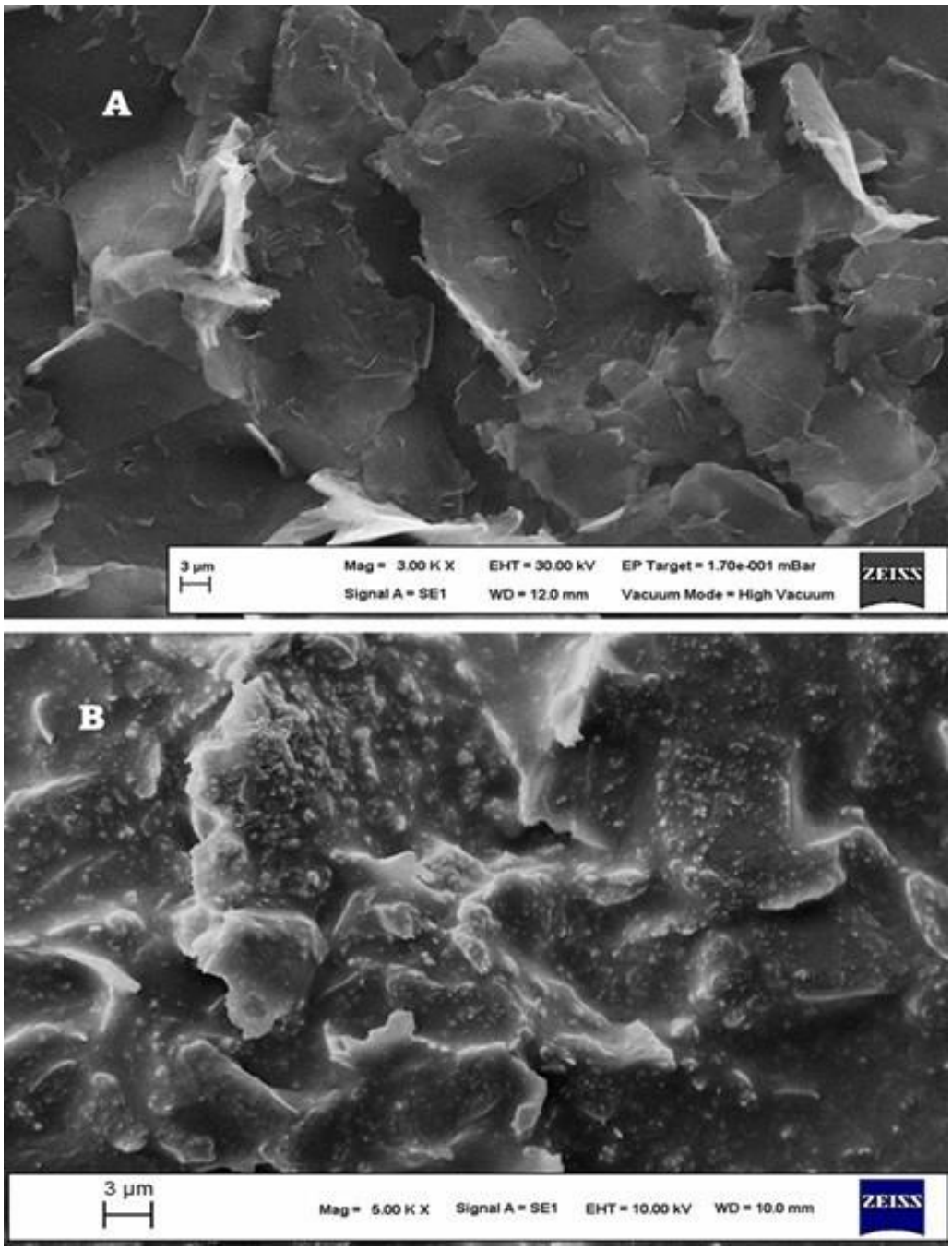

Figure 4.16. SEM images of (A) GN and (B) GN@ITO

XRD patterns of both GN and GN@ITO are illustrated in Figure 4.19. The diffraction peaks observed at 2θ values of 21°, 30°, 35°, 46°, 51°, and 60.5° correspond to crystalline planes of ITO, while the prominent peak at 26° is characteristic of graphitic carbon in graphene nanoplatelets. Together, these results confirm that the synthesized electrode material consists of well-dispersed ITO nanoparticles anchored on a GN matrix.

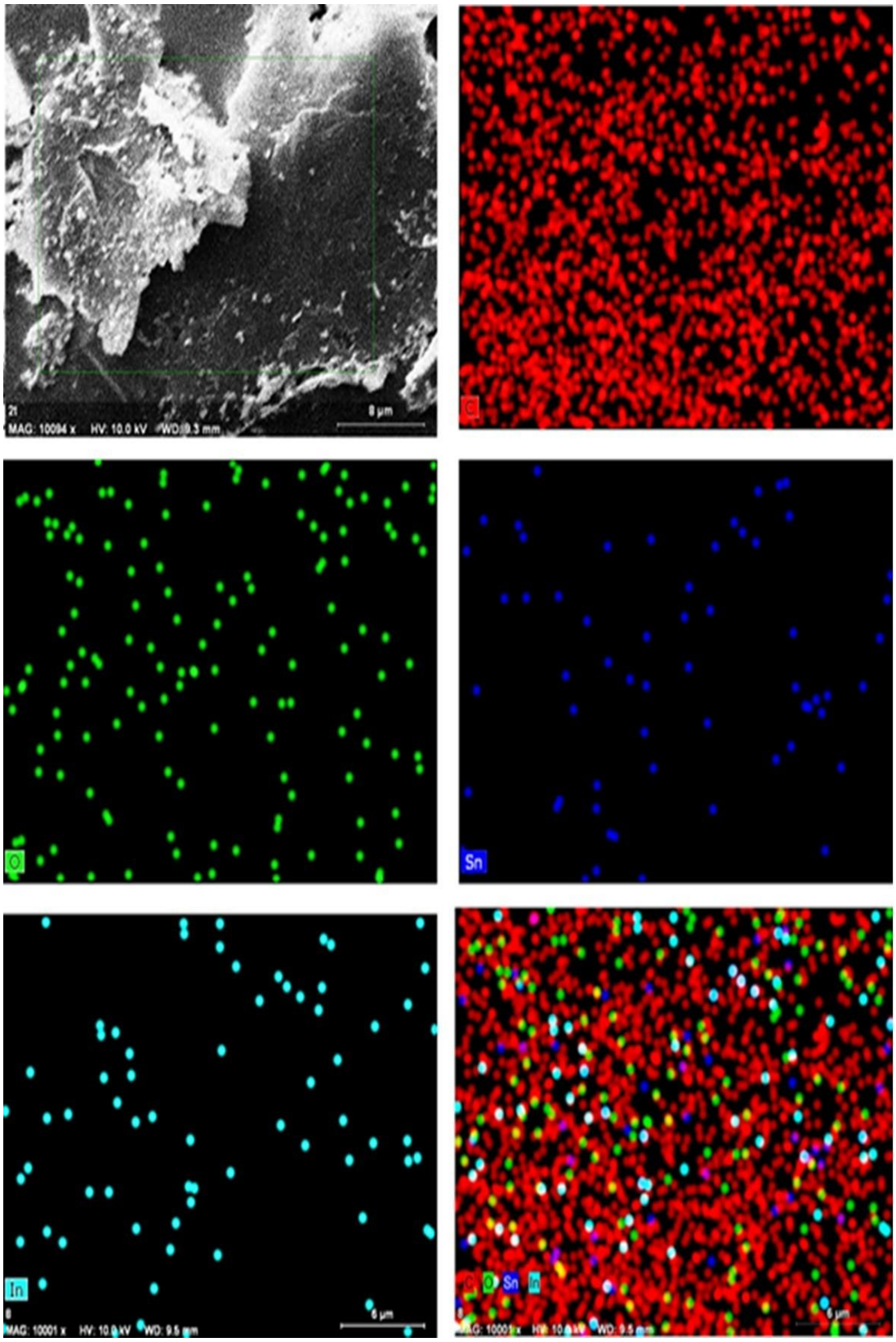

Figure 4.17. EDX spectrum of GN@ITO

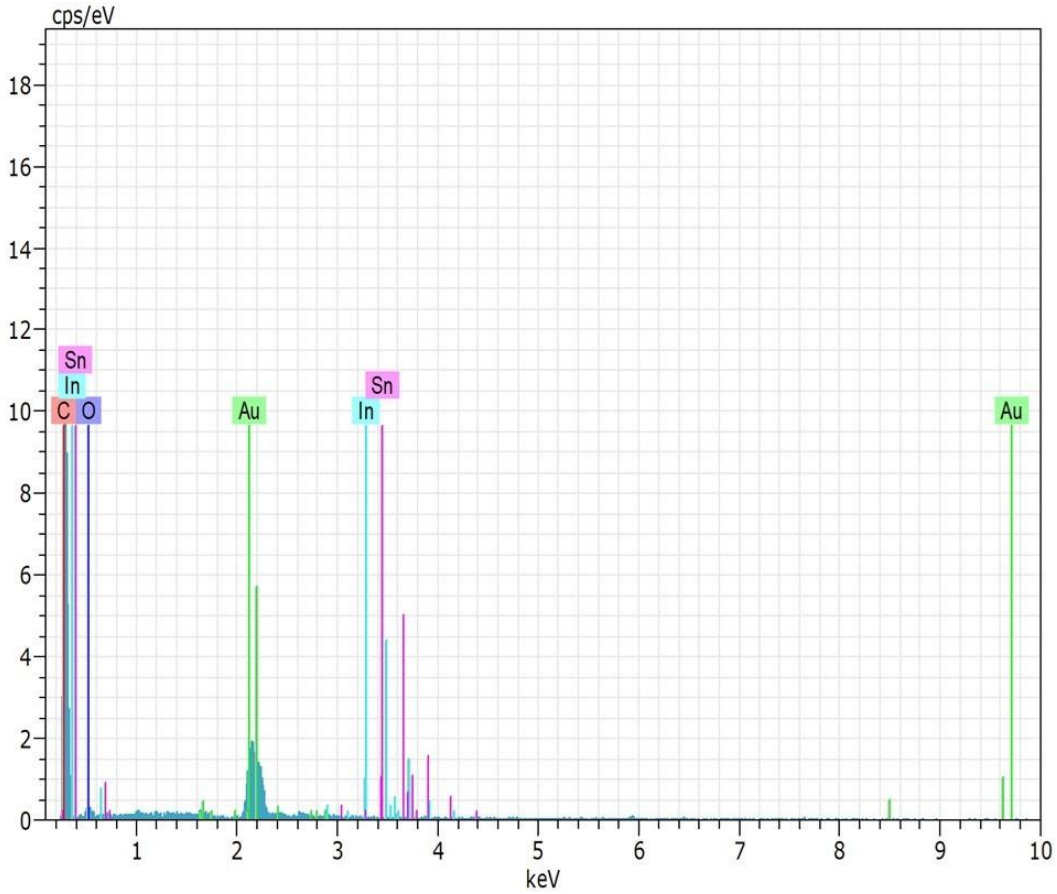

Figure 4.18. EDX spectrum of GN@ITO

4.2.2. Optimization

The effect of suspension volume of GN/ITO was examined by CV. Voltammetric measurements suggested that 5 µL suspension could be appropriate to achieve improvement in behavior of yohimbine (Figure 4.20A-B). Additionally, the suspension of GN/ITO should be sonicated for at least 60 minutes to maintain reproducibility for yohimbine. The effect of the mass ratio of GN to ITO on the sensor's performance was systematically investigated for yohimbine detection. Figure 4.20C presents the voltammograms obtained using GCEs modified with different GN:ITO mass ratios. Among the tested compositions, a GN:ITO ratio of 5:1 yielded the highest peak current response for yohimbine, indicating the most favorable electrocatalytic activity (Figure 4.20D). No further enhancement in the peak response was observed with higher proportions of ITO, confirming 5:1 as the optimal ratio for electrode modification in this study.

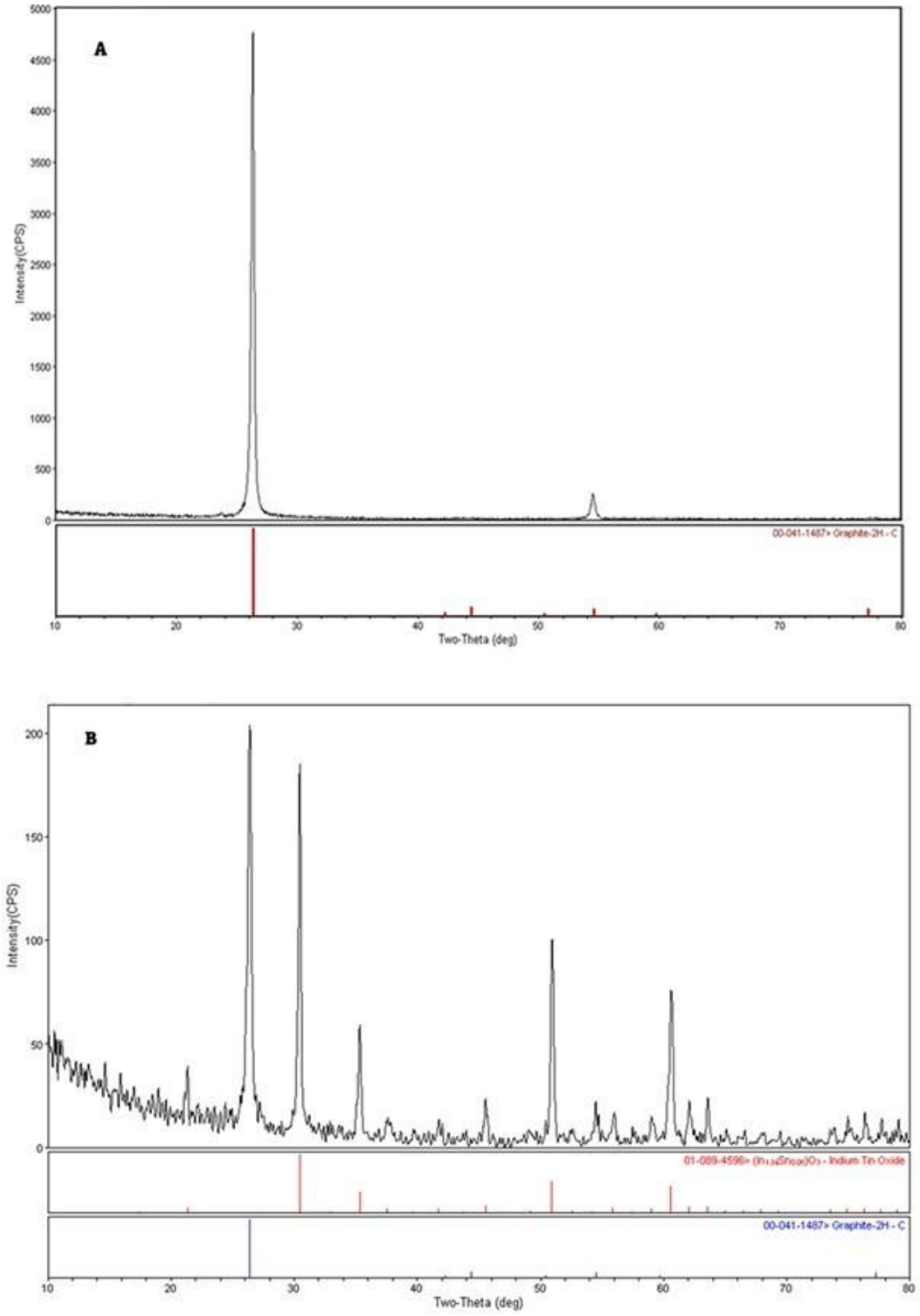

Figure 4.19. XRD spectra of (A) GN and (B) GN@ITO

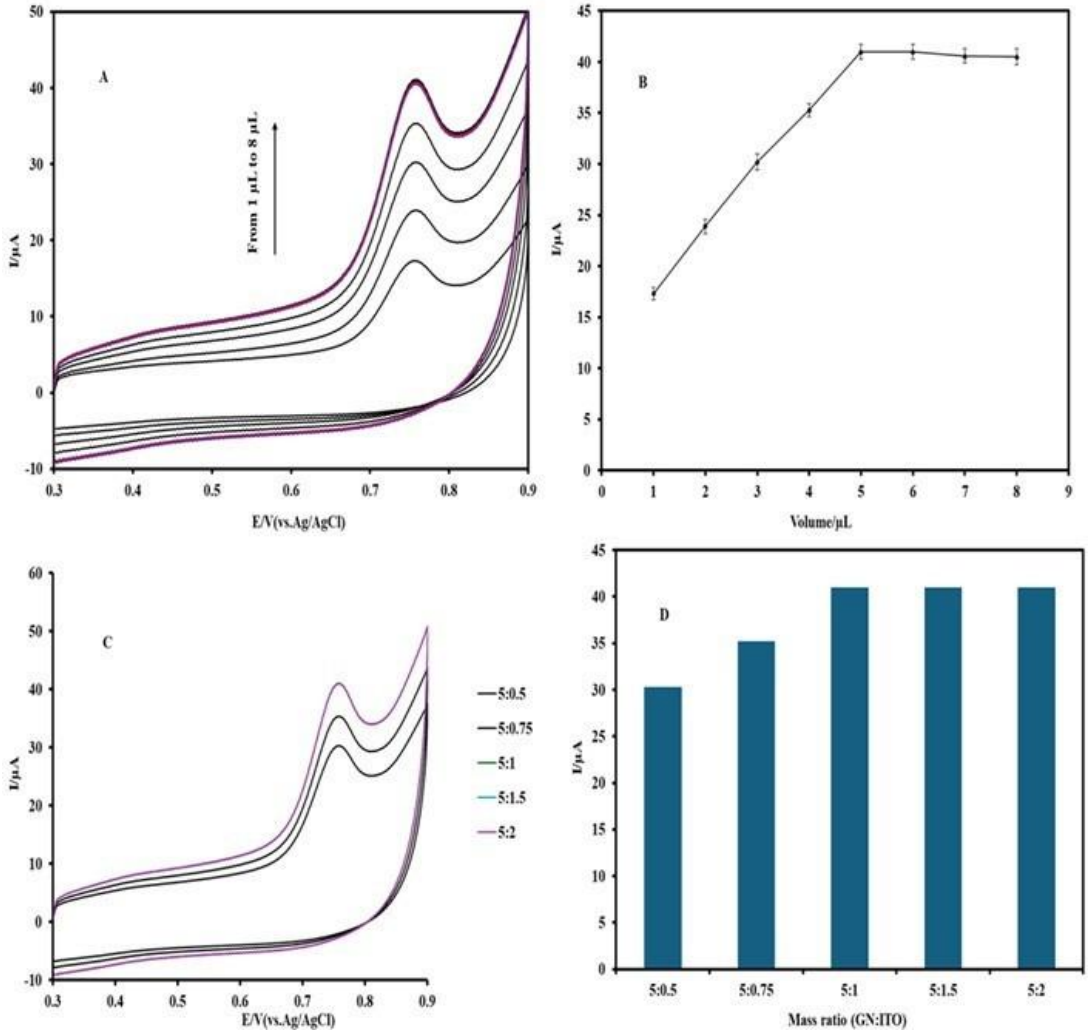

Figure 4.20. A) CVs of 16 µM yohimbine on GCE modified with different volume of GN@ITO suspension. (B) Peak current versus volume. (C) CVs of 16 µM yohimbine recorded on GCE modified with various mass ratios of GN to ITO. (D) Bar chart showing the variation of peak current with different mass ratios of GN to ITO in the modified electrode.

4.2.3. Charge transfer resistance

Rct of electrodes was determined by EIS using a frequency range between 0.01 Hz and 0.1 MHz with an amplitude of 0.025 V. Nyquist diagrams were used to estimate Rct values (Figure 4.21A). The measurements showed that the Rct for (a) GCE, (b) GN/GCE, and (c) GCE/GN@ITO were 693 Ω, 389 Ω, and 249 Ω, respectively. The GCE/GN@ITO system possessed the lowest Rct value, indicating that GN@ITO is a promising material and could be applied in electroanalysis. The significantly reduced charge transfer resistance observed for the GCE/GN@ITO electrode demonstrates the synergistic effect of GN and ITO nanoparticles in facilitating efficient electron transfer. This enhancement in conductivity, combined with the high surface area and electrocatalytic properties of the composite material,

contributes to the improved electrochemical performance of the proposed sensor. These findings confirm that the GN@ITO-modified electrode offers a reliable and effective platform for sensitive and selective analytical applications, particularly for the detection of yohimbine.

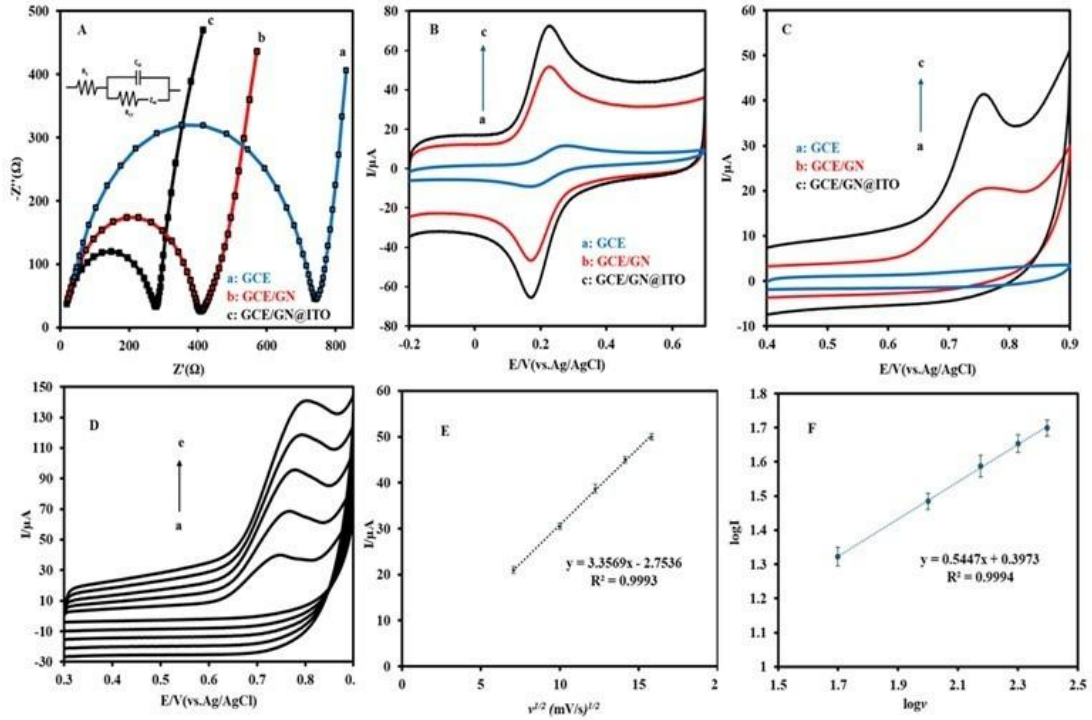

Figure 4.21. (A) Nyquist curves of 1 mM K3[Fe(CN)6] by (a) bare GCE, (b) GN/GCE, and (c) GCE/GN@ITO. (A) CVs of 1 mM K3[Fe(CN)6] in 0.1 M KCl recorded by (a) GCE, (b) GN/GCE, and (c) GCE/GN@ITO with scan rate of 50 mV/s. (B) CVs of 16 µM yohimbine in 0.1 M PBS (pH7) utilizing GCE (a), GN/GCE (b), and GCE/GN@ITO (c). Scan rate: 0.05 V/s. (D) CVs of 16 µM yohimbine on GCE/GN@ITO for scan rates of (a) 50 mV/s, (b) 100 mV7s, (c) 150 mV/s, (d) 200 mV/s and (e) 250 mV/s. (E) Plot of Ip versus v1/2. (F) Plot of logI versus logv.

4.2.4. Measurement of electroactive surface area

Voltammograms of 1 mM K3[Fe(CN)6] with different sweep rates were to calculate the electrochemically active surface area using Randles–Sevcik equation: Ip=2.69×105n32ACD12v12 where Ip refers to peak response, n refers to number of electrons, A is electrochemically active surface area of modified electrode, C is the analytical concentration, D is a coefficient related with diffusion, and v refers to sweep rate. CVs for 1 mM K3[Fe(CN)6] on GCE, GCE/GN, and GCE/GN@ITO. However, comparison voltammograms are presented in Figure 4.21B. The slope of Ip versus v1/2 was used to calculate electrochemically active area of electrodes. The

electro-active area for GCE, GN/GCE, and GCE/GN@ITO was 0.066, 0.2, and 0.5 cm2, respectively. Voltammetry exhibited that GCE/GN@ITO has the largest electrochemically active area in comparison with GCE and GN/GCE. The substantial increase in electroactive surface area observed for the GCE/GN@ITO electrode highlights the advantageous combination of GN and ITO nanoparticles in the electrode modification. The enlarged surface area allows for more active sites and greater accessibility for electron transfer processes, which is critical for enhancing sensor sensitivity. Compared to bare GCE and GN-modified GCE, the GCE/GN@ITO system exhibited superior electrochemical characteristics, reinforcing its potential as an efficient platform for electrochemical sensing. These results, along with the low charge transfer resistance and favorable voltammetric behavior, confirm that the proposed GN@ITO composite is a highly effective material for developing sensitive and reliable electroanalytical sensors.

4.2.5. Electrochemical properties of yohimbine

Electrochemical properties of yohimbine were investigated on GCE, GN/GCE, and GCE/GN@ITO by CV. Figure 4.21C presents voltammograms for 16 µM yohimbine on GCE, GCE/GN, and GCE/GN@ITO. A broad poor response was observed at an oxidation potential of Epa of 0.829 V for yohimbine on GCE. However, GCE modified with GN exhibited an oxidation peak at 0.761 V. Moreover, a well-defined anodic response appeared at 0.754 V on GCE modified with GN@ITO. Obviously, Epa shifted gradually from 0.829 V to 0.861 V and 0.754 V on GCE, GCE/GN, GCE/GN@ITO. Such a gradual shift might be attributed to the high catalytic activity. Also, current response gradually increased from bare GCE to GCE/GN and GCE/GN@ITO. The proposed electrochemical platform (GCE/GN@ITO), integrating GN and ITO with oxygen vacancies, exhibited groundbreaking performance for yohimbine oxidation, characterized by its reduced charge transfer resistance, and exceptional catalytic activity. Ep-Ep/2=48/αn mV The αn was was found as 0.98. This reveals that two-electrons are transferred in the process because the value of α is assumed as 0.5 for an irreversible process. The diffusion coefficient of yohimbine was also determined using GCE/GN@ITO. For a totally irreversible electrode reaction, the Randles-Sevcik equation is: Ip=2.99×105n(an)12ACD12v12 where Ip refers to peak response, n refers to number of electrons, α is electron transfer coefficient, A is electrochemically active surface area of GCE/GN@ITO, C is the analytical concentration, D is a coefficient related with diffusion, and v refers to scan rate. The diffusion coefficient of yohimbine was calculated to be 1.96×10-6 cm2/s. These observations demonstrate

the promising catalytic performance of the GCE/GN@ITO system toward yohimbine oxidation. The enhancement in peak current and the significant shift toward lower oxidation potentials indicate facilitated electron transfer and improved kinetics at the electrode surface. This enhancement can be attributed to the synergistic effects of GN, which has good conductivity, and ITO, which contribute to electrocatalytic activity through oxygen vacancies and favorable electronic properties. Together, these components create a highly active interface that promotes efficient yohimbine oxidation. The improved peak definition, higher current response, and reduced overpotential collectively suggest that the proposed GCE/GN@ITO sensor offers a promising platform for sensitive and reliable detection of yohimbine, outperforming both bare and singly modified electrodes.

Furthermore, the yohimbine oxidation was an irreversible process since no backward response was observed. Additionally, the following equation valid for a diffusion controlled irreversible process was used to calculate the number of electrons (Smarzewska et al., 2014).

4.2.6. The effect of scan rate

The proposed platform (GCE/GN@ITO) was also utilized to perform cyclic voltammetry for various scan rates to acquire its possible mechanism. Figure 4.21D presents voltammograms of 16 µM yohimbine on GCE/GN@ITO at various scan rates. Figure 4.21E presents a plot of Ip vs v1/2. The linear plot indicated that oxidation of yohimbine on GCE/GN@ITO was a diffusion-controlled process. The linear graph of logI -logv yields a slope of 0.54. This value also confirmed a diffusion-controlled mechanism for yohimbine (Figure 4.21F).

4.2.7. The effect of pH

The number of protons in oxidation reaction was determined on GCE/GN@ITO. Voltammograms of 40 nM yohimbine recorded on parameters of step potential:5 mV-Amplitude:20 mV-Frequency:10 Hz for different values of solution pH are given in Figure 4.22A. The value of protons was found by the equation of Ep= E0-59m/n pH. The slope of the plot of Epa versus pH was found to be -56.0 mV/pH (Figure 4.22B). This revealed the ratio of protons and electrons is 1:! in the yohimbine oxidation. In addition, voltammetric studies exhibited that the most improved response was observed in a solution of pH 7. Further measurements were conducted in pH 7.

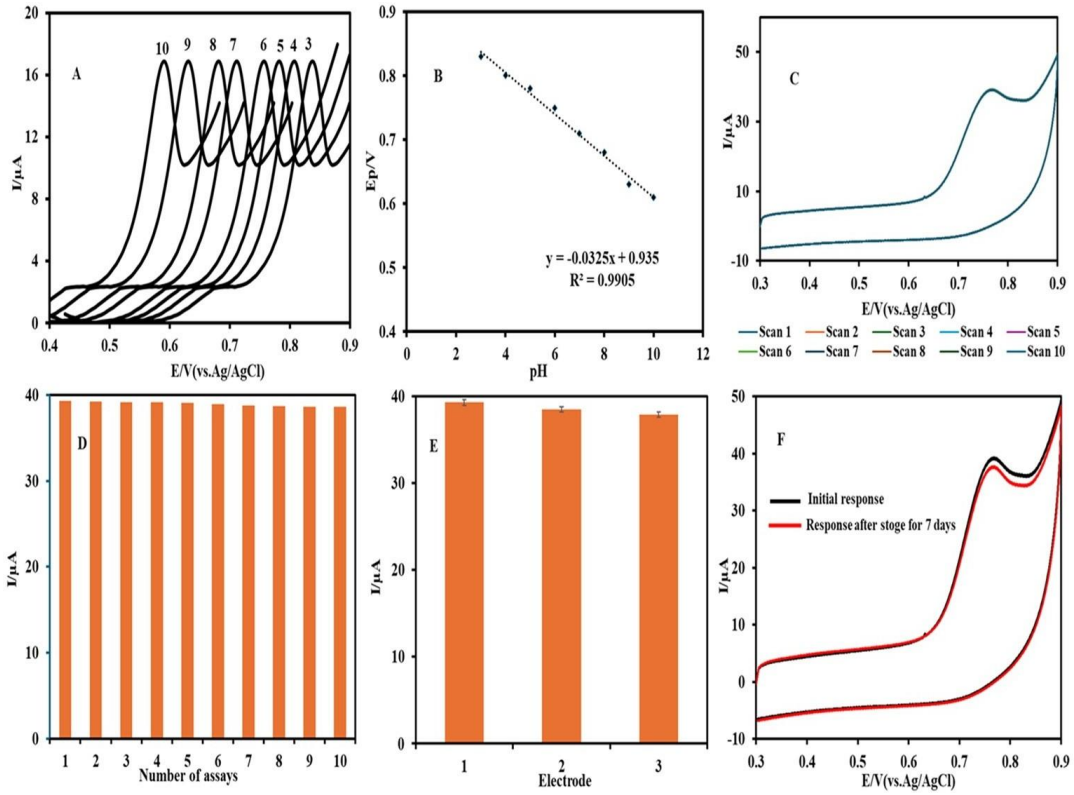

Figure 4.22. A) Voltammograms of 40 nM yohimbine recorded in various pH values (B) Graph of Ep versus pH. (C) Repetitive CVs of 16 µM yohimbine. (D) Bar for peak responses in repeatability voltammograms. (E) Current responses of multiple electrodes. (F) Initially recorded repetitive CVs of 16 µM yohimbine (black) and storage after 7 days (red).

4.2.8. Analytical performance of GCE/GN@ITO

The analytical performance of GCE/GN@ITO was systematically evaluate to,demonstrate its outstanding reliability. The repeatability of the electrode for yohimbine detection was exceptional, as consecutive CVs of 16 µM yohimbine (Figure 4.22C) yielded a value of less than 1.0% as relative standard deviation (RSD) (Figure 4.22D). This low variation is an indication of the remarkable stability. Similarly, the reproducibility of the GCE/GN@ITO platform was confirmed using three independently fabricated electrodes, which exhibited consistent RSD value of less than 2.0%, (Figure 4.22E). These results emphasize the reproducible fabrication process and uniform electrocatalytic activity of the electrode. In addition, the stability of the proposed sensor was excellent as the peak current decrease of yohimbine after 7 days was less than 5% (Figure 4.22F).

Moreover, the selectivity of GCE/GN@ITO was also investigated. SWVs of various concentrations of yohimbine in the presence of 20 µM ascorbic acid, 1 µM

dopamine, and 0.6 µM uric acid are presented in Figure 4.23A. No influence was observed at GCE/GN@ITO. Additionally, voltammograms of the sensor demonstrated excellent selectivity, as the presence of common interfering substances of ascorbic acid, dopamine, uric acid, acetaminophen, glucose, sodium and potassium did not affect the yohimbine voltammetric peak (Figure 4.23B). The peak current recovery of yohimbine on the proposed electrode in the presence of various interfering species is also presented as a bar chart in Figure 4.23C. This resilience against interference is attributed to the synergistic properties of GN and ITO nanoparticles, which enhance the electrode's sensitivity and selectivity through superior catalytic activity and efficient electron transfer. Overall, the GCE/GN@ITO electrode exhibits groundbreaking analytical performance, combining exceptional repeatability, reproducibility, and selectivity. These attributes establish it as a powerful and reliable platform for the precise and interference-free determination of yohimbine in complex matrices.

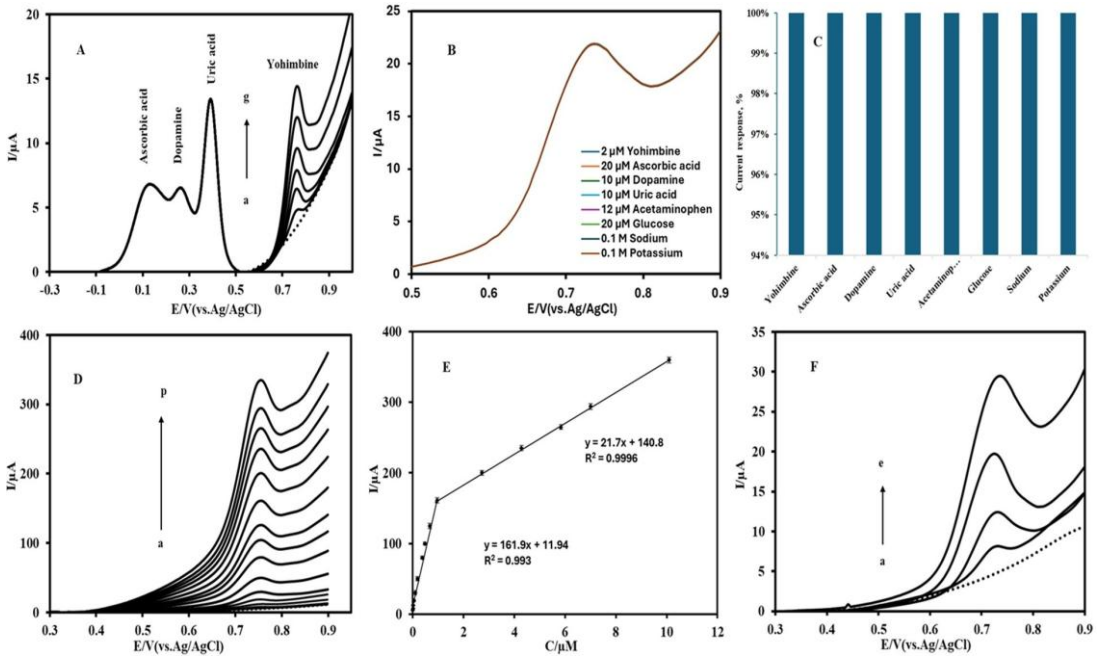

Figure 4.23. (A) SWVs of increasing yohimbine concentrations with ascorbic acid, dopamine and uric acid at GCE/GN@ITO. (D) SWVs for various concentrations of yohimbine on GCE/GN@ITO. (E) Plot of Ip versus concentration. (F) SWVs for (a) blank (PBS solution), (b) yohimbine sample and standard additions of stock solution of yohimbine concentrations of (c) 10 nM, (d) 24 nM, (e) 47 nM.

4.2.9. Linear range and detection limit

The voltammetric platform (GCE/GN@ITO) was used for recording yohimbine voltammograms at different concentrations by SWV (Figure 4.23D).

Figure 4.23E presents a dynamic working range with a concentration range of 4.0×10-9~2.1×10-6 M. The calibration measurements produced regression equations of Ip(μA)=161.9C(μM)+11.94(R2= 0.9981) and Ip(μA)=21.7C(μM)+140.8(R2= 0.9996). The detection limit (LOD) on GCE/GN@ITO was calculated to be 5.0×10-10 M (for 3sb/m). A comparative analysis of the proposed GCE/GN@ITO sensor with previously reported electrochemical methods for yohimbine detection highlights its superior performance across multiple analytical parameters (Table 4.4). Compared to previously reported sensors and methods for yohimbine detection (Chen and Bryden, 2015, Farouk et al., 2011, Švorc and Kalcher, 2014, Švorc et al., 2014, Rodsud and Limbut, 2019, Düzmen et al., 2024, Beyyavaş and Aslanoglu, 2024), the GCE/GN@ITO platform offers a significantly wider linear detection range (4.0×10-9 to 2.1×10-6 M) and a much lower limit of detection (LOD) of 5.0×10-10 M. In addition, the sensitivity of the proposed sensor was calculated as 161.9 μA/μM, which is notably higher than those reported in previous studies.

These enhancements are largely attributed to the interaction of GN with ITO, that contributes to an increased electroactive surface area, enhanced electron transfer, and the available of surface oxygen vacancies on ITO that facilitate efficient electrocatalysis. The sensor also exhibits excellent repeatability and long-term stability, which are often not thoroughly addressed in earlier works. Altogether, these findings confirm that the GCE/GN@ITO sensor outperforms existing methods, making it a reliable and highly sensitive platform for the trace-level detection of yohimbine in real-world applications.

Table 4.4. Analytical parameters of various analysis methods for yohimbine

Method/Electrode	Sensitivity (μA/μM)	LOD (M)	Linear range (M)	Reference
HPLC-MS	-	2.5×10^{-7}	1.3×10^{-5}-2.0×10^{-4}	(Chen and Bryden, 2015)
UV-vis	-	3.1×10^{-7}	5.1×10^{-6}-5.1×10^{-5}	(Farouk et al., 2011)
DPV-BDDE	0.0342	1.3×10^{-7}	2.5×10^{-7}-9.1×10^{-5}	(Švorc et al., 2014)
FIA-BDDE	0.0062	1.5×10^{-7}	3.0×10^{-7}-1.0×10^{-4}	(Švorc and Kalcher, 2014)
ASV-GCE/GRNP	2.35	7.0×10^{-8}	2.0×10^{-7}-3.0×10^{-5}	(Rodsud and Limbut, 2019)
GCE/CNFs-Er_2O_3	1.15	8.0×10^{-9}	2.0×10^{-8}-1.6×10^{-5}	(Düzmen et al., 2024)
GCE/GRNP-Dy_2O_3	46.91	5.7×10^{-9}	8.0×10^{-9}-7.8×10^{-7}	(Beyyavaş and Aslanoglu, 2024)
GCE/GN@ITO	161.9	5.0×10^{-10}	4.0×10^{-9}-2.1×10^{-6}	This study

4.2.10. Possible detection mechanism

The electrochemical detection of yohimbine on the GCE/GN@ITO electrode is primarily facilitated by the unique properties of GN and ITO composite. The high electroactive surface area of GN provides abundant active sites for the oxidation of yohimbine molecules, leading to enhanced sensitivity (Jiménez-Suárez and Prolongo, 2020, Pereira et al., 2020). Graphene's large surface area could lead efficient

interaction with yohimbine, promoting rapid electron transfer, which is crucial for improving the sensor's detection capability (Jiménez-Suárez and Prolongo, 2020, Pereira et al., 2020).

Additionally, the presence of oxygen vacancies on the graphene surface further enhances the sensor's performance. These vacancies act as additional active sites for molecule oxidation, improving the overall electrochemical response. The ITO component contributes to the conductivity of the composite, reducing charge transfer resistance and facilitating quicker electron movement at the electrode surface (Ottoni et al., 2016). As a result, the GCE/GN@ITO electrode exhibits reduced impedance and faster electrochemical reactions, enabling highly sensitive detection of yohimbine even at low concentrations.

Together, these factors allow for rapid, sensitive, and reliable determination of yohimbine, making the GCE/GN@ITO electrode an effective tool for voltammetric detection in complex samples like dietary supplements.

4.2.11. Analytical applications

The contents of three capsules were accurately weighed, and the average mass of a single capsule was dispersed in 10 mL of methanol. The solution was diluted to 25 mL using PBS and subjected to sonication for 10 minutes to ensure homogeneity. A known volume of the prepared solution was then transferred to the electrochemical media. The voltammetric results for the analysis of the supplements are summarized in Table 4.5. Additionally, SWVs illustrating the standard additions of varying yohimbine concentrations are presented in Figure 4.23E. The voltammetric measurements revealed that a yohimbine capsule contains 4.960±0.073, corresponding to a recovery rate of 99.2%. Moreover, standard addition experiments yielded highly satisfactory recovery values ranging from 99.3% to 100.2%, with low relative standard deviations (RSDs) of 1.8%–2.2%. These findings demonstrate the exceptional accuracy and precision achievable using the GCE/GN@ITO electrode for the quantitative analysis of supplements. Such a promising performance of GCE/GN@ITO is attributed to the synergistic behavior of its components. Graphene nanoplatelets (GN) provide high surface area and superior conductivity, facilitating rapid electron transfer for yohimbine oxidations. Meanwhile, ITO contribute their electrocatalytic activity, chemical stability, and high conductivity, further enhancing the electrode's sensitivity and selectivity. Together, these features enable the GCE/GN@ITO system to deliver remarkable sensitivity, precision, and

reproducibility, establishing it as a cutting-edge platform for the voltammetric detection of pharmaceutical compounds. For comparison purposes, results of a traditional UV-visible spectrophotometric technique were used to quantify yohimbine content in capsule formulations (Beyyavaş and Aslanoglu, 2024). The corresponding results, summarized in Table 2, indicate a measured yohimbine concentration of 5.001 ± 0.190 mg, with recovery rates ranging from 98.0% to 103.7%. To statistically evaluate the consistency between the voltammetric and spectrophotometric approaches, a t-test was performed. At the 95% confidence interval, the calculated t value was 0.349, which falls well below the critical threshold of 2.77. This suggests that the differences between the two analytical methods are statistically insignificant. Therefore, the analysis supports that the voltammetric technique utilizing GCE/GN@ITO provides dependable and accurate quantification of yohimbine in dietary supplements.

Table 4.5. Analysis of capsules

Method	Yohimbine (mg)	Added (nM)	Expected (nM)	Found (nM)	Recovery %	RSD
Voltammetry	4.960±0.073	-	-	16.8±0.26	-	1.6
		10.0	26.8	26.6±0.56	99.4	2.1
		24.0	40.8	40.5±0.73	99.3	1.8
		47.0	63.8	63.9±1.4	100.2	2.2
Method	**Yohimbine (mg)**	**Added (μM)**	**Expected (μM)**	**Found (μM)**	**Recovery %**	**RSD %**
Spectroscopy	5.001±0.190	-	-	66.3±2.5	-	3.8
		30.0	96.3	99.3±2.4	103.1	2.4
		60.0	126.3	130.6±4.2	103.7	3.2
		120.0	186.3	182.6±5.3	98.0	2.9

4.3. The Application of ATO-GNP/GCE

4.3.1. Material characterization

The morphology, composition, and structure of the ATO-GNP nanocomposite were examined by SEM, EDX, and XRD. As illustrated in Figure 4.24, SEM image reveals a uniform and well-dispersed decoration of ATO nanoparticles on the surface of the layered GNP matrix. The GNPs provide a large, conductive, and textured substrate, facilitating homogeneous nanoparticle attachment and forming a highly interconnected electroactive interface that promotes efficient electron transfer.

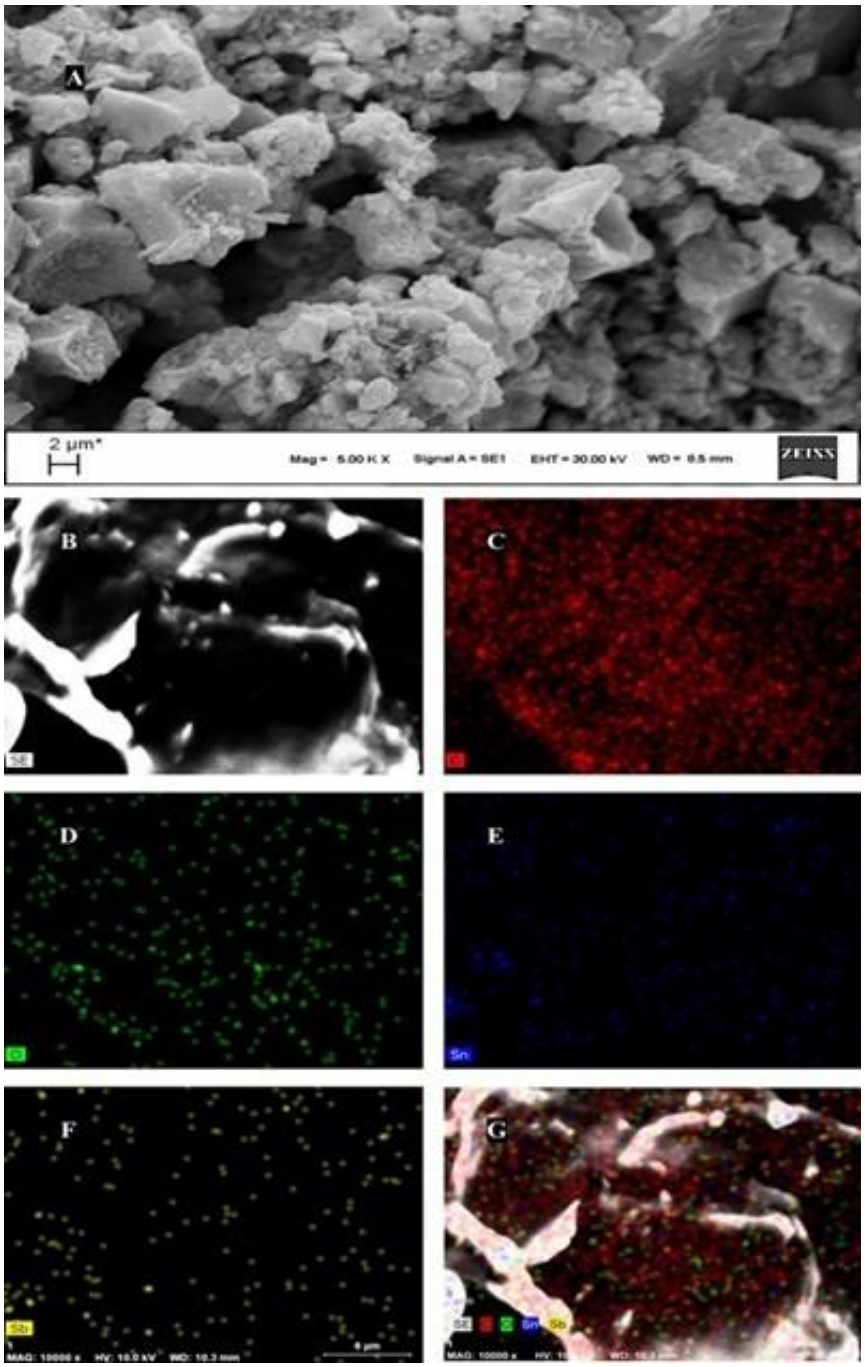

Figure 4.24. SEM and mapping images

Elemental mapping measuremenst also confirmed the distribution of the constituents in the composite material. The back-scattered electron (BSE) image of the nanocomposite is shown in Figure 4.24B. Carbon mapping (Figure 4.24C) shows the interconnected network of GNPs, while the oxygen map (Figure 4.24D) is an indication of surface oxides, consistent with the oxidic nature of ATO nanoparticles. The antimony and tin elemental maps (Figure 4.24E and 4.24F) reveal the distribution of ATO throughout the composite layer. The combined overlay maps (Figure 4.24G) further verify the successful and homogeneous integration of ATO on

GNP layers.

The EDX measurement (Figure 4.25) confirmsed the availability of carbon, antimony, tin and oxygen verifying the presnce of all elements within the composite.

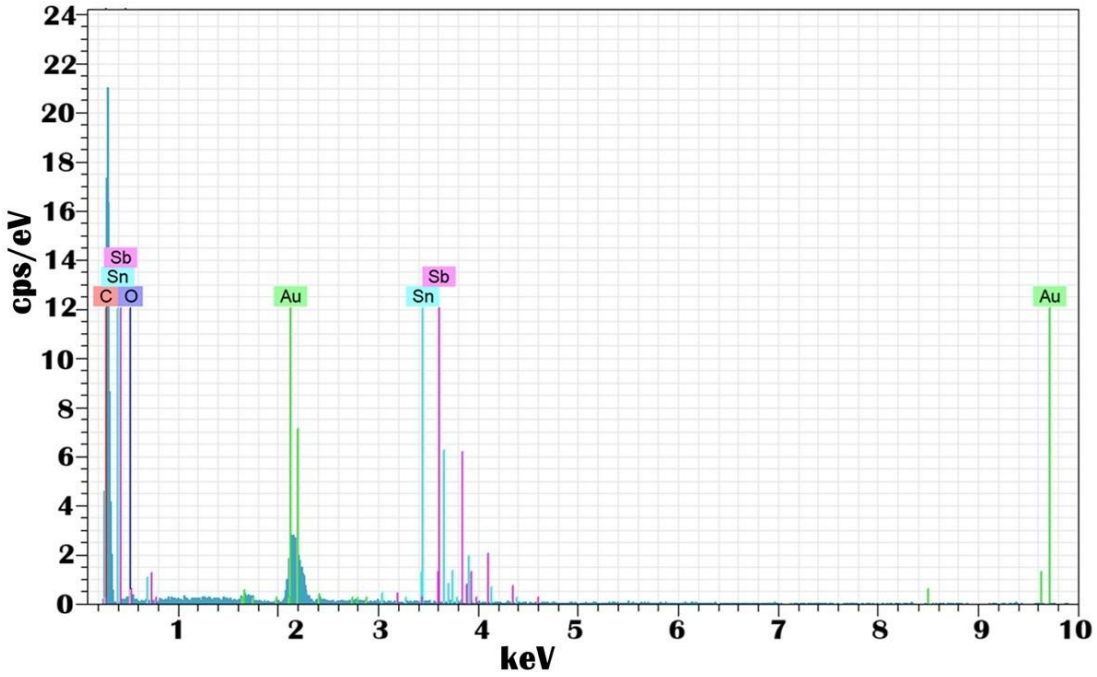

Figure 4.25. EDX spectrum

Additionally, the XRD patterns of GNP, ATO, and the ATO-GNP composite are presented in Figure 4.26. The black curve shows the diffraction pattern of GNP, which exhibited a strong peak at 2θ ≈ 26.5°, corresponding to the (002) plane of graphitic C atoms.

In addition, a weak reflection at 54°, attributed to the (004) plane also confirmed structure of GNP. The XRD pattern of ATO (red curve) displays distinct reflections at 2θ values of 26.4°, 33.5°, 38.0°, 52.0°, 54.5°, and 64.5°, which can be indexed to the (110), (101), (200), (211), (220), and (310) planes of crystalline ATO (J. Montero et al., 2014), consistent with the standard diffraction data of SnO2 (JCPDS No. 00-41-1445) and Sb2O3 (JCPDS No. 00-41-1449).

Moreover, the blue curve reveals the presence of both GNP- and ATO-related diffraction peaks, indicating successful integration of ATO nanoparticles onto the GNP framework. The intense (002) peak of graphitic carbon at 26.5° overlaps with the (110) reflection of ATO at 26.4°, resulting in a merged and slightly broadened

peak due to the close interplanar spacing of both components. This overlap is a common phenomenon in carbon-based nanocomposites containing metal oxides and signifies intimate interfacial contact between the GNP and ATO phases. The other characteristic peaks of ATO remain visible in the composite, confirming that the crystalline integrity of ATO was preserved during synthesis. These results collectively confirm the coexistence of both graphitic and oxide phases and verify the successful formation of the ATO-GNP nanocomposite on the electrode surface.

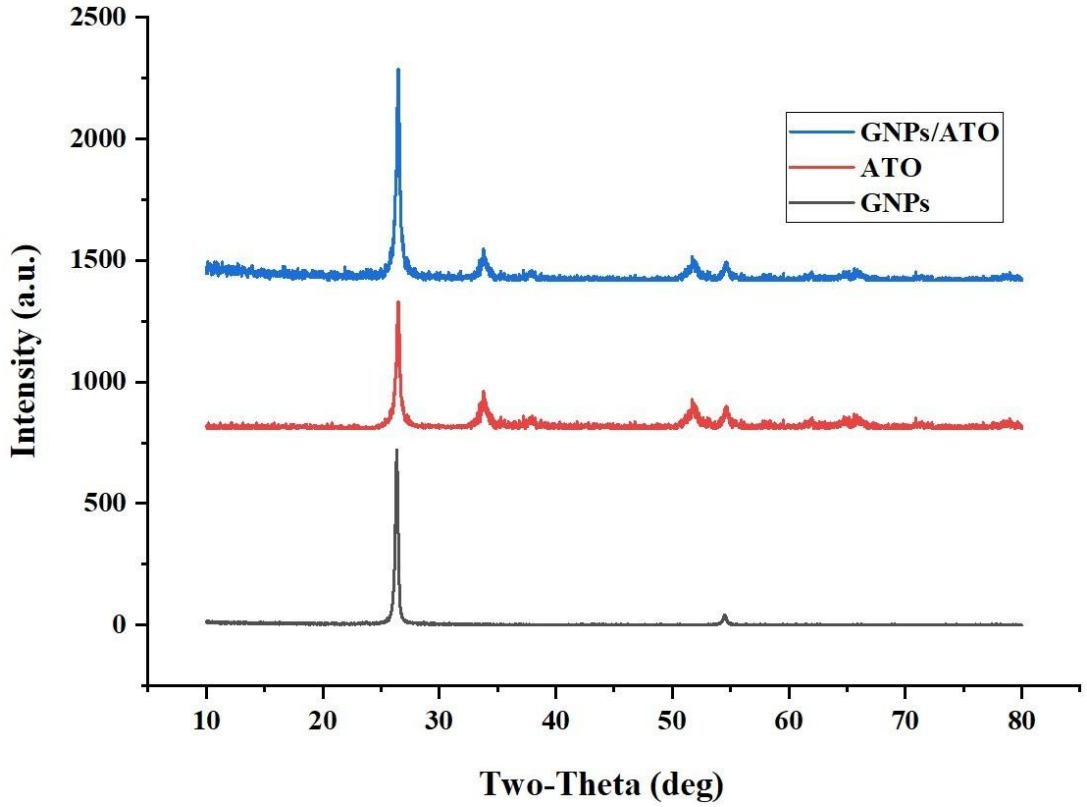

Figure 4.26. XRD spectra of materials

4.3.2. Electrochemical impedance spectroscopy (EIS)

EIS was applied to investigate the Rct values of electrodes. Nyquist plots were obtained in 1.0 mM K3[Fe(CN)6]/K4[Fe(CN)6] with 0.1 M KCl and are presented in Figure 4.27A. The typical semicircular shape observed in the high- frequency region corresponds to the electron transfer resistance at the electrode–electrolyte interface.

GCE exhibited a large semicircle with a high Rct value of 699.0±2.4 Ω, indicating slow electron transfer kinetics owing to its lower electroactive surface area and limited conductivity. Modification of GCE with GNP resulted in a significant

decrease of Rct to 383.6±2.8 Ω, reflecting increased charge mobility and an enlarged surface area afforded by the highly conductive and layered behavior of GNP. The abundant edge-plane defects and excellent conductivity of GNP facilitate electron transport across the interface, thereby enhancing the charge transfer process. Moreover, a GCE modified only ATO nanoparticles yielded an Rct value of 311.0±3.0 Ω, showing a decrease when compared to GNP-modified electrode. Further incorporation of ATO nanoparticles into the GNP matrix led to a pronounced reduction of Rct to 256.7±3.5 Ω, the lowest among the studied electrodes. This remarkable decrease can be attributed to the synergistic interplay between GNP and ATO nanoparticles. While GNP provides a conductive scaffold with high surface area, ATO nanoparticles contribute catalytic activity and additional active sites, effectively accelerating electron transfer kinetics.

To further elucidate the charge characteristics, EIS data on ATO-GNP/GCE were fitted by an circuit model (Figure 3A-inset). The circuit model was found to be Rs + (Rct + (W ‖ C1)) + C2. Rs is solution resistance,, and C1 is double-layer capacitance. Also, W is the Warburg diffusion element while C2 is pseudocapacitance (Manikandan et al., 2024). The fitting parameters of Rs = 18.0 Ω, Rct = 256 Ω, C1 = 50.3 nF, W = 6.395×10^{-3} $s^{1/2}/\Omega$, and C2 = 13.6 µF were obtained. It should be noted that Rct reflects the electron-transfer barrier; the parallel combination W‖C1 corresponds to interfacial charging processessemi-infinite diffusion (Manikandan et al., 2024); and C2 represents the pseudocapacitive contribution due to ion accumulation within the nanostructured composite (Randviir and Banks, 2013). The Nyquist plot of ATO-GNP/GCE displays a semicircle followed by a nearly vertical line, typical of a mixed diffusion-kinetic process, suggesting improved conductivity.

It is noteworthy that although ATO intrinsically exhibits high electrical conductivity and catalytic activity, excessive ATO loading can cause nanoparticle agglomeration and excessive surface coverage, partially blocking the active sites of the GNP framework. At the optimized composition, however, the strong synergistic coupling between the highly conductive GNP network and catalytically active ATO nanoparticles promotes rapid interfacial charge transfer and electron mobility, resulting in a markedly reduced Rct and superior electrochemical performance of the ATO-GNP/GCE sensor.

The progressive decrease in Rct values across the electrode series—bare GCE > GNP/GCE > ATO/GCE >ATO-GNP/GCE —demonstrates the stepwise

improvement in interfacial charge transfer properties. The ATO-GNP modified electrode therefore exhibits superior electrical characteristics, making it highly suitable for sensitive and reliable electrochemical sensing of HVA.

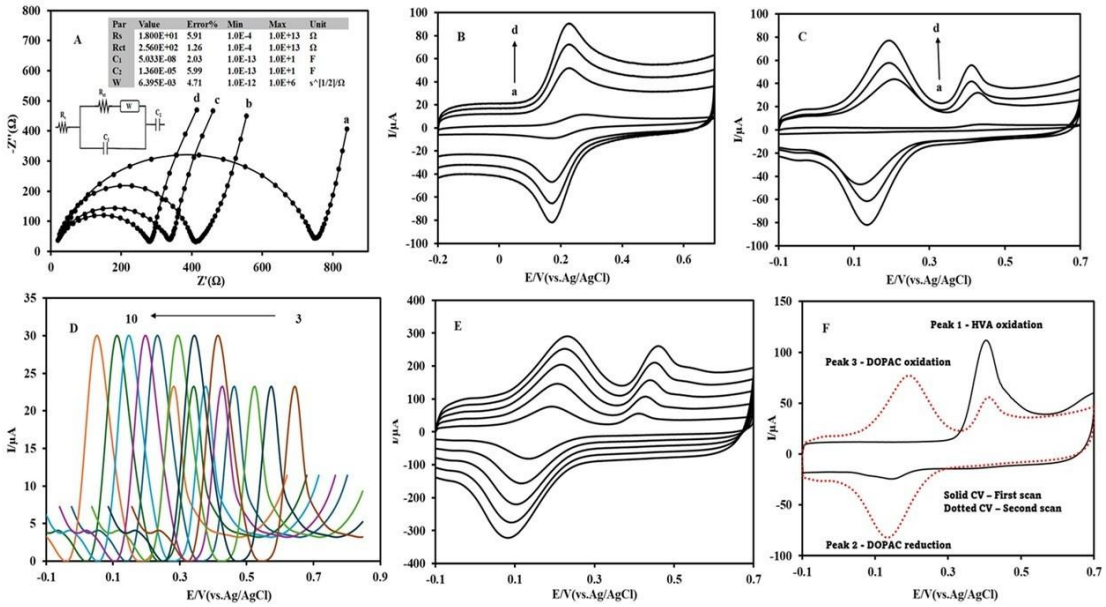

Figure 4.27. (A) EIS of 1 mM K3[Fe(CN)6]/K4[Fe(CN)6] with 0.1 M KCl for (a) bare GCE, (b) GNP/GCE, (c) ATO/GCE and (d) ATO-GNP/GCE. (B) CVs of 1 mM K3[Fe(CN)6] on the same electrodes. (C) Voltammograms of 5 µM HVA oxidation on (a) bare GCE, (b) GNP/GCE, (c) ATO/GCE and (d) ATO-GNP/GCE. (D) SWVs of HVA recorded at various pH values. (E) CVs of 5 µM HVA at various scan rates using ATO-GNP/GCE. (F) Consecutive CVs of 5 µM HVA on ATO-GNP/GCE (Solid: first and dotted: second voltammogram). Scan rate 50 mV/s.

4.3.3. Electroactive surface area

The active surface area on electrodes was studied by CV using a 1.0 mM K3[Fe(CN)6] with supporting electrolyte of 0.1 M KCl. The studies were performed at varying sweep rates, and tthe Randles–Sevcik equation was used to calculate the surface area..

Figure 4.27B presents the CV curves along with the corresponding linear plots utilized to determine the surface areas. The active area was 0.066 cm2 for bare GCE, 0.20 cm2 for GNP/GCE, 0.29 cm2 for ATO/GCE and 0.53 cm2 for the ATO-GNP/GCE sensor. This progressive increase underscores the advantageous contributions of each component in the modified electrodes.

The enhancement observed for GNP/GCE is due to the high surface area and excellent electrical conductivity of GNP. GNP's multilayered structure

can facilitate rapid electron transfer.

The further increase upon incorporating ATO nanoparticles arises from their uniform distribution on GNP, which provides catalytic sites. Additionally, the catalytic behavior of ATO enable sustained performance for rapid electron transfer.

The synergistic interaction of GNP with ATO nanoparticles results in enhanced accessibility towards analyte, and a significantly enlarged electrochemically active surface area. This characteristic is essential for achieving improved sensitivity and amplified signal response in electrochemical sensing studies.

4.3.4. Voltammetric behavior of HVA

The electrochemical oxidation of HVA was investigated by CV in 0.1 M PB, pH 7, comparing electrodes of GCE, GNP/GCE, ATO/GCE and ATO-GNP/GCE. As shown in Figure 4.27C, GCE showed a broad and a weak oxidation peak at 0.442 V, indicating poor voltammetric activity toward HVA. After modification with GNP, a broad oxidation peak appeared near 0.427 V, reflecting improved electron transfer and increased active surface area due to the conductive GNP layer. However, the GNP/GCE also produced another oxidation peak at 0.215 and corresponding reduction peak at 0.115 V, with the ΔEp value of 50 mV.

Remarkably, the ATO-GNP/GCE platform produced a sharper and more intense oxidation peak at approximately 0.412 V with significantly higher current response, indicating enhanced electrocatalytic activity and favorable kinetics toward HVA oxidation. Another redox couple was also observed at the proposed electrode (ATO-GNP/GCE), oxidation occurred at 0.193 and reduction occurred at 0.140 V, with an ΔEp of 53 mV. This shows that the irreversible oxidation peak shifted to more negative potentials at ATO-GNP/GCE when compared to GCE and GNP/GCE.

Additionally, the value of ΔEp for the redox couple was also reduced at the proposed electrode. The enhanced electrochemical response of the ATO-GNP/GCE platform toward HVA originates from the synergistic functions of both components. ATO nanoparticles, as highly conductive n-type semiconductors, provide abundant electrocatalytic sites, facilitate rapid charge transfer, and contribute redox-active surface oxygen species that promote the oxidation of phenolic groups in HVA.

GNPs, on the other hand, supply a large electroactive surface area, high intrinsic conductivity, and strong π–π interactions with the aromatic ring of HVA, thereby enhancing its surface adsorption and electron exchange efficiency. The intimate interfacial contact between ATO nanoparticles and GNP layers establishes a three-dimensional conductive network that accelerates electron tunneling and collectively accounts for the observed amplification of the anodic peak current.

The effect of solution pH on Epa of HVA and DOPAC was studied using SWV. The oxidation peak potential shifted negatively with increasing pH (Figure 4.27D), consistent with proton involvement in the redox reaction. Graph of Epa vs. pH showed slopes of –0.050 and –0.0502 for HVA and DOPAC respectively, indicating 1:1 ratio for the number of protons and electrons participate in the oxidation of both HVA and DOPAC electrode reaction. Based on these results, both processes involve the transfer of two-protons along with two-electrons.

To determine the nature of electrode reaction at ATO-GNP/GCE, CVs of HVA were obtained at different sweep rates (Figure 4.27E). The peak current was proportional to the sweep rate (v), and a log-log plot of peak response versus sweep rate yielded a slope close to 1.0, indicating that HVA undergoes a primarily adsorption-controlled process.

Further kinetic analysis using following Laviron's equation for irreversible reactions provided insights into the number of electrons transferred. $Ep=E°+RT(/\alpha nF)lnRTk°\alpha nF+(RT/\alpha nF)lnv$.. A linear relationship between peak potential (Epa) and lnv allowed calculation of number of electrons (n). A plot of Epa versus lnv yielded a slope of 0.0288 for the irreversible process of HVA (peak 1) (Mulla et al., 2009). The results suggested that two electrons are transferred in HVA oxidation as the value of α can be assumed as 0.5 for a totally irreversible process (Chan et al., 2017).

Furthermore, the number of electrons available in the quasi-reversible transformation of DOPAC (corresponding to peak 2 and peak 3) was determined using the following relationships: $Epa=E°+RT(1-\alpha)nFlnv$ and $Epc=E°-RT\alpha nFlnv$. According to these equations, the slopes of plots (both anodic and cathodic peak potential) versus the natural logarithm of the scan rate are given by $RT/(1–\alpha)$ nF and $RT/\alpha nF$, respectively. The experimental data yielded the linear equations: Epa (V) = 0.0281lnv (V/s) + 0.2793 (R^2 = 0.9983) and Epc (V) = -0.0291lnv (V/s) + 0.0474 (R^2 = 0.9932). Based on these slopes, the product αn was calculated to be 0.88. From

this, the electron transfer coefficient (α) was determined as 0.44, leading to a calculated number of electrons (n) of 1.8, which approximates to 2. This result indicates that the quasi-reversible redox process involving peaks 2 and 3 proceeds via a two-electron transfer process.

The electrode reaction mechanism of HVA was thoroughly examined using the ATO-GNP/GCE sensor. Figure 4.27F illustrates the cyclic voltammograms obtained from successive scans of 5.0×10-6 M HVA in 0.1 M PBS at pH 7. As depicted in Scheme 3.3, the proposed electrochemical pathway aligns with the mechanism described by Mulla et al. (Mulla et al., 2009). In this process, the oxidation of HVA proceeds via demethylation to yield 4-aceto-o-quinone, which corresponds to the anodic peak (peak 1) observed at 0.412 V, as indicated by the solid voltammogram. During the reverse scan, a cathodic peak (peak 2) appears at
0.193 V, which is attributed to the reduction of the intermediate to DOPAC. In subsequent cycles, DOPAC undergoes re-oxidation to regenerate 4-aceto-o-quinone, resulting in the second anodic signal (peak 3) at 0.140 V, with continuous HVA oxidation contributing further to this conversion (Mulla et al., 2009, Buleandra et al., 2025).

4.3.5. Optimization of sensor parameters

To maximize electrochemical efficiency for the precise detection of HVA, critical factors—including the amount of composite suspension, the accumulation duration, and the GNP-to-ATO nanoparticle mass ratio—were carefully fine-tuned through CV.

The effect of the suspension volume applied to GCE on platform response was investigated by modification of electrode with varying volumes of the dispersion of GNP-ATO. CVs of 5.0 µM HVA were obtained with identical conditions (Figure 4.28A). As illustrated in graph of peak current against volume (Figure 4.28B-C), the highest current was obtained at a volume of 5 µL. Volumes exceeding this threshold resulted in a plateau or slight decline in current, likely due to saturation of the electrode surface and hindered mass transport. Thus, 5 µL as the optimal volume for the modification of the electrode was selected for further experiments.

Given that the oxidation of HVA on the GNP-ATO electrode is adsorption-controlled, the effect of accumulation time on peak current was evaluated using time periods of 30 - 300 seconds. During the accumulation step, the electrode was

immersed in HVA solution, and CV measurements were performed at a scan rate of 50 mV/s (Figure 4.28D). The current increased with time and reached the highest peak current at 150 seconds (Figure 4.28E-F). Longer accumulation periods did not enhance the response and, in some cases, caused a slight decrease, presumably due to surface saturation or desorption effects. Thus, 150 seconds were selected as the accumulation time for further experiments. Once the accumulation step is completed, the surface was rinsed with PBS prior to analysis.

To identify the best composition of mass ratios of GNPs to ATO nanoparticles (5:0.5, 5:0.75, 5:1, 5:1.5, and 5:2) were examined. Cyclic voltammograms of HVA were studied by electrodes modified with different GNP:ATO ratios (Figure 4.28G). The corresponding plot of peak current versus mass ratio (Figure 4.28H-I) demonstrated that a 5:1 mass ratio yielded the highest and most well-defined oxidation peak. Increasing the ATO content beyond this ratio resulted in diminished current responses, likely due to nanoparticle agglomeration or excessive surface coverage causing active site blockage.

Although ATO possesses high intrinsic electrical conductivity and catalytic activity, the overall electrochemical response of the composite is governed by the balance between nanoparticle loading and surface accessibility. At the optimized GNP:ATO ratio of 5:1, ATO nanoparticles are well-dispersed on the conductive GNP matrix, ensuring efficient charge transfer and abundant active sites. However, increasing the ATO content beyond this ratio results in partial nanoparticle agglomeration and excessive surface coverage, which reduce the effective electroactive area and impede electron transport through the GNP network.

Consequently, the current response decreases despite ATO's high conductivity, emphasizing the importance of maintaining an optimal dispersion and interfacial contact between the two components. Consequently, the 5:1 mass ratio was selected to obtain the highest peak response for HVA study.

Such a systematic optimization resulted in high sensitivity, reproducible signals, and good sensor performance to improve the analytical capability of the proposed voltammetric platform for HVA detection.

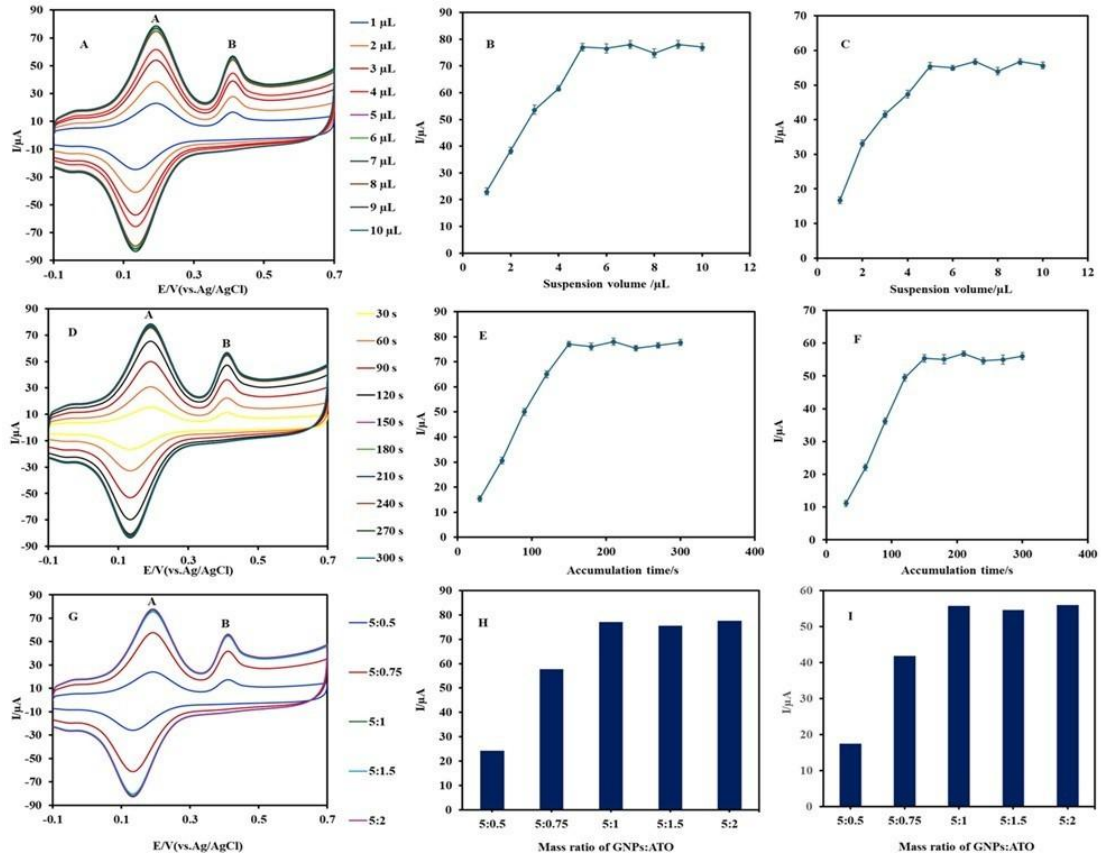

Figure 4.28. A) CVs of 5 µM HVA recorded with varying suspension volumes on ATO-GNP/GCE at an accumulation time of 150 s and scan rate of 50 mV/s. (B) Plot of peak current versus suspension volume for peak A. (C) Plot of peak current versus suspension volume for peak B. (D) CVs of 5 µM HVA for different accumulation times under the same conditions. (E) Graph of peak current versus accumulation time for peak A. (E) Graph of peak current versus accumulation time for peak B. (G) CVs comparing different mass ratios of GNP:ATO for 5 µM HVA detection. (H) Bar chart of peak currents at different GNP:ATO ratios for peak A. (I) Bar chart of peak currents at different GNP:ATO ratios for peak B.

4.3.6. Assessment of analytical performance

The quantitave performance of ATO-GNP/GCE for HVA determination was thoroughly investigated in terms of stability, selectivity, reproducibility and repeatability..

Repeatability was checled with conducting ten successive scans of 4.0 µM HVA using ATO-GNP/GCE. RSD was found to be 1.1%, indicating signal stability as short-term precision.

Reproducibility was tested using three ATO/GNPs-modified electrodes. The RSD of 3.4% confirmed consistent electrode fabrication and reliable sensor

performance across different electrodes. According to a recent report (Stefani et al., 2017), the concentration of HVA in biological fluids of mild stage Parkinson's disease patients is approximately 11.91 nM. Therefore, the repeatability and reproducibility of the proposed electrode was also performed in a solution containing 10 nM HVA. SWVs of 10 nM HVA are presented in Figure 4.29A. To emphasize the subtle differences among individual scans, the current axis was zoomed in, revealing that the curves are not identical but closely aligned (Figure 4.29B). The RSD of the anodic peak current was 1.2 % for ten scans, further confirming the outstanding repeatability of the electrode. The raw voltammograms for the three electrodes are provided in Figure S5A-C. The resulting RSD of 3.5% confirms consistent electrode fabrication and reliable sensor performance across different electrodes.

Selectivity of ATO-GNP/GCE examined by recording responses of 1.6 μM HVA in the presence of potential interfering species commonly found in biological and environmental samples. These included 4 μM glucose, 3 μM ascorbic acid, 3 μM clenbuterol, 5 μM terbutaline, 5 μM tramadol, 5 μM tryptophan, 5 μM tartrazine, 7 μM quinoline yellow and 8 μM allura red. The sensor showed negligible interference from these species, confirming its high selectivity and anti-interference capability for HVA detection.

Selectivity of ATO-GNP/GCE was also performed to examine its response to HVA in the presence of potential interfering molecules, which are found in biological fluids of mild stage Parkinson's disease patients. For this purpose, SWVs of 10 nM HVA in the presence of 0.5 nM dopamine, 0.2 nM DOPAC, 0.5 nM levodopa (Figure 4.29C). The current axis was zoomed in to emphasize the subtle differences among individual scans (Figure 4.29D). This clearly shows that dopamine, DOPAC and levodopa have no influence of the reliable detection of HVA on the proposed electrode.

Stability was evaluated upon the storage of ATO-GNP and measuring its response to 4.0 μM HVA over a period of 15 days. The electrode retained over 95.5% of its initial peak current, demonstrating good electrochemical stability.

The stability was also evaluated upon the storage of ATO-GNP/GCE measuring its response to 10 nM HVA in artificial blood sample over a period of 15 days (Figure 4.29E). The electrode retained about 95.0% of its initial signal even in blood sample, demonstrating excellent long-term stability.

The superior performance of ATO-GNP/GCE arises from the synergistic combination of ATO nanoparticles and graphene nanoplatelets. ATO contributes excellent chemical stability and catalytic activity, while GNPs provide outstanding conductivity, a high surface area, and mechanical strength. This combination results in a robust sensing platform capable of delivering sensitive and selective HVA detection in complex sample matrices.

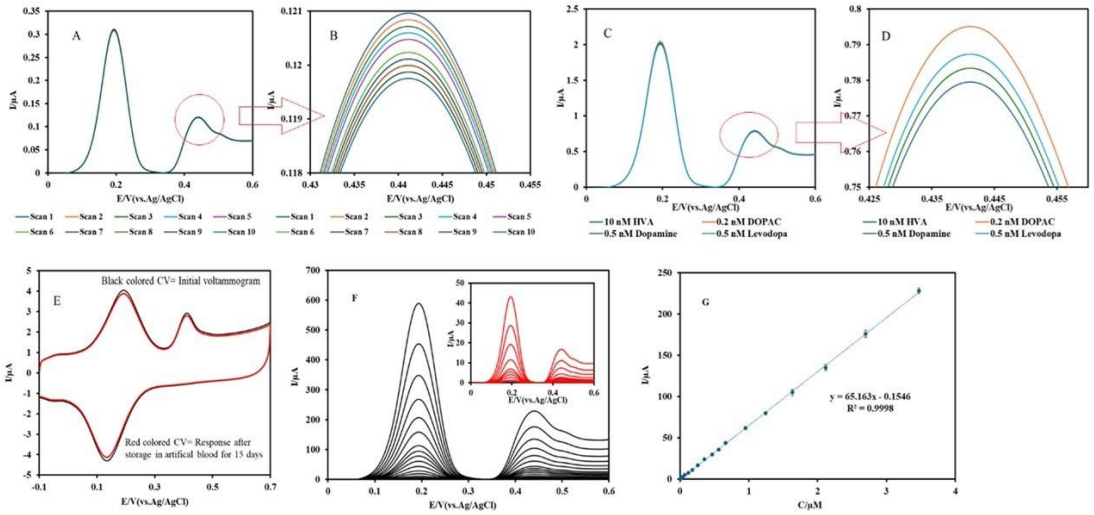

Figure 4.29. (A) Consecutive SWVs demonstrating repeatability for 1.5 nM HVA on ATO-GNP/GCE. (B) The current axis is zoomed in to demonstrate that the voltammograms are close but not identical, consistent with high repeatability. (C) SWVs showing the current response of 10 nM HVA in the presence of various coexisting species. (D) The current axis is zoomed in to demonstrate that the voltammograms are close but not identical, consistent with high selectivity. (E) CVs showing the initial and 15-day stability test of 10 nM HVA in artificial blood. (F) SWVs of HVA at concentations from 4.0×10-9 M to 3.5×10-6 M (Inset: SWVs of lower concentrations of HVA). (G) Curve of current response versus HVA concentrations.

4.3.7. Determination of linear working range

The quantitative detection capability of the GCE modified with GNP and ATO (ATO-GNP/GCE) toward HVA was evaluated using SWV. As shown in Figure 4.29F, the peak current increased proportionally by increasing concentrations of HVA, demonstrating a strong and consistent relationship of current–concentration. SWVs of lower concentrations of HVA are given as inset. The calibration curve, plotting peak currents versus concentrations of HVA, is presented in Figure 42.9G with a plot for the lower concentrations. The sensor exhibited excellent linearity over a wide concentration range from 4.0×10-9 M to 3.5×10-6 M. The equation obatined

for calibration for this linear range was: Ip (μA) = (65.163 ± 0.071) C (μM) - (0.1546 ± 0.0068) (R^2 = 0.9998, n = 3). The LOD, calculated by the 3σ/m method (where σ is the standard deviation of the signal of blank phosphate buffer and m is the slope of peak current versus concentration in the calibration plot), was determined to be (4.5 ± 0.1)×10-10 M, indicating high sensitivity toward HVA detection.

The calibration plot demonstrated a wide linear range, with no sign of current saturation observed within this interval. This behavior confirms that the electrooxidation of HVA at the ATO-GNP/GCE surface remains adsorption-controlled across the tested concentrations. The excellent surface accessibility and high density of active adsorption sites provided by the GNP-ATO nanocomposite prevent premature site blockage and maintain a proportional increase in current response. Nevertheless, beyond 3.5×10^{-6} M, the relationship between current and concentration begins to deviate from linearity, suggesting the onset of partial surface saturation or competitive adsorption effects at elevated analyte levels.

The observed sensitivity of 65.163 μA/μM highlights the efficient electron transfer and strong interaction between HVA molecules and the composite sensing surface. The large active surface area and conductivity of GNP, combined with the catalytic activity and stability of ATO, synergistically enhance the voltammetric response. Additionally, the enlarged electroactive surface area and reduced Rct, as confirmed by prior characterization, contribute to the improved analytical performance of the sensor. Compared to the reported sensors presented in Table 4.6 (Santhy Antherjanam et al., 2023, Yolanda Dineiro et al., 2005, Shishkanova et al., 2018, Khamlichi et al., 2017, Khulood Abu Al-Ola et al., 2021), the ATO-GNP/GCE platform exhibits competitive or superior analytical performance, combining a broad linear range and a lower detection limit with excellent reproducibility and stability. The results establish the ATO-GNP/GCE platform as a reliable and high- performance modified electrode for sensitive and selective detection of HVA. Its wide linear concentration range, lower LOD, and excellent sensitivity make it a good candidate for low-level monitoring in clinical diagnostics and medical research.

Table 4.6. A table showing the comparison of various electrodes for HVA

Electrode material	Linear range (M)	LOD (M)	Sensitivity (μA/μM)	Reference
Poly(ASA)	3.0×10^{-6}-6.1×10^{-5}	1.8×10^{-6}	0.03462	(Antherjanam et al., 2023)
ZFO/CNTs	4.1×10^{-7}-3.2×10^{-6}	1.4×10^{-7}	6.679	(Abu Al-Ola et al., 2021)
Lecuine	4.0×10^{-7}-1.0×10^{-4}	1.0×10^{-7}	-	(Khamlichi et al., 2017)
Poly(CTB)-G	4.0×10^{-5}-1.0×10^{-4}	2.2×10^{-6}	1.7105	(Shishkanova et al., 2018)
MIP	5.0×10^{-8}-1.0×10^{-5}	7.0×10^{-9}	0.044	(Dineiro et al., 2005)
GNPs/ATO	4.0×10^{-9}-3.5×10^{-6}	4.5×10^{-10}	65.163	This study

4.3.8. Sample analysis and practical applicability

The practical applicability of the developed ATO–GNP/GCE sensor was evaluated using spiked artificial blood and urine to assess its analytical performance in complex biological matrices. According to a recent report (Stefani et al., 2017), the concentration of HVA in human biological fluids of mild stage Parkinson's disease patients is approximately 11.91 nM. Therefore, spiking experiments were performed at physiologically relevant concentrations of 5, 10, and 15 nM to better reflect real conditions.

The practical applicability of the developed ATO–GNP/GCE sensor was first demonstrated through the analysis of artificial blood sample, where the sensor achieved recoveries ranging from 99.0% to 102.0% with RSDs between 1.5% and 2.5%, confirming its excellent accuracy and precision for trace-level HVA detection in complex blood matrices (Table 4.7).

Similarly, the sensor's performance was validated using artificial urine sample spiked with the same HVA concentrations. The recoveries for urine samples were found to be in the range of 98.0–101.0%, with RSD values between 2.0% and 2.5%, demonstrating the sensor's strong repeatability, selectivity, and robustness against matrix interferences.

These results confirm that the proposed ATO–GNP-modified electrode retains excellent analytical performance even at nanomolar HVA levels comparable to those found in physiological conditions. Hence, while the platform was primarily designed to establish electroanalytical feasibility, the obtained results highlight its strong potential for future adaptation to biomedical and diagnostic applications.

Table 4.7. Analysis of samples using the proposed electrode

Sample	Added (nM)	Found (nM)	Recovery	RSD
Artificial Blood	5	5.1±0.1	102.0	2.0
	10	10.15±0.25	101.5	2.5
	15	14.85±0.22	99.0	1.5
Artificial Urine	5	4.95±0.10	99.0	2.0
	10	10.1±0.25	101.0	2.5
	15	14.7±0.3	98.0	2.0

5. DISCUSSION

accurate, sensitive, and selective determination of analytes of major health importance: the food dye sunset yellow (SY), the dietary supplement alkaloid yohimbine (YHM), and the clinically relevant neurotransmitter metabolite homovanillic acid (HVA). Although each analyte originates from a different domain—food industry contaminants, supplement regulation, and neurological diagnostics respectively—common analytical challenges persist, such as low-level detection, matrix interferences, and the need for rapid, cost-effective analysis. To address these challenges, three modified glassy carbon electrodes incorporating combinations of carbon-based nanostructures with metal oxide nanoparticles (AZO, ITO, ATO) were fabricated and tested. Their electrocatalytic behaviors were systematically examined using voltammetry and electrochemical impedance spectroscopy (EIS), demonstrating the essential role of nanostructure-engineered materials in boosting electrochemical performance.

5.1. Enhanced Electrocatalytic Activity and Electron Transfer

A major finding across all three platforms is the significant enhancement in electron transfer kinetics resulting from the synergistic interactions between carbon nanomaterials and metal oxide nanoparticles. Carbon materials are well recognized for their high conductivity, exceptional surface area, and π–π interactions with various analytes. Meanwhile, metal oxides—particularly those with high bandgap energy and mixed valence properties—contribute to catalytic activity and more efficient charge migration at the electrode–solution interface.

In the case of the GCE/MWCNTs/AZO electrode, the tubular geometry of MWCNTs provides highly conductive pathways that facilitate rapid electron transport. AZO nanoparticles introduce additional active catalytic sites and promote electron tunneling effects due to aluminum-induced oxygen vacancies. EIS results confirmed a dramatic reduction in charge transfer resistance (Rct), which directly correlates with the superior analytical performance toward SY oxidation. The improved conductivity allowed the anodic peak signal of SY to intensify significantly, particularly at the optimized accumulation time of 210 seconds, demonstrating the benefit of adsorption-driven preconcentration.

Similarly, the GCE/GN@ITO configuration leveraged the layered morphology of graphene nanoplatelets to enhance electron transfer through a two- dimensional conjugated structure, while ITO nanoparticles increased catalytic

turnover thanks to their semiconductor behavior and controlled oxygen vacancies. A notable shift in oxidation potential relative to bare GCE and GCE/GN indicated a lowered overpotential, confirming the electrocatalytic effects.

In the ATO-GNP/GCE platform, the presence of antimony tin oxide, known for its strong redox activity and high conductivity, resulted in a catalytic interface that efficiently facilitated the irreversible oxidation of HVA. Given the biological complexity of HVA-containing fluids, this electrode required highly efficient electron exchange to ensure stable responses even in matrix-rich serum and urine. The significant reduction in Rct and rise in electroactive surface area provided by this nanohybrid system reaffirmed the necessity of incorporating electrocatalytically active metal oxides.

5.2. Analytical Performance Comparison

One of the strengths of this thesis is the evaluation of platforms under similar electrochemical techniques and performance metrics, enabling a comparative insight into their efficiency. All three systems achieved nanomolar sensing capabilities, showcasing how nanostructured electrodes overcome the inherent limitations of bare carbon electrodes.

These outcomes demonstrate that tailoring electrode surface chemistry to target analyte properties directly improves analytical efficiency: Sunset yellow benefits from a high adsorption capability due to the aromatic structure of MWCNTs enabling π–π stacking. Yohimbine, a tertiary alkaloid, interacts favorably with GN's active basal planes and oxygen defect centers on ITO. HVA oxidation involves proton-coupled electron transfer, and ATO provides an optimized environment for such redox mechanisms.

The broad linear ranges cover regulatory threshold levels for SY in beverages and pharmaceuticals, ensure pharmaceutical-quality control in YHM supplements, and support clinical diagnostic relevance for HVA—particularly regarding dopamine metabolism disorders.

5.3. Selectivity and Interference Studies

A common challenge in electroanalytical applications is the presence of multiple interfering substances that can impact analyte recognition. Selectivity improvements in this thesis stem from both:

- Electrode/analyte interaction specificity

- π–π interactions for sunset yellow

- Electrostatic affinity and hydrogen bonding environments for yohimbine

- Protonic involvement in HVA oxidation kinetics

- Surface-controlled preconcentration effects

- Especially notable in the sunset yellow study through accumulation time modulation

All sensors showed minimal interference from common ions and structurally similar molecules present in real samples. The HVA platform demonstrated that the signal remained highly stable even in protein-rich media like blood, confirming surface resistance to fouling—a significant improvement given the notorious biofouling issues in clinical electrochemistry.

5.4. Real Sample Success and Practical Implications

The most meaningful demonstration of platform success lies in its performance in real-world samples:

The close agreement with standard methods such as UV–Vis spectroscopy confirms analytical reliability. This not only validates sensor performance but also highlights their potential as low-cost and portable alternatives to bulky and expensive chromatographic techniques.

5.5. Sensor Durability, Reproducibility, and Fabrication Scalability

Robust sensor fabrication is critical for industrial and clinical deployment. All developed platforms demonstrated: Low RSD values (<3.5%) indicating reproducibility in repeated cycles, Excellent storage stability, especially ATO–GNP retaining >95% response after 15 days, Straightforward fabrication using drop- casting and drying — low-cost and suitable for mass production, These features enhance commercial viability and open avenues for point-of-care diagnostic devices and on-site food analysis kits.

5.6. Mechanistic Insights and Structure–Function Relationships

Each analyte interaction illuminates specific electrocatalytic mechanisms:

Sunset yellow:

-Oxidation involves azo-group cleavage

-Enhanced by surface adsorption in MWCNTs network

Yohimbine:

-Oxidation involves amine-containing molecular sites

-Facilitated by active oxygen vacancies in ITO

HVA:

-Proton-dependent oxidation, indicating biological pH relevance

-Stabilized by electron mediation from ATO mixed valence states

These mechanistic details reinforce the principle that electrode material selection must reflect the target analyte's redox chemistry for optimal performance.

5.7. Overall Scientific Contribution

This thesis contributes to the field of electrochemical sensing by:

- Demonstrating how material synergy drives analytical superiority

- Extending applicability across diverse scientific sectors

- Providing a reusable framework for designing next-generation electrosensors

- The findings ultimately establish that nanocomposites combining conductive carbon materials with catalytic metal oxides yield:

- Enhanced signal strength

- Accelerated electron transfer

- Lower oxidation potentials

- Higher sensitivity and operational stability

This interdisciplinary approach bridges food safety monitoring, regulatory control of supplements, and clinical biochemical assessment—proving the concept of a single material-design strategy with versatile application potential.

The integration of carbon nanomaterials with electrocatalytically active metal oxides forms a powerful strategy to overcome longstanding analytical limitations. This thesis demonstrates that such engineered nanohybrids can deliver superior electrochemical sensing of chemically diverse analytes across multiple application domains while maintaining practicality, reproducibility, and cost-effectiveness.

6. CONCLUSION

A sensitive voltammetric method of analysis was developed based on MWCNTs and aluminum doped zinc oxide (AZO) on a glassy carbon electrode (GCE). The proposed voltammetric platform possessed a large active surface area and low of Rct value. These enabled improved voltammetric behaviour for sunset yellow. The developed platform demonstrated to provide high reproducibility and good selectivity for sunset yellow. A linear concentration of 4.0×10-9 - 7.5×10-6 M was obtained by GCE/MWCNTs/AZO and an LOD of 9.5×10-10 M for sunset yellow. The developed method was successfully used for the quantification of dye compound in a nation-wide consumed powder drink. The results obtained at developed platform were also compared with the measurement recorded at conventional UV-visible method. Applicability of GCE/MWCNTs/AZO was assured in a pharmaceutical product. Good recoveries along with reasonable values of RSD% demonstrated the applicability of GCE/MWCNTs/AZO.

This study also introduces a high-performance electrochemical platform based on GN and ITO nanoparticles for the reliable and accurate detection of yohimbine in dietary supplements and biological fluids. The integration of GN and ITO onto the GCE surface results in a highly efficient sensor with exceptional electrocatalytic properties. Analyses demonstrated that the GCE/GN@ITO system significantly enhances electron transfer kinetics by reducing Rct and increasing the electroactive surface area.The remarkable electrochemical performance of the GCE/GN@ITO sensor is attributed to the synergistic interaction between GN and ITO. GN offers a high surface area, excellent conductivity, and strong adsorption capabilities, while ITO enhances catalytic activity, good stability, and introduces oxygen defects that facilitate the oxidation of yohimbine. These combined features enable precise and sensitive quantification of yohimbine, with a wide range (4.0×10-9 ~ 2.1×10-6 M) and a low LOD of 5.0×10-10 M. The sensor's versatility is further demonstrated by its successful application in food supplement analysis, where it accurately quantified the yohimbine content in capsules (4.960±0.073 mg per capsule). The platform also displayed excellent recovery rates and low RSDs in biological samples, highlighting its reliability for practical applications. In conclusion, the GCE/GN@ITO electrochemical platform sets a new standard in electrochemical quantification, offering good performance for pharmaceutical and clinical diagnostics. Its precise, rapid, and reliable detection capabilities have significant implications for advancing public health and safety.

Furthermore, a novel and highly sensitive voltammetric platform was developed by coating a GCE with GNP and ATO (ATO-GNP/GCE) for the selective determination of HVA. The synergistic combination of conductive GNPs and catalytically active ATO resulted in significantly enhanced electrochemical performance, including a substantially lowered Rct and increased electroactive surface area. Voltammetric studies demonstrated that the ATO-GNP/GCE sensor outperformed both bare and GNP-only modified electrodes, delivering stronger current responses, improved sensitivity, and superior electrocatalytic activity toward HVA oxidation. ATO-GNP/GCE exhibited a broad linear detection range, a low LOD, and good repeatability, reproducibility, and selectivity, with common substances found in fluids. Critically, ATO-GNP/GCE was applied to complex samples, such as blood and urine, achieving high recovery rates with low RSDs. These findings validate the sensor's accuracy, reliability, and practical utility. This study highlights the promising potential of the ATO-GNP/GCE platform as a robust and effective tool for the trace-level quantification of HVA, with important applications in clinical diagnostics, particularly for disorders related to dopamine metabolism, and biomedical research. The integration of graphene-based nanomaterials with ATO offers a versatile strategy for designing advanced electrochemical sensors with enhanced analytical performance.

7. RECOMMENDATIONS

Although the developed GCE/MWCNTs/AZO, GN@ITO/GCE, and ATO-GNP/GCE sensing platforms demonstrated superior electrocatalytic performance and excellent analytical reliability for the detection of sunset yellow, yohimbine, homovanillic acid (HVA), and further studies are recommended to broaden their practical applicability and scientific impact:

Considering the structural similarity of many pharmacological agents and neurotransmitter-related biomarkers, future work could focus on simultaneous multi-species detection. Integrating selective signal-separation strategies may enable real-time analysis of complex biological matrices.

The highly sensitive responses obtained in laboratory conditions suggest that these platforms could be integrated into portable electrochemical devices. Miniaturization, wireless data transmission, and disposable electrode formats should be explored to facilitate field-based pharmaceutical inspection and bedside diagnostic use.

To further enhance durability and anti-fouling behavior, future studies may employ polymeric coatings, ionic liquids, or peptide-based functional layers. Extensive stability assessment under varying temperature, humidity, and storage conditions is crucial for commercialization prospects.

Density functional theory modeling, in situ Raman spectroelectrochemistry, or XPS studies could provide deeper mechanistic understanding regarding electron-transfer pathways and adsorption interactions between the analytes and nanostructured modifiers.

Expanding testing to large sample sets, including various pharmaceutical products, human biofluids, and food supplement brands, will strengthen the reliability and regulatory potential of the sensors. Correlation studies with gold- standard techniques (HPLC, LC-MS) should be systematically performed.

Since some nanomaterials present environmental or cost-related limitations, future research may explore greener synthesis routes and evaluate scalability for industrial manufacturing.

REFERENCES

Abbas, H. A., Radwan, A. L. A., Khaled, E., & Hassan, R. Y. A. (2021). Synthesis and characterization of nanostructured copper and lanthanum co-doped zirconia for voltammetric sensing of tumor biomarkers. *Electrochemical Science Advances, 2*(5).

Ai, Y. J., Liang, P., Wu, Y. X., Dong, Q. M., Li, J. B., Bai, Y., Xu, B. J., Yu, Z., & Ni, D. (2018). Rapid qualitative and quantitative determination of food colorants by both Raman spectra and Surface-enhanced Raman Scattering (SERS). *Food Chem, 241*, 427-433.

Azab, S. M. (2019). A comprehensive structural comparison between cellulose and starch polymers functionalized cobalt nanoparticles sensors for the nanomolar detection of paracetamol. *Journal of Electroanalytical Chemistry, 840*, 319-327.

Švorc, Ľ., & Kalcher, K. (2014). Flow-injection amperometric determination of yohimbine alkaloid in dietary supplements using a boron-doped diamond electrode. *Sensors and Actuators B: Chemical, 205*, 215-218.

Švorc, Ľ., Stanković, D. M., Mehmeti, E., & Kalcher, K. (2014). Sensitive electrochemical determination of yohimbine in primary bark of natural aphrodisiacs using boron-doped diamond electrode. *Anal. Methods, 6*(13), 4853-4859.

Alkahlout, A., Al Dahoudi, N., Grobelsek, I., Jilavi, M., & de Oliveira, P. W. (2014). Synthesis and Characterization of Aluminum Doped Zinc Oxide Nanostructures via Hydrothermal Route. *Journal of Materials, 2014*, 1-8.

Amutha, E., Rajaduraipandian, S., Sivakavinesan, M., & Annadurai, G. (2022). Hydrothermal synthesis and characterization of the antimony-tin oxide nanomaterial and its application as a high-performance asymmetric supercapacitor, photocatalyst, and antibacterial agent. *Nanoscale Adv, 5*(1), 255-267.

Arvand, M., Parhizi, Y., & Mirfathi, S. H. (2015). Simultaneous Voltammetric Determination of Synthetic Colorants in Foods Using a Magnetic Core–Shell Fe3O4@SiO2/MWCNTs Nanocomposite Modified Carbon Paste Electrode. *Food Analytical Methods, 9*(4), 863-875.

Asran, A. M., Mohamed, M. A., Abd El-Rahman, M. K., & Mousavi, M. P. S. (2023). Green ecofriendly electrochemical sensing platform for the sensitive determination of doxycycline. *Heliyon, 9*(4), e15223.

Balram, D., Lian, K. Y., Sebastian, N., Al-Mubaddel, F. S., & Noman, M. T. (2022). Ultrasensitive detection of food colorant sunset yellow using nickel nanoparticles promoted lettuce-like spinel Co(3)O(4) anchored GO nanosheets. *Food Chem Toxicol, 159*, 112725.

Baytak, A. K., & Aslanoglu, M. (2020). A comparison study of adsorptive transfer voltammetry and solution phase voltammetry for the determination of caffeic

acid. *Arabian Journal of Chemistry, 13*(5), 5539-5551.

Baytak, A. K., Teker, T., Duzmen, S., & Aslanoglu, M. (2016). A novel voltammetric sensor based on carbon nanotubes and nanoparticles of antimony tin oxide for the determination of ractopamine. *Mater Sci Eng C Mater Biol Appl, 59*, 368-374.

Beyyavaş, E., & Aslanoglu, M. (2024). Developing a sensitive electrochemical platform constructed with nanoparticles of dysprosium supported on graphene nanoplatelets for the determination of yohimbine. *Microchemical Journal, 207*, 111902.

Blanco-López, M. C., Lobo-Castañón, M. J., Ordieres, A. J. M., & Tuñón-Blanco, P. (2007). Electrochemical Behavior of Catecholamines and Related Compounds at In Situ Surfactant Modified Carbon Paste Electrodes. *Electroanalysis, 19*(2-3), 207-213.

Borchers, A., & Pieler, T. (2010). Programming pluripotent precursor cells derived from Xenopus embryos to generate specific tissues and organs. *Genes (Basel), 1*(3), 413-426.

Buleandra, M., Voica, L. G., Popa, D. E., Badea, I. A., Iorgulescu, E. E., & Cheregi, M. C. (2025). Electrochemical Study and Determination of Homovanillic Acid, the Final Metabolite of Dopamine, Using an Unmodified Disposable Electrode. *Molecules, 30*(2).

Cai, Y., Li, X., Wu, K., & Yang, X. (2019). Electrochemical sensing performance of Eu-BTC and Er-BTC frameworks toward Sunset Yellow. *Anal Chim Acta, 1062*, 78-86.

Carcione, R., Battistoni, S., Palmieri, E., Orlanducci, S., & Tamburri, E. (2023). Pretreatment strategies of titanium substrates to modulate the electrochemical properties of CVD-grown Ti-doped diamond electrodes for dopamine detection. *Surface and Coatings Technology, 467*, 129662.

Chan, H. T. H., Kätelhön, E., & Compton, R. G. (2017). Voltammetry using multiple cycles: Porous electrodes. *Journal of Electroanalytical Chemistry, 799*, 126-133.

Chandana, G. N., Shivaswamy, M. B., Asha, M. S., Jeevitha, S., Nagendra Prasad, H. S., Hemanth, B. S., Sangamesha, M. A., Madhukar, B. S., Mallesha, L., & Manjunatha, J. G. (2024). Ecofriendly synthesis of NiZnFe2O5 nanoparticle by papaya leaf extract for electrochemical detection of ascorbic acid in orange juice and pharmaceuticals. *Journal of Electrochemical Science and Engineering*.

Chebotarev, A., Koicheva, A., Bevziuk, K., Pliuta, K., & Snigur, D. (2019). Simultaneous determination of Sunset Yellow and Tartrazine in soft drinks on carbon-paste electrode modified by silica impregnated with cetylpyridinium chloride. *Journal of Food Measurement and Characterization, 13*(3), 1964-1972.

Chen, P., & Bryden, N. (2015). Determination of Yohimbine in Yohimbe Bark and Related Dietary Supplements Using UHPLC-UV/MS: Single-Laboratory Validation. *J AOAC Int, 98*(4), 896-901.

Darabi, R., & Shabani-Nooshabadi, M. (2021). NiFe2O4-rGO/ionic liquid modified carbon paste electrode: An amplified electrochemical sensitive sensor for determination of Sunset Yellow in the presence of Tartrazine and Allura Red. *Food Chem, 339*, 127841.

David, I. G., Bizgan, A. M., Popa, D. E., Buleandra, M., Moldovan, Z., Badea, I. A., Tekiner, T. A., Basaga, H., & Ciucu, A. A. (2015). Rapid determination of total polyphenolic content in tea samples based on caffeic acid voltammetric behaviour on a disposable graphite electrode. *Food Chem, 173*, 1059-1065.

de Lima, L. F., Maciel, C. C., Ferreira, A. L., de Almeida, J. C., & Ferreira, M. (2020). Nickel (II) phthalocyanine-tetrasulfonic-Au nanoparticles nanocomposite film for tartrazine electrochemical sensing. *Materials Letters, 262*, 127186.

Dejmkova, H., Adamkova, H., Barek, J., & Zima, J. (2017). Voltammetric and amperometric determination of selected catecholamine metabolites using glassy carbon paste electrode. *Monatshefte für Chemie - Chemical Monthly, 148*(3), 511-515.

Deng, K., Li, C., Li, X., & HaowenHuang. (2016). Simultaneous detection of sunset yellow and tartrazine using the nanohybrid of gold nanorods decorated graphene oxide. *Journal of Electroanalytical Chemistry, 780* 296-302.

Deng, Y., Wu, J., Tu, K., Xu, H., Ma, L., Chen, J., & Qian, S. (2017). Fabrication of an electrochemical sensor based on a graphene/Au composite for the determination of clenbuterol in beef samples. *International Journal of Electrochemical Science, 12*(7), 6108-6117.

Devika Sudha Ravindran, Swathi Mukundan, & Kuma, K. G. (2021). A Simple and Efficient Turn-Off Fluorescence Sensor for the Nanomolar Detection of Homovanillic Acid Using Protein Mediated Blue Emitting Nickel Nanoclusters. *ChemistrySelect, 6*, 2477 -2482.

Diñeiro, Y., Menéndez, M. I., Blanco-López, M. C., Lobo-Castañón, M. J., Miranda-Ordieres, A. J., & Tuñón-Blanco, P. (2005). Computational Approach to the Rational Design of Molecularly Imprinted Polymers for Voltammetric Sensing of Homovanillic Acid. *Analytical Chemistry, 77*(20), 6741-6746.

Ding, Z., Deng, P., Wu, Y., Tian, Y., Li, G., Liu, J., & He, Q. (2019). A Novel Modified Electrode for Detection of the Food Colorant Sunset Yellow Based on Nanohybrid of MnO(2) Nanorods-Decorated Electrochemically Reduced Graphene Oxide. *Molecules, 24*(6), 1178.

Dorraji, P. S., & Jalali, F. (2017). Electrochemical fabrication of a novel ZnO/cysteic acid nanocomposite modified electrode and its application to simultaneous determination of sunset yellow and tartrazine. *Food Chem, 227*, 73-77.

Düzmen, Ş., & Aslanoglu, M. (2023). Development of a voltammetric method of analysis using praseodymium oxide-carbon nanotubes for the sensitive detection of dopamine in the presence of tramadol, paracetamol and ascorbic acid. *Electroanalysis, 35*(7).

Düzmen, Ş., Teker, T., & Aslanoglu, M. (2024). A nanostructure based voltammetric platform constructed with carbon nanofibers and erbium nanoparticles for the determination of yohimbine and its DNA binding. *Journal of Electroanalytical Chemistry, 974*, 118710.

Ebube Uwaya, G., & Bisetty, K. (2023). A sensitive ZIF-67/ MWCNTs composite-based sensor for the detection of sunset yellow in food and beverages. *Journal of Electroanalytical Chemistry, 951*, 117899.

El-Gendy, D. M., Mohamed, M. A., Amirghasemi, F., Atty, S. A., Abd El-Rahman, M. K., & Mousavi, M. P. S. (2023). From aluminum foil to personalized medicine: Ecofriendly one-step electrode modification for rapid detection of ertapenem and co-administered medications. *Journal of Science: Advanced Materials and Devices, 8*(3), 100601.

Fan, Y., Zuo, Y., Liu, J., Wang, C., Zhao, X., Ma, J., & Wang, M. (2024). Fabrication of 3D CuFe(2)O(4)/Cu(0) hierarchical nanostructures on carbon fiber paper by simple hydrothermal method for efficient detection of malachite green, sunset yellow and tartrazine in food samples. *Food Chem, 459*, 140378.

Farouk, M., Abd El-Aziz, L., El-Gindy, A. E., & Shokry, E. (2011). Validated methods for determination of yohimbine hydrochloride in the presence of its degradation products. *Bulletin of Faculty of Pharmacy, Cairo University, 49*(2), 67-79.

Fernandez, E., Vidal, L., & Canals, A. (2018). Rapid determination of hydrophilic phenols in olive oil by vortex-assisted reversed-phase dispersive liquid-liquid microextraction and screen-printed carbon electrodes. *Talanta, 181*, 44-51.

Figueira Alves, G., Vinícius de Faria, L., Pedrosa Lisboa, T., Cunha de Souza, C., Luiz Mendes Fernandes, B., Auxiliadora Costa Matos, M., & Camargo Matos, R. (2022). A portable and affordable paper electrochemical platform for the simultaneous detection of sunset yellow and tartrazine in food beverages and desserts. *Microchemical Journal, 181*, 107799.

Foroughi, M. M., Jahani, S., Aramesh-Boroujeni, Z., Fathabadi, M. V., Rafsanjani, H. H., & Dolatabad, M. R. (2021). Template-free synthesis of ZnO/Fe3O4/Carbon magnetic nanocomposite: Nanotubes with hexagonal cross sections and their electrocatalytic property for simultaneous determination of oxymorphone and heroin. *Microchemical Journal, 170*, 106679.

Foroughi, M. M., Jahani, S., Aramesh-Boroujeni, Z., Rostaminasab Dolatabad, M., & Shahbazkhani, K. (2021). Synthesis of 3D cubic of Eu3+/Cu2O with clover-like faces nanostructures and their application as an electrochemical sensor

for determination of antiretroviral drug nevirapine. *Ceramics International, 47*(14), 19727-19736.

Fu, T., Qin, X., Ma, Y., Yuan, X., Wu, S., Ye, X., & Dang, Y. (2022). Yohimbine hydrochloride inhibits skin melanin synthesis by regulating wnt/beta-catenin and p38/MAPK signal pathways. *J Dermatol Sci, 107*(1), 17-23.

Gan, T., Sun, J., Wu, Q., Jing, Q., & Yu, S. (2013). Graphene Decorated with Nickel Nanoparticles as a Sensitive Substrate for Simultaneous Determination of Sunset Yellow and Tartrazine in Food Samples. *Electroanalysis, 25*(6), 1505-1512.

Gómez, M., Arancibia, V., Rojas, C., & Nagles, E. (2012). Adsorptive Stripping Voltammetric Determination of Tartrazine and Sunset Yellow in Gelatins and Soft Drink Powder in the presence of Cetylpyridinium Bromide. *Int. J. Electrochem. Sci., , 7* 7493 - 7502.

García-Salinas, F., Vázquez-Durán, A., & Yáñez-Limón, J. M. (2023). Comparative study of Al-doped ZnO films deposited by sol–gel and by sputtering using a sintered target from ZnO nanoparticles synthesized by sol–gel. *Boletín de la Sociedad Española de Cerámica y Vidrio, 62*(2), 134-144.

Garkani Nejad, F., Asadi, M. H., Sheikhshoaie, I., Dourandish, Z., Zaimbashi, R., & Beitollahi, H. (2022). Construction of modified screen-printed graphite electrode for the application in electrochemical detection of sunset yellow in food samples. *Food and Chemical Toxicology, 166*, 113243.

Garkani Nejad, F., Asadi, M. H., Sheikhshoaie, I., Dourandish, Z., Zaimbashi, R., & Beitollahi, H. (2022). Construction of modified screen-printed graphite electrode for the application in electrochemical detection of sunset yellow in food samples. *Food Chem Toxicol, 166*, 113243.

Ghasemi, Z., Beitollahi, H., Garkani Nejad, F., & Dourandish, Z. (2024). MIL-101 (Fe)-NH2/multi-walled carbon nanotubes nanocomposite modified glassy carbon electrode for simultaneous voltammetric determination of methotrexate and calcium folinate. *Microchemical Journal, 207*, 112252.

Ghorbani-Bidkorbeh, F., Shahrokhian, S., Mohammadi, A., & Dinarvand, R. (2010). Simultaneous voltammetric determination of tramadol and acetaminophen using carbon nanoparticles modified glassy carbon electrode. *Electrochimica Acta, 55*(8), 2752-2759.

Gowda, A. R. A., Kavyashree, M. B., Sangamesha, M. A., Shivaswamy, M. B., Jeevitha, S., Shivaraju, H. P., & Prasad, H. S. N. (2025). The rGO@S- CeMgZn nanocomposite: new insights into the selective and simultaneous electrochemical detection of ciprofloxacin and acetaminophen in biological fluids. *New Journal of Chemistry*.

Goyal, A., Yuen, J., Sinicrope, S., Winter, B., Randall, L., Rusheen, A. E., Blaha, C. D., Bennet, K. E., Lee, K. H., Shin, H., & Oh, Y. (2024). Resolution of tonic concentrations of highly similar neurotransmitters using voltammetry and

deep learning. *Mol Psychiatry, 29*(10), 3076-3085.

Hajmalek, S., Jahani, S., & Foroughi, M. M. (2021). Simultaneous voltammetric determination of tramadol and paracetamol exploiting glassy carbon electrode modified with FeNi3 nanoalloy in biological and pharmaceutical media. *ChemistrySelect, 6*, 8797 –8808.

Hassan A.M. Hendawy, & Khaled, E. (2025). Ferrite nanostructures as promising candidates for voltammetric monitoring of the tumor marker vanillylmandelic acid. *Egyptian Journal of Chemistry, 68*, 123-133.

Hatefi-Mehrjardi, A., Ghaemi, N., Karimi, M. A., Ghasemi, M., & Islami-Ramchahi, S. (2014). Poly-(Alizarin Red S)-Modified Glassy Carbon Electrode for Simultaneous Electrochemical Determination of Levodopa, Homovanillic Acid and Ascorbic Acid. *Electroanalysis, 26*(11), 2491-2500.

He, Q., Liu, J., Liu, X., Xia, Y., Li, G., Deng, P., & Chen, D. (2018). Novel Electrochemical Sensors Based on Cuprous Oxide-Electrochemically Reduced Graphene Oxide Nanocomposites Modified Electrode toward Sensitive Detection of Sunset Yellow. *Molecules, 23*(9).

He, Q., Ma, S., Wang, J., Chen, K., Dong, J., Zhou, J., Chen, D., & Ning, Y. (2022). Graphene Oxide-Based Fluorometric Determination of the eta Gene in Pseudomonas aeruginosa Using Nicking Enzyme-Mediated Cyclic Signal Amplification. *Analytical Letters, 55*(7), 1027-1039.

Hidalgo, J., Turdean, G. L., Falciola, L., Pifferi, V., Galambos, I., Jankovics, H., Toth, E., & Hidalgo, L. (2025). A functionalized multiwalled carbon nanotubes decorated with an engineered flagellin protein as a modified electrode for the detection of diclofenac sodium. *Microchemical Journal, 216*, 114698.

Hodapp, B., Haggerty, A., Feldman, R., & Timpe, J. (2022). Intracranial hemorrhage after a single dose of Yohimbine in a chronic user of clonidine. *Am J Emerg Med, 62*, 145 e141-145 e144.

Hrdlicka, V., Barek, J., & Navratil, T. (2021). Differential pulse voltammetric determination of homovanillic acid as a tumor biomarker in human urine after hollow fiber-based liquid-phase microextraction. *Talanta, 221*, 121594.

Iwasaki, Y., Matsumoto, H., Okumura, M., Inoue, H., Kaji, Y., Ando, C., & Kamei, J. (2022). Determination of neurotransmitters in mouse brain using miniaturized and tableted QuEChERS for the sample preparation. *J Pharm Biomed Anal, 217*, 114809.

J. Montero, C. Guillen, C. G. Granqvist, J. Herrero, & Niklasson, G. A. (2014). Preferential Orientation and Surface Oxidation Control in Reactively Sputter Deposited Nanocrystalline SnO2:Sb Films: Electrochemical and Optical Results. *ECS Journal of Solid State Science and Technology, 3 (11), 3*, N151-N153

Jeevitha, S., Prasad, H. S. N., Shivaswamy, M. B., Asha, M. S., Arjun, S. R.,

Chandana, G. N., Sangamesha, M. A., Madhukar, B. S., Hemanth, B. S., & Thomas, S. (2024). Facile green preparation of ZnFe2O4 nanoparticles using papaya leaf extract for electrochemical detection of acetaminophen in Zerodol P and Dolo drops. *Ionics, 30*(12), 8617-8630.

Ji, L., Cheng, Q., Wu, K., & Yang, X. (2016). Cu-BTC frameworks-based electrochemical sensing platform for rapid and simple determination of Sunset yellow and Tartrazine. *Sensors and Actuators B: Chemical, 231*, 12-17.

Ji, L., Peng, L., Chen, T., Li, X., Zhu, X., & Hu, P. (2022). Facile synthesis of Fe- BTC and electrochemical enhancement effect for sunset yellow determination. *Talanta Open, 5*, 100084.

Jiménez-Suárez, A., & Prolongo, S. G. (2020). Graphene Nanoplatelets. *Applied Sciences, 10*(5), 1753.

Jin, Y., Wang, T., Song, J., Zhang, Y., Guo, W., & Li, G. (2025). A sensitive electrochemical sensing platform for the detection of Marbofloxacin using ZrMo2O8/MWCNT-COOH composites. *Journal of Environmental Chemical Engineering, 13*(2), 115629.

Karabiberoğlu, Ş. U., Ayan, E. M., & Dursun, Z. (2013). Electroanalysis of Caffeic Acid in Red Wine and Investigation of Thermodynamic Parameters Using an Ag Nanoparticles Modified Poly(Thiophene) Film Glassy Carbon Electrode. *Electroanalysis, 25*(8), 1933-1945.

Karapınar, S., Teker, T., Düzmen, Ş., & Aslanoglu, M. (2024). Decorating graphene nanoplatelets with praseodymium oxide for the sensitive electrochemical determination of papaverine. *Measurement, 238*, 115345.

Kaya, S. I., Cetinkaya, A., & Ozkan, S. A. (2021). Latest advances on the nanomaterials-based electrochemical analysis of azo toxic dyes Sunset Yellow and Tartrazine in food samples. *Food Chem Toxicol, 156*, 112524.

Khamlichi, R. E., Bouchta, D., Anouar, E. H., Atia, M. B., Attar, A., Choukairi, M., Tazi, S., Ihssane, R., Faiza, C., Khalid, D., & Khalid, R. T. (2017). A novel l-leucine modified Sol-Gel-Carbon electrode for simultaneous electrochemical detection of homovanillic acid, dopamine and uric acid in neuroblastoma diagnosis. *Mater Sci Eng C Mater Biol Appl, 71*, 870-878.

Khazaee Nejad, S., Ma, H., Al-Shami, A., Soleimani, A., Mohamed, M. A., Dankwah, P., Lee, H. J., & Mousavi, M. P. S. (2024). Sustainable agriculture with LEAFS: a low-cost electrochemical analyzer of foliage stress. *Sensors & Diagnostics, 3*(3), 400-411.

Khulood Abu Al-Ola, Alia Abdulaziz Alfi, Ahmed Hameed, Alaa M. Munshi, Zehba A. Al-Ahmed, Ali A. Keshk, Mohamed E. Khalifa, & El-Metwaly, N. M. (2021). Zinc Ferrite Nanostructure/Multi-Walled Carbon Nanotubes (ZFO/MWCNTs) Nanocomposite as Sensor for Homovanillic Acid Detection in Urine Samples for Cancer Therapy Monitoring. *Int. J. Electrochem. Sci., 16*, 210838.

Kolozof, P.-A., Florou, A. B., Spyrou, K., Hrbac, J., & Prodromidis, M. I. (2020). In-situ tailoring of the electrocatalytic properties of screen-printed graphite electrodes with sparked generated molybdenum nanoparticles for the simultaneous voltammetric determination of sunset yellow and tartrazine. *Sensors and Actuators B: Chemical, 304*, 127268.

Koyun, O. (2018). Poly(L-Cysteine) Modified Pencil Graphite Electrode for Determination of Sunset Yellow in Food and Beverage Samples by Differential Pulse Voltammetry. *International Journal of Electrochemical Science*, 159-174.

Laviron, E. (1974). Adsorption, autoinhibition and autocatalysis in polarography and in linear potential sweep voltammetry. *Electroanalytical Chemistry and Interracial Electrochemistry, 52*, 355 393.

Li, J., Liu, M., Jiang, J., Liu, B., Tong, H., Xu, Z., Yang, C., & Qian, D. (2019). Morphology-controlled electrochemical sensing properties of CuS crystals for tartrazine and sunset yellow. *Sensors and Actuators B: Chemical, 288*, 552-563.

Li, L., Zheng, H., Guo, L., Qu, L., & Yu, L. (2019). Construction of novel electrochemical sensors based on bimetallic nanoparticle functionalized graphene for determination of sunset yellow in soft drink. *Journal of Electroanalytical Chemistry, 833*, 393-400.

Li, S., Liang, J., Wei, P., Liu, Q., Xie, L., Luo, Y., & Sun, X. (2022). ITO@TiO2 nanoarray: An efficient and robust nitrite reduction reaction electrocatalyst toward NH3 production under ambient conditions. *eScience, 2*(4), 382-388.

Li, S., Liu, P., Wang, Y., Li, Y., Ren, Y., Yang, Q., & Ma, Y. (2025). Porous g- C3N4 tubes in-situ anchored by waste biomass-derived carbon dots for photocatalytic reduction of sunset yellow and Escherichia coli in juice. *Applied Surface Science, 682*, 161584.

Li, T., Ma, X., Xue, G., Ju, X., Liu, J., & Wang, L. (2022). Determination of sunset yellow in beverage based on solution-gated graphene transistors with multi-walled carbon nanotube functionalized gate electrodes. *Journal of Electroanalytical Chemistry, 922*, 116758.

Li, Y., Ren, F., Li, J., Chen, Y., Liu, J., & Yang, C. (2025). 1D/2D SnO2/rGO composites-modified GCE for highly sensitive nonenzymatic electrochemical determination of chloramphenicol. *Journal of Alloys and Compounds, 1014*, 178637.

Li, Y., Wang, J., Feng, B., Duan, K., & Weng, J. (2015). Synthesis and characterization of antimony-doped tin oxide (ATO) nanoparticles with high conductivity using a facile ammonia-diffusion co-precipitation method. *Journal of Alloys and Compounds, 634*, 37-42.

Liu, G., Guan, X., Zhang, P., Tan, Q., Li, T., Jin, X., Xu, H., Li, C., & Zhao, J. (2025). A Fully Integrated Wearable Microfluidic Electrochemical Sensor

with Ultrasonic Connecting and Hot-Pressing Bonded Multilayer Structure for Sweat Biomarker Analysis. *Analytical Chemistry, 97*(41), 22858-22870.

Liu, J., Li, J., Chen, Y., Tan, X., & Yang, C. (2025). α-Fe2O3/rGO composites for non-enzymatic electrochemical sensing of UA and Trp and mechanism study through DFT calculation. *Diamond and Related Materials, 156*, 112413.

Liu, S., Chen, S., Tian, L., He, Q., Wang, X., Lu, F., & Ning, Y. (2023). A graphene-oxide-based fluorometric assay for norA gene transcription in MRSA using Nb.BbvCI-assisted target recycling and T7 exonuclease-triggered cascade dual recycling signal amplification. *Talanta, 259*, 124549.

Lu, J. Y., Guo, Z., Huang, W. T., Bao, M., He, B., Li, G., Lei, J., & Li, Y. (2024). Peptide-graphene logic sensing system for dual-mode detection of exosomes, molecular information processing and protection. *Talanta, 267*, 125261.

Manikandan, M., Manikandan, E., Swetha, V., Kurpaa, S., Vijay, S., & Kiruthika, V. (2024). Nickel-copper-cobalt mixed oxide electrode material for high performance asymmetric supercapacitor. *Sci Rep, 14*(1), 10821.

M.B. Shivaswamy, H.S. Nagendra Prasad, Kiran B. Manjappa, S. Madhushree, B.S. Hemanth, B.S. Madhukar, R. Kavya, M.A. Sangamesha, & Anand, A. P. (2024). Unveiling The Multi Functionality of CeCuIn 2 O 5 Nanoparticles: A Promising Approach For UV-Light Photocatalysis, Electrochemical Sensing and Antibacterial Applications. *Analytical & Bioanalytical Electrochemistry, 16*(4), 830-845.

Manikandan, V. S., Adhikari, B., & Chen, A. (2018). Nanomaterial based electrochemical sensors for the safety and quality control of food and beverages. *Analyst, 143*(19), 4537-4554.

Margonis, C. M., Ho, M., Travis, B. D., Brennessel, W. W., & McNamara, W. R. (2021). Iron polypyridyl complex adsorbed on carbon surfaces for hydrogen generation. *Chemical Communications, 57*, 7697-7700.

Marquez-Mariño, K., Penagos-Llanos, J., García-Beltrán, O., Nagles, E., & Hurtado, J. J. (2018). Development of a Novel Electrochemical Sensor Based on a Carbon Paste Electrode Decorated with Nd2O3 for the Simultaneous Detection of Tartrazine and Sunset Yellow. *Electroanalysis, 30*(11), 2760-2767.

Mittal, S., Alexander, K. S., & Dollimore, D. (2000). A high-performance liquid chromatography assay for yohimbine HCl analysis. *Drug Dev Ind Pharm, 26*(10), 1059-1065.

Moarefdoust, M. M., Jahani, S., Moradalizadeh, M., Motaghi, M. M., & Foroughi, M. M. (2021). An electrochemical sensor based on hierarchical nickel oxide nanostructures doped with indium ions for voltammetric simultaneous determination of sunset yellow and tartrazine colorants in soft drink powders. *Anal Methods, 13*(21), 2396-2404.

Mohamed, M. A., Eldin, G. M. G., Ismail, S. M., Zine, N., Elaissari, A., Jaffrezic-

Renault, N., & Errachid, A. (2021). Innovative electrochemical sensor for the precise determination of the new antiviral COVID-19 treatment Favipiravir in the presence of coadministered drugs. *Journal of Electroanalytical Chemistry, 895*, 115422.

Mohammed, M. A., Attia, A. K., & Elwy, H. M. (2016). Electrochemical Sensor Based on Multiwalled Carbon Nanotube, Alizarine Red S and Chitosan for Simultaneous Determination of Oxomemazine Hydrochloride, Paracetamol and Guaifenesin. *Electroanalysis, 29*(2), 506-513.

Mulla, I. A., Lowry, J. P., Serra, P. A., & O'Neill, R. D. (2009). Development of a voltammetric technique for monitoring brain dopamine metabolism: compensation for interference caused by DOPAC electrogenerated during homovanillic acid detection. *Analyst, 134*(5), 893-898.

Nimbalkar, A. R., Patil, N. B., Ganbavle, V. V., Mohite, S. V., Madhale, K. V., & Patil, M. G. (2019). Sol-gel derived aluminium doped zinc oxide thin films: A view of aluminium doping effect on physicochemical and NO2 sensing properties. *Journal of Alloys and Compounds, 775*, 466-473.

Ning, Y., Duan, Y., Feng, Y., & Deng, L. (2014). Label-Free Fluorescent Aptasensor Based on a Graphene Oxide Self-Assembled Probe for the Determination of Adenosine Triphosphate. *Analytical Letters, 47*(14), 2350-2360.

O'Neill, R. D. (2005). Long-Term Monitoring of Brain Dopamine Metabolism In Vivo with Carbon Paste Electrodes. *Sensors, 9*, 317-342.

Ottoni, C. A., Randello de Souza, R., Silva, S. G. d., Spinacé, E. V., Brambilla de Souza, R. F., & Neto, A. O. (2016). Performance of Pd Electrocatalyst Supported on a Physical Mixture Indium Tin Oxide–carbon for Glycerol Electro–oxidation in Alkaline Media. *Electroanalysis, 29*(4), 960-964.

Patil, N. J., Vishnuraj, R., Mani, G. K., Rangarajan, M., & Srinivasan, P. (2025). Silver decorated CuO-mesoporous graphitic carbon nitride as electrochemical sweat sensor for sensing ammonium ions: A membrane-free voltammetric approach. *Electrochimica Acta, 535*, 146716.

Peña-Gonzalez, A. (2018). Detection of Sunset Yellow by Adsorption Voltammetry at Glassy Carbon Electrode Modified with Chitosan. *International Journal of Electrochemical Science*, 5005-5015.

Penagos-Llanos, J., García-Beltrán, O., Calderón, J. A., Hurtado-Murillo, J. J., Nagles, E., & Hurtado, J. J. (2019). Simultaneous determination of tartrazine, sunset yellow and allura red in foods using a new cobalt-decorated carbon paste electrode. *Journal of Electroanalytical Chemistry, 852*, 113517.

Penagos-Llanos, J., García-Beltrán, O., Nagles, E., & Hurtado, J. J. (2020). A New Electrochemical Method to Detect Sunset Yellow, Tartrazine and Thiomersal in a Pharmaceutical Dose Using a Carbon Paste Electrode Decorated with Molybdenum Oxide. *Electroanalysis, 32*(10), 2174-2182.

Pereira, P., Ferreira, D. P., Araujo, J. C., Ferreira, A., & Fangueiro, R. (2020). The

Potential of Graphene Nanoplatelets in the Development of Smart and Multifunctional Ecocomposites. *Polymers (Basel), 12*(10).

Pogacean, F., Coros, M., Mirel, V., Magerusan, L., Barbu-Tudoran, L., Vulpoi, A., Stefan-van Staden, R.-I., & Pruneanu, S. (2019). Graphene-based materials produced by graphite electrochemical exfoliation in acidic solutions: Application to Sunset Yellow voltammetric detection. *Microchemical Journal, 147*, 112-120.

Qi, X., Xia, Y., Wu, J., Wan, X., Wang, T., Li, Q., & Li, G. (2025). Robust determination of marbofloxacin based on bimetallic Au@Ag nanoparticle-decorated black phosphorus nanosheets supported molecularly imprinted polymer film. *Materials Today Chemistry, 45*, 102687.

Qin, P., Yang, Y., Li, W., Zhang, J., Zhou, Q., & Lu, M. (2019). Amino- functionalized mesoporous silica nanospheres (MSN-NH2) as sorbent for extraction and concentration of synthetic dyes from foodstuffs prior to HPLC analysis. *Analytical Methods, 11*(1), 105-112.

Qiu, X., Lu, L., Leng, J., Yu, Y., Wang, W., Jiang, M., & Bai, L. (2016). An enhanced electrochemical platform based on graphene oxide and multi-walled carbon nanotubes nanocomposite for sensitive determination of Sunset Yellow and Tartrazine. *Food Chemistry, 190*, 889-895.

Rafiq, M. Z., Siddique, A., Fazle Rabbee, M., Jillani, S. M. S., Al-Humaidi, J. Y., Dildar, A., Qamar, M. T., Haider, S. K., Akhtar, M. N., Fazal, M. A., Khan, M. A., Mizanur Rahman Khan, M., Sheikh, T. A., & Rahman, M. M. (2024). Sensitive detection of urea based on Dy2O3-Co3O4@ZrO2 nanocomposite by electrochemical approach for environmental assessment. *Microchemical Journal, 207*, 111915.

Randviir, E. P., & Banks, C. E. (2013). Electrochemical impedance spectroscopy: an overview of bioanalytical applications. *Analytical Methods, 5*(5), 1098.

Regmi, G., Rijal, S., & Velumani, S. (2023). Aluminum-doped zinc oxide (AZO) ultra-thin films deposited by radio frequency sputtering for flexible Cu(In,Ga)Se2 solar cells. *Memories - Materials, Devices, Circuits and Systems, 5*, 100064.

Ren, L., Xu, B., Wang, G., Yin, X., Liu, Y., Yang, W., & Chen, Y. (2020). Fabrication of an antimony doped tin oxide-graphene nanocomposite for highly effective capacitive deionization of saline water. *RSC Adv, 10*(64), 39130-39136.

Rene Pfeifera, Priscila Tamiasso Martinhonb, Celia Sousab, Josino Costa Moreirac, Marco Antonio Chaer Nascimentob, Jiří Bareka, & Vyskočila, V. ((2019). The role of 3,4-dihydroxyphenylacetic acid adsorption in the oxidation of homovanillic acid at a glassy carbon rotating disc electrode. *Journal of Electroanalytical Chemistry, 838* 129-135.

Rodsud, S., & Limbut, W. (2019). A Simple Electrochemical Sensor Based on

Graphene Nanoplatelets Modified Glassy Carbon Electrode (GrNPs/GCE) for Highly Sensitive Detection of Yohimbine (YOH). *Journal of The Electrochemical Society, 166*(10), B771-B779.

Romero-Alfano, I., Stevanovic, M., Goyenechea, J., Prats, E., Barata, C., Raldua, D., & Gomez-Canela, C. (2025). Ultra-sensitive UHPLC-MS/MS method for simultaneous quantification of 31 neurochemicals in zebrafish larvae and brain. *Talanta, 295*, 128334.

Rozi, N., Ahmad, A., Yook Heng, L., Shyuan, L. K., & Hanifah, S. A. (2018). Electrochemical Sunset Yellow Biosensor Based on Photocured Polyacrylamide Membrane for Food Dye Monitoring. *Sensors (Basel), 18*(1).

Sahraei, R., Farmany, A., & Mortazavi, S. S. (2013). A nanosilver-based spectrophotometry method for sensitive determination of tartrazine in food samples. *Food Chem, 138*(2-3), 1239-1242.

Sakthivel, M., Sivakumar, M., Chen, S.-M., & Pandi, K. (2018). Electrochemical synthesis of poly(3,4-ethylenedioxythiophene) on terbium hexacyanoferrate for sensitive determination of tartrazine. *Sensors and Actuators B: Chemical, 256*, 195-203.

Sanati, A. L., Karimi-Maleh, H., Badiei, A., Biparva, P., & Ensafi, A. A. (2014). A voltammetric sensor based on NiO/CNTs ionic liquid carbon paste electrode for determination of morphine in the presence of diclofenac. *Mater Sci Eng C Mater Biol Appl, 35*, 379-385.

Santhy Antherjanam, Beena Saraswathyamma, & Kumar, S. M. S. (2023). Simultaneous electrochemical determination of the tumour biomarkers homovanillic acid and vanillylmandelic acid using a modified pencil graphite electrode. *Microchemical Journal, 190* 108659.

Sarakhman, O., Benková, A., & Švorc, Ľ. (2022). A modern and powerful electrochemical sensing platform for purines determination: Voltammetric determination of uric acid and caffeine in biological samples on miniaturized thick-film boron-doped diamond electrode. *Microchemical Journal, 175*, 107132.

Setoudeh, N., Jahani, S., Kazemipour, M., Foroughi, M. M., & Hassani Nadiki, H. (2020). Zeolitic imidazolate frameworks and cobalt-tannic acid nanocomposite modified carbon paste electrode for simultaneous determination of dopamine, uric acid, acetaminophen and tryptophan: Investigation of kinetic parameters of surface electrode and its analytical performance. *Journal of Electroanalytical Chemistry, 863*, 114045.

Shan, W. L., Lu, Q., Li, H. Y., Wang, Z. X., Zhang, R., Wei, M. J., Kong, F. Y., & Wang, W. (2025). A single N-rich covalent organic framework-based sensor for electrochemical sensing of 2,4,6-trichlorophenol. *Food Chem, 493*(Pt 4), 146092.

Shishkanova, T. V., Broncová, G., Fitl, P., Král, V., & Barek, J. (2018).

Voltammetric Detection of Catecholamine Metabolites Using Tröger's Base Modified Electrode. *Electroanalysis, 30*(4), 734-739.

Shishkanova, T. V., Kralik, F., & Synytsya, A. (2023). Voltammetric Detection of Vanillylmandelic Acid and Homovanillic Acid Using Urea-Derivative-Modified Graphite Electrode. *Sensors (Basel), 23*(7).

Shume, W. M., Zereffa, E. A., Fakrudeen, S. P., Al-Farraj, S., Sillanpää, M., & Murthy, H. C. A. (2023). Ni1Zn1-xLayFe2-yO4@rGO nanocomposite as electrochemical sensor for simultaneous analysis of food colorants-sunset yellow and tartrazine. *Inorganic Chemistry Communications, 155*, 111071.

Sierra-Rosales, P., Berríos, C., Miranda-Rojas, S., & Squella, J. A. (2018). Experimental and theoretical insights into the electrooxidation pathway of azo-colorants on glassy carbon electrode. *Electrochimica Acta, 290*, 556-567.

Silva Mariano, R., Coldibeli, B., Scalianti Ceravolo, G., & Romão Sartori, E. (2024). Ultra-sensitive determination of serotonergic antidepressant vortioxetine in pharmaceutical and blood samples at the boron-doped diamond electrode. *Journal of Electroanalytical Chemistry, 952*, 117962.

Simona Baluchováa, Jiří Bareka, Luciana I.N. Toméb, Christopher M.A. Brettb, & Schwarzová-Pecková, K. (2018). Vanillylmandelic and Homovanillic acid: Electroanalysis at non-modified and polymer-modified carbon-based electrodes. *Journal of Electroanalytical Chemistry, 821*, 22-32.

Singh, M., & Scotognella, F. (2023). Recent Progress in Solution Processed Aluminum and co-Doped ZnO for Transparent Conductive Oxide Applications. *Micromachines (Basel), 14*(3).

Smarzewska, S., Guziejewski, D., Skowron, M., Skrzypek, S., & Ciesielski, W. (2014). Voltammetric behavior and quantitative determination of ambazone concentrations in urine and in a pharmaceutical formulation. *Open Chemistry, 12*(12), 1239-1245.

Soliman, S. S., Mahmoud, A. M., & El Mously, D. A. (2025). Nickel monoligand-MOF modified electrochemical sensor for the detection of neuroblastoma biomarker homovanillic acid. *Sensing and Bio-Sensing Research, 50*, 100909.

Stefani, A., Pierantozzi, M., Olivola, E., Galati, S., Cerroni, R., D'Angelo, V., Hainsworth, A. H., Saviozzi, V., Fedele, E., & Liguori, C. (2017). Homovanillic acid in CSF of mild stage Parkinson's disease patients correlates with motor impairment. *Neurochem Int, 105*, 58-63.

Subramanian, B., Jeeva Jothi, K., Mohideen, M. M., Karthikeyan, R., Santhana Krishna Kumar, A., Ayyakannu Sundaram, G., Thirumalai, K., Albaqami, M. D., Mohammad, S., & Swaminathan, M. (2024). Synthesis and Characterization of Dy2O3@TiO2 Nanocomposites for Enhanced Photocatalytic and Electrocatalytic Applications. *ACS Engineering Au, 4*(5), 474-490.

Sun, H., Song, J., Zhao, C., Tian, S., Cheng, Z., Tian, L., & Qi, T. (2025). Enhancing

NO sensing performance using a bismuth-doping strategy for Yttria-stabilized zirconia-based electrochemical sensors. *Chemical Engineering Journal, 526*, 170679.

Sun, R., Lv, R., Li, Y., Du, T., Chen, L., Zhang, Y., Zhang, X., Zhang, L., Ma, H., Sun, H., & Qi, Y. (2023). Simple and sensitive electrochemical detection of sunset yellow and Sudan I in food based on AuNPs/Zr-MOF-Graphene. *Food Control, 145*, 109491.

T. Selvaraju, & Ramaraj, R. (2007). Simultaneous detection of ascorbic acid, uric acid and homovanillic acid at copper modified electrode. *Electrochimica Acta, 52*(2998-3005).

Tahtaisleyen, S., Gorduk, O., & Sahin, Y. (2020). Electrochemical Determination of Tartrazine Using a Graphene/Poly(L-Phenylalanine) Modified Pencil Graphite Electrode. *Analytical Letters*, 1-21.

Tajik, S., & Beitollahi, H. (2022). Hydrothermal synthesis of CuFe(2)O(4) nanoparticles for highly sensitive electrochemical detection of sunset yellow. *Food Chem Toxicol, 165*, 113048.

Tang, Y., Wang, Y., Liu, G., & Sun, D. (2016). Determination of sunset yellow and tartrazine using silver and poly (L-cysteine) composite film modified glassy carbon electrode. *Indian Journal of Chemistry, Vol. 55A.* , 298-303.

Teker, T., & Aslanoglu, M. (2024). Developing a sensitive voltammetric platform constructed with dysprosium nanoparticles supported on gadolinium oxide–carbon nanotube for the determination of centrophenoxine. *Microchemical Journal, 198*, 110199.

Teker, T., & Aslanoglu, M. (2021). Development of a Dy(2)O(3)@Eu(2)O(3)-carbon nanofiber based electrode for highly sensitive detection of papaverine. *Anal Chim Acta, 1183*, 338972.

Tian, L., Chen, S., & Ning, Y. (2025). Monitoring of lasR gene transcription in Pseudomonas aeruginosa via a graphene oxide-based fluorometric bioassay coupling strand displacement-triggered target recycling and exonuclease III-assisted signal amplification. *Microchemical Journal, 208*, 112617.

Tran, Q. T., Phung, T. T., Nguyen, Q. T., Le, T. G., & Lagrost, C. (2019). Highly sensitive and rapid determination of sunset yellow in drinks using a low-cost carbon material-based electrochemical sensor. *Anal Bioanal Chem, 411*(28), 7539-7549.

Trani, A., Petrucci, R., Marrosu, G., Zane, D., & Curulli, A. (2017). Selective electrochemical determination of caffeine at a gold-chitosan nanocomposite sensor: May little change on nanocomposites synthesis affect selectivity? *Journal of Electroanalytical Chemistry, 788*, 99-106.

Wang, M., Zhang, J., Gao, Y., Yang, X., Gao, Y., & Zhao, J. (2013). Determination of Sunset Yellow in Soft Drinks at Attapulgite Modified Expanded Graphite Paste Electrode. *Journal of The Electrochemical Society, 161*(3), H86-H91.

Wang, T., Xia, Y., Wan, X., Zhang, Y., Chen, N., Jin, Y., & Li, G. (2024). A facile and efficient voltammetric sensor for marbofloxacin detection based on zirconium-based metal-organic framework UiO-66/nitrogen-doped graphene nanocomposite. *Microchemical Journal, 201*, 110673.

Wang, T., Xu, S., Liu, L., Zhang, Y., & Li, G. (2025). A highly stable voltammetric sensor for trace ofloxacin determination coupling molecularly imprinting film with AuNP and UiO-66 MOF dual-encapsulated black phosphorus nanosheets. *Materials Today Chemistry, 43*, 102468.

Wu, J., Xia, Y., Wang, T., Zhang, Y., & Li, G. (2025). Efficient voltammetric platform combining a molecularly imprinted polymer and silver-nanoparticle- decorated black phosphorus nanosheets for selective determination of Gatifloxacin. *Food Chem X, 25*, 102094.

Wu, T., Wang, Q., Peng, X., & Guo, Y. (2021). Facile Synthesis of Gold/Graphene Nanocomposites for Simultaneous Determination of Sunset Yellow and Tartrazine in Soft Drinks. *Electroanalysis, 34*(1), 83-90.

Xu, J., Zhang, Y., Zhou, H., Wang, M., Xu, P., & Zhang, J. (2012). An Amperometric Sensor for Sunset Yellow FCF Detection Based on Molecularly Imprinted Polypyrrole. *Engineering, 04*(10), 159-162.

Xu, W., Lei, R., Cao, W., Guo, C., Zhang, X., & Wang, S. (2013). Voltammetric Method Using Multi-Walled Carbon Nanotubes Modified Glassy Carbon Electrode for the Determination of Terbutaline Sulfate in Pork Sample. *Journal of Analytical Sciences, Methods and Instrumentation, 03*(02), 75-79.

Yang, C., Trikantzopoulos, E., Jacobs, C. B., & Venton, B. J. (2017). Evaluation of carbon nanotube fiber microelectrodes for neurotransmitter detection: Correlation of electrochemical performance and surface properties. *Anal Chim Acta, 965*, 1-8.

Yang, F., Wang, J., Yin, K., & Pang, H. (2022). An Electrochemical Sensor for Sunset Yellow Detection Based on Cu@Cu(2)O-BNPC Formed by Modified Porous Carbon. *ACS Omega, 7*(36), 32068-32077.

Yi, J., Zeng, L., Wu, Q., Yang, L., & Xie, T. (2018). Sensitive Simultaneous Determination of Synthetic Food Colorants in Preserved Fruit Samples by Capillary Electrophoresis with Contactless Conductivity Detection. *Food Analytical Methods, 11*(6), 1608-1618.

Yolanda Dineiro, M. Isabel Menendez, M. Carmen Blanco-Lopez, M. Jesus Lobo-Castanon, Arturo J. Miranda-Ordieres, & Tunon-Blanco, P. (2005). Computational Approach to the Rational Design of Molecularly Imprinted Polymers for Voltammetric Sensing of Homovanillic Acid. *Analytical Chemistry 77*, 6741-6746.

Zhang, M., Tang, Y., Tian, X., Wang, H., Wang, J., & Zhang, Q. (2021). Magnetron co-sputtering optimized aluminum-doped zinc oxide (AZO) film for high-response formaldehyde sensing. *Journal of Alloys and Compounds, 880*,

160510.

Zhang, S., Ling, P., Chen, Y., Liu, J., & Yang, C. (2023). 2D/2D porous Co3O4/rGO nanosheets act as an electrochemical sensor for voltammetric tryptophan detection. *Diamond and Related Materials, 135*, 109811.

Zhao, Y., Zhang, Y., Li, Y., Yang, M., Yuan, J., Cao, Y., Xu, L., Ma, X., Lin, S., An, J., & Wang, S. (2021). Yohimbine hydrochloride inhibits benign prostatic hyperplasia by downregulating steroid 5alpha-reductase type 2. *Eur J Pharmacol, 908*, 174334.

Zhou, Y., Zhang, H., Chang, Z., Ye, B., & Xu, M. (2016). Simultaneous Determination of Clenbuterol and Salbutamol with a Graphene-Nafion Nanocomposite Modified Electrode. *International Journal of Electrochemical Science, 11*(6), 5154-5164.

Zhu, L., Han, X., Zhu, J., Du, L., Liu, L., & Gong, W. (2021). Severe acute intoxication with yohimbine: Four simultaneous poisoning cases. *Forensic Sci Int, 320*, 110705.

Zhu, M., Zeng, C., Ye, J., & Sun, Y. (2018). Simultaneous in vivo voltammetric determination of dopamine and 5-Hydroxytryptamine in the mouse brain. *Applied Surface Science, 455*, 646-652.